UNIVERSITÄT ZU LÜBECK

From the Institute for Endocrinology & Diabetes

of the University of Lübeck

Directors: Prof. Dr. rer. nat. Jens Mittag

and Prof. Dr. med. Sebastian Schmid

"A big heart needs an open mind –

Dissecting central versus peripheral actions of thyroid hormones in a mouse model of the Allan-Herndon-Dudley Syndrome"

Dissertation for Fulfillment of Requirements

for the Doctoral Degree

of the University of Lübeck

from the Department of Natural Sciences

Submitted by

Beate Herrmann

from Bergisch Gladbach, Germany

Lübeck, 2020

First referee: Prof. Dr. rer. nat. Jens Mittag

Second referee: Prof. Dr. med. Olaf Hiort

Date of oral examination: October 30th, 2020

Approved for printing. Lübeck, November 2nd, 2020

Publications

Parts of this thesis were already published in a peer-reviewed journal due to priority reasons.

Herrmann B, Harder L, Oelkrug R, Chen J, Gachkar S, Nock S, Resch J, Korkowski M, Heuer H, Mittag J (2020)
Central Hypothyroidism Impairs Heart Rate Stability and Prevents Thyroid Hormone-Induced Cardiac Hypertrophy and Pyrexia. *Thyroid*, 10.1089/thy.2019.0705. Advance online publication. https://doi.org/10.1089/thy.2019.0705

Publications that were not part of this thesis:

Gachkar S, Oelkrug R, Herrmann B, Scanlan T.S, Sun Q, Biebermann H, Hoefig C.S, Schomburg L, Mittag J (2020)
N- and O-Acetylated 3-Iodothyronamines Have No Metabolic or Thermogenic Effects in Male Mice. *European thyroid journal*, 9(2), 57–66. https://doi.org/10.1159/000504887

Johann K, Reis M.C, Harder L, Herrmann B, Gachkar S, Mittag J, Oelkrug R (2018)
Effects of sildenafil treatment on thermogenesis and glucose homeostasis in diet-induced obese mice. *Nutrition & diabetes*, 8(1), 9. https://doi.org/10.1038/s41387-018-0026-0

Oelkrug R, Herrmann B, Geissler C, Harder L, Koch C, Lehnert H, Oster H, Kirchner H, Mittag J (2017)
Dwarfism and insulin resistance in male offspring caused by α1-adrenergic antagonism during pregnancy. *Molecular metabolism*, 6(10), 1126–1136. https://doi.org/10.1016/j.molmet.2017.06.016.

Zusammenfassung

Schilddrüsenhormone (SDH) spielen eine zentrale Rolle unter anderem im Stoffwechsel, Wachstum, Herzkreislaufsystem, in der Thermoregulation sowie in der Gehirnentwicklung. Bei Abweichungen von den SDH-Serumspiegeln kann es unter anderem zu einer Hypo- oder Hyperthyreose kommen. Letzteres ist gekennzeichnet durch Tachykardie, Gewichtsverlust und Wärmeunverträglichkeit, während Patienten mit einer Hypothyreose entgegengesetzte Symptome aufzeigen. Der Ursprung dieser Symptome wurde bislang durch eine direkte SDH-Wirkung an den jeweiligen Organen beschrieben. Dies wurde jedoch kürzlich in Frage gestellt, da gezeigt werden konnte, dass die direkte Gabe von 3,3',5-Triiodthyronin (T3) in das Nagergehirn die Auswirkungen einer systemischen Hyperthyreose nachahmen kann.

Zur weiteren Aufklärung befasst sich die vorliegende Dissertation mit der Analyse der peripheren SDH-Beiträge im Vergleich zu ihren zentralen Effekten bezüglich der auftretenden Symptome einer Hyperthyreose. Der Fokus liegt hierbei auf der Thermoregulation und dem kardiovaskulären System. Hierzu wurden Mäuse verwendet, denen die zwei SDH-Transporter, der Monokarboxylat-Transporter 8 (MCT8) und das organische Anionen transportierende Polypeptid 1c1 (OATP1C1), fehlen (*M/O* doppel-knockout (dko)). Dies führt in den Mäusen zu einer peripheren Hyperthyreose, wohingegen sich das Gehirn in einem sehr hypothyreoten Zustand befindet. Diese Mäuse rekapitulieren den Phänotyp des Allan-Herndon-Dudley Syndroms (AHDS) im Menschen, eine seltene vererbbare Erkrankung mit Mutationen in MCT8 die zu schwerer geistiger Retardierung führt. Des Weiteren wurden Wildtyp (WT) Mäuse oral mit T3 behandelt, um eine ähnliche periphere Hyperthyreose bei einer parallelen zentralen Hyperthyreose zu induzieren. Der Vergleich beider Mausmodelle ermöglichte somit die Identifizierung von Symptomen einer Hyperthyreose, die gleichzeitig eine zentrale SDH-Wirkung erfordern, nämlich die kardiale Hypertrophie sowie die Erhöhung der Körpertemperatur. Darüber hinaus erwies sich der SDH-Status des Gehirns als entscheidend für die Regulation der Herzratenfrequenz, da *M/O* dko Mäuse abnorme Episoden von Tachykardie und Bradykardie aufwiesen. Schließlich wurde die Sicherheit der systemischen Verabreichung des SDH-Analogons 3,3',5-Triiodthyroessigsäure (Triac) an WT-Mäusen getestet, da dieser Wirkstoff zurzeit in klinischen Studien bei AHDS Patienten eingesetzt wird. Die Daten zeigen eine hepatische Hyperthyreose, wohingegen sich der Skelettmuskel in einem Zustand der Hypothyreose zu befinden scheint – eine wichtige Beobachtung, die bei der Planung von klinischen Studien mit Triac berücksichtigt werden sollte.

Zusammenfassend lässt sich sagen, dass der Vergleich der *M/O* dko Mäuse mit den T3-behandelten Mäusen deutliche phänotypische Merkmale zeigte, die die zentrale Wirkung von SDH erfordern. Insbesondere die gestörte autonome Kontrolle der *M/O* dko Mäuse ist von großer translationaler Relevanz, da tachykarde Episoden zu Herzrhythmusstörungen und zum plötzlichen Tod führen können – ein Phänomen das auch bei AHDS Patienten beobachtet wird.

Abstract

Thyroid hormones (THs) play a pivotal role in metabolism, growth, and development of the human body as they target almost every cell in the body. Therefore, optimal TH concentrations are ensured through a tightly regulated system. If this system is out of balance hypo- or hyperthyroidism can develop. The key hallmarks of hyperthyroidism are tachycardia, weight loss, and heat intolerance, whereas patients with hypothyroidism show opposite symptoms. For a long time, it was generally accepted that the described symptoms are the direct actions of THs in the respective peripheral tissues. This classical paradigm was recently challenged by studies showing that direct administration of 3,3',5-triiodothyronine (T3) into the rodent brain can mimic the effects of whole-body hyperthyroidism. Due to the plethora of TH effects and communication routes, it is however difficult to dissect the peripheral versus the central effects under physiological conditions *in vivo*, as they include important regulatory check points such as the blood-brain-barrier.

The aim of the present study was to dissect the peripheral contributions of TH action versus its central effects for the symptoms occurring in hyperthyroidism, with a focus on thermoregulation and cardiovascular function. To this end, mice lacking the TH transporters monocarboxylate transporter 8 (MCT8) and organic anion transporting polypeptide 1c1 (OATP1C1) (*M/O* double knockout (dko)) were used as they display peripheral hyperthyroidism while the brain is in a profoundly hypothyroid state. These mice recapitulate the phenotype of the Allan-Herndon-Dudley Syndrome (AHDS), a genetic human disorder caused by mutations in MCT8, which is characterized by severe mental retardation. Therefore, the *M/O* dko mice were compared to wildtype (WT) mice treated orally with T3 to induce a similar peripheral hyperthyroidism and importantly, also centrally. This allowed the identification of hyperthyroid symptoms that require a simultaneous central hyperthyroidism, namely the TH-induced cardiac hypertrophy and elevation in daytime body temperature. Furthermore, the TH status of the brain was found to be crucial for the heart rate frequency distribution, as the *M/O* dko mice displayed abnormal episodes of tachycardia and bradycardia. Finally, the safety of systemic administration of the TH analogue 3,3',5-triiodothyroacetic acid (Triac) was tested in WT mice, as this compound is currently used in clinical trials to reverse the defects observed in AHDS. The data revealed a hepatic hyperthyroid state, whereas the skeletal muscle seems to be in a hypothyroid state – an important observation that needs to be taken into consideration when designing the endpoints to observe in clinical trials employing Triac.

In summary, the comparison of the *M/O* dko with the T3-treated mouse model revealed distinct phenotypic traits that require the central action of THs. Especially, the impaired autonomic control is likely of great translational relevance, as tachycardic episodes can lead to cardiac arrhythmias and sudden death, which is also observed in AHDS patients.

Content

1. Introduction

Thyroid hormones (THs) play a crucial role in metabolism, growth, and development of the human body as they target almost every cell in the body. The first thyroid gland abnormalities have been described earlier than 1500 BC and included an abnormal enlargement of the thyroid gland, which has been termed goitre (1). Today, thyroid dysfunction belongs to the leading endocrine disorders worldwide. Furthermore, the prevalence of diagnosed TH disorders was 18.9 % in a population-based study in Northeast Germany (2). However, the numbers differ dependent on the respective area, as the global distribution of iodine, an indispensable component of THs, is uneven (reviewed in (3)). In addition to the differences in iodine supplementation, the cause of a thyroid disorder may also be genetic origin. Some of these inherited disorders are rare and not well known among clinicians, which leads to treatment delays and misdiagnosis. Our knowledge about the actions of THs as a highly multi-layered and tightly controlled system has significantly improved but in many cases the importance is still underestimated. Therefore, the overall aims are to understand the thyroid complexity with its individual connections and contributions, to increase awareness of rare disorders as well as to optimize treatment options.

1.1. The main regulatory systems

To ensure smooth functionality of the multifaceted processes, which are required for the survival and wellbeing of mammals, several regulatory systems have developed. The endocrine system acts along with the nervous system in the regulation and maintenance of homeostasis. The nervous system relies on a special cell type, the neuron. These neurons act in precise pathways to transmit electro-chemical impulses. The nervous system consists of the central nervous system (CNS) and the peripheral nervous system. The latter system includes nerves of the autonomic nervous system, which sends automatically and continuously motor impulses to internal organs (e.g. heart rate, breathing rate, body temperature) through an antagonistic functional relationship of the sympathetic (SNS; “fight or flight response”) and parasympathetic nervous system (PSNS; “rest and digest function”), which will be described in more detail (Chapter 1.3.1 Autonomic nervous system). The endocrine system, in contrast to the nervous system acts through chemical messengers, called hormones. After production in the endocrine glands, these hormones are secreted into the blood and carried to their destined cells, which have receptors for these specific hormones. Due to the powerful actions of hormones, their release needs to be tightly controlled, often by a feedback mechanism consisting of several layers. One example is the hypothalamus-pituitary-thyroid (HPT) axis as described in the following chapter.

1.1.1. The hypothalamus-pituitary-thyroid axis

The connection and correct communication between the hypothalamus, the pituitary, and the thyroid gland is required for production and secretion of THs (**Figure 1**). In the hypothalamus, the neurons in the paraventricular nucleus, a highly conserved brain region adjacent to the third ventricle, synthesize, and release the thyrotropin-releasing hormone (TRH) in response to environmental and physiological stimuli. TRH acts then on the pituitary gland and induces the secretion of the thyroid-stimulating hormone (TSH), which results in the stimulation of the thyroid to produce THs. To achieve stable, circulating TH concentrations THs signal back to the hypothalamus and the pituitary. This reduces the production and secretion of THs by the thyroid gland (reviewed in (4, 5)).

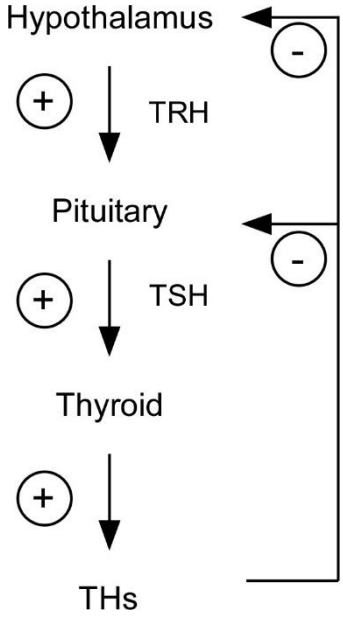

Figure 1: Schematic overview of thy hypothalamus-pituitary-axis.
Hypothalamic neurons release TRH, which leads to the secretion of TSH from the pituitary and this results in the production of THs. TRH and TSH are regulated via a negative-feedback loop through THs. THs, thyroid hormones; TRH, thyrotropin-releasing hormone; TSH, thyroid-stimulating hormone.

1.1.2. Biosynthesis of thyroid hormones

The thyroid gland consists of two lobes shaping a butterfly and is located in the base of the neck. It produces the prohormone 3,3',5,5'-tetraiodothyronine (T4, thyroxine) and the active form 3,3',5-triiodothyronine (T3, triiodothyronine). Microscopically, the thyroid gland consists of thyroid follicles in which the follicular cells (thyrocytes) enclose the follicle colloid (lumen). After TH synthesis in the lumen, several proteolytic steps via endopeptidases occur and the liberated T4 and to a lesser amount T3 are transported across the cell membrane into the blood. This transport is facilitated by TH specific transporters (e.g. monocarboxylate transporter 8 (MCT8))(6). In the blood, the majority of T4 and T3 is bound to carrier proteins such as thyroxine-binding globulin, albumin, and thyroid binding prealbumin resulting in only 0.03% of free T4 and 0.3% of free T3

(summarized in (5)). Mainly the prohormone T4 is secreted as it has a half-life of seven days in human compared to the much shorter half-life of one day of T3 (7, 8). In mice, the half-life is much shorter with eight hours of T4 and two hours of T3 (9). Once the THs reach their destined tissue TH transporters are required for their uptake, which will be further discussed (Chapter 1.6. Thyroid hormone transporter).

1.1.3. Metabolism and action of thyroid hormones

As the THs play such an important role, their concentration has to be regulated and adjusted on numerous levels. The first level is covered by the regulation of the synthesis as described above. Another regulatory mechanism to ensure sufficient T3 concentration occurs via conversion of T4 to T3 directly in the target tissue, where it is needed (reviewed in (10, 11)). This conversion and other metabolic reactions are catalyzed by a family of selenoenzymes, the iodothyronine deiodinase type 1-3 (DIO 1-3), with each deiodinase favoring an inner or outer ring-deiodination (12). Depending on the tissue and the developmental stage, two types of deiodinases can catalyze the same reaction. The conversion from T4 to T3 is catalyzed by outer-ring deiodination (ORD) by DIO1 and DIO2, whereas the inner-ring deiodination (IRD) catalyzed by DIO1 or DIO3 results in the conversion of T4 into reverse T3. T3 can be inactivated by IRD through DIO1 and DIO3 to produce 3,3'-diiodothyronine (3,3'-T2). Furthermore, reverse T3 can be further inactivated to 3,3'-T2 via ORD by DIO1 and DIO2 (reviewed in (13, 14)). Additional metabolites of T3 and reverse T3 are 3,5-T2 and 3',5',-T2, respectively (reviewed in (15)). *Dio1* is mainly expressed in the liver, kidney, and thyroid gland in human and rodents (reviewed in (16, 17)), whereas *Dio2* is predominantly expressed in the brain, pituitary, brown adipose tissue, and skeletal muscle (reviewed in (9)). The activity of DIO3 is higher during late developmental and early postnatal stages with high expression levels in embryonal tissues because as the main inactivating enzyme it ensures the optimal TH supply to the fetus during pregnancy (18). Additionally, to the deiodination route, alternate pathways of TH metabolism have been described. These pathways include conjugation (sulfation, sulfonation, and glucuronidation of the phenolic hydroxyl group), ether cleavage, and oxidative deamination of the alanine side-chain resulting in the formation of the corresponding iodothyroacetic acids (the most studied forms are 3,3',5,5'-tetraiodothyroacetic acid (TA4, Tetrac) and 3,3',5-triiodothyroacetic acid (TA3, Triac)) (reviewed in (19)). It has been shown, that TA3 formation occurs by oxidative deamination via thyronamine intermediates; however, the exact enzymes performing these reactions remain to be identified (20).

THs exert their main function through regulating gene expression of responsive genes. This occurs through the binding of T3 to nuclear TH receptors (TR). The first TRs were cloned in 1986 and derive in humans from two genes, *THRA* and *THRB*, located on different chromosomes namely 17 and 3, respectively (in mice *Thra* is located on chromosome eleven and *Thrb* on chromosome 14) (reviewed in (21-23)). From these two isoforms several splicing forms have

been described, but only three of them have been proven to bind T3: TRα1, TRβ1, and TRβ2. These TRs show a high tissue specificity with TRβ1 mainly expressed in liver, kidney, and brain, the TRβ2 is the main TR involved in the HPT axis, and TRα1 is predominantly expressed in the brain, heart, muscle, and bone (reviewed in (24-26)). Nevertheless, co-expression of some of the isoforms have been reported as well, for example in brown adipose tissue. Here, the TRα and TRβ isoforms play different roles but both isoforms are required for an adequate adaptive thermogenesis response (reviewed in (26)), which will be described (Chapter 1.4.1 Brown adipose tissue).

The TRs regulate transcription through a bimodal switch model, which is illustrated in **Figure 2**. The unliganded TRs bind to TH-response elements, which are regulatory sequences in the deoxyribonucleic acid (DNA). Preferentially, the TRs bind as heterodimers with the retinoid X receptor but it is also able to bind as monomers or homodimers. This unliganded binding results in the repression of transcription, which is mediated by recruitment of transcriptional nuclear co-repressors and histone deacetylases (27, 28). The binding of T3 induces a conformational change of TR, causing the release of co-repressors and the recruitment of nuclear co-activators along with histone acetyl transferases, thereby leading to gene activation (29, 30). Besides this genomic (canonical) action of THs, also non-genomic actions (non-canonical) have been described which are based on fast, transcriptional-independent actions but the underlying mechanisms are not fully understood yet (reviewed in (31)).

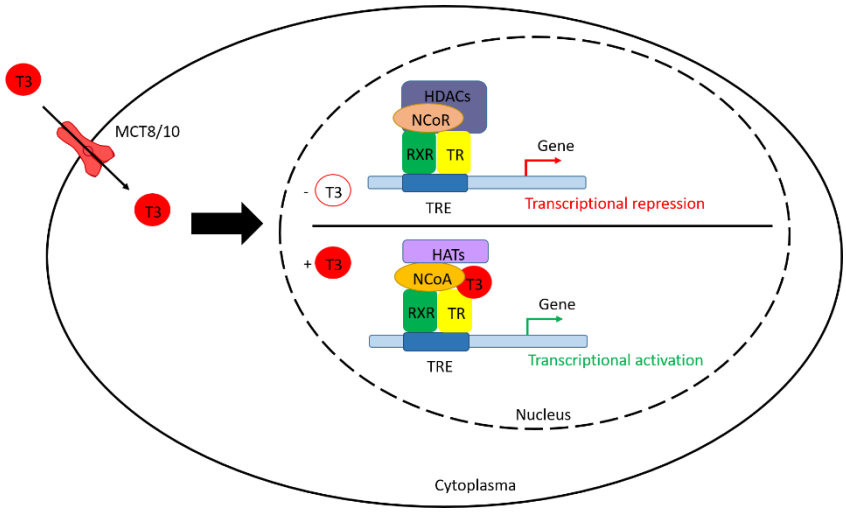

Figure 2: Simplified illustrated transcriptional regulation by TH (Modified from (32, 33)).
The unliganded TR can bind to the TRE preferentially as heterodimer with RXR. This unliganded binding results in the repression of transcription which is performed by the presence of NCoR and HDACs. When T3 enters the cell via specific transporters e.g. MCT8/10, it binds to the TR in the nucleus resulting in a conformational change. This causes the release of the co-repressor and the recruitment of NCoA along with HATs and ultimately resulting in transcriptional activation.
HATs, acetyl transferases; HDACs, histone deacetylases; MCT8/10, monocarboxylate transporter 8/10; NCoA, nuclear co-activators; NCoR, nuclear co-repressors; RXR, retinoid X receptor; TR, thyroid hormone receptor; TRE, thyroid hormone-response element.

1.2. Clinical symptoms of hypo- and hyperthyroidism

As mentioned above the regulation and production of THs involve several interfaces, which rely on each other. This multilayered coordinated regulatory system is essential to ensure the optimal environment for each individual tissue; however, it also makes it vulnerable on numerous levels. Hypothyroidism (a reduction in THs) and hyperthyroidism (an excess in THs) belong to the most common endocrine disorders worldwide, with the first reported endocrine deficiency disorder in 1850 (34). Hypothyroidism can have several causes and is distinguished between primary (diseases in the thyroid gland) and secondary (diseases in the hypothalamus or pituitary) hypothyroidism. The most common cause of primary hypothyroidism in developed countries is an autoimmune disease called Hashimoto's disease, where antibodies either against an enzyme in the thyroid (thyroid peroxidase) or thyroglobulin are produced by the immune system (reviewed in (35)). However, worldwide the most common cause is iodine deficiency (3). Subclinical (mild) hypothyroidism is characterized by increased TSH concentration and normal serum TH concentrations (36), whereas overt hypothyroidism is diagnosed with elevated TSH concentration in the presence of low free T4 concentrations (37). Patients with subclinical hypothyroidism have either minor or no symptoms at all, whereas patients with overt hypothyroidism show a wide range of symptoms as THs influence numerous tissues. These symptoms include among others bradycardia (reviewed in (5, 38)), weight gain with increased cholesterol levels (reviewed in (5, 39, 40)) and cold intolerance (reviewed in (41)). These symptoms can be mostly reversed by hormone substitution (either by T4 alone or a combination of T3 and T4), which differs from the consequences of reduced TH availability during development (Chapter 1.7. Thyroid hormone transporter deficiency in human and animal models). In contrast to hypothyroidism, hyperthyroidism results from an inappropriately elevated TH synthesis and secretion and is a form of thyrotoxicosis (a clinical state due to excess of THs independent of the origin of THs) (42, 43)). The most common form of hyperthyroidism is the Grave's disease, also a form of autoimmune disease, in which agonistic antibodies bind to TSH receptors resulting in ongoing TSH stimulation and in overproduction of THs (44). Hyperthyroidism is differentiated as well into a subclinical and an overt form with low or undetectable serum TSH concentration with normal free T3 and T4 concentrations and undetectable serum TSH concentration with elevated serum free T3 and T4 concentrations, respectively (reviewed in (42)). Patients with hyperthyroidism show opposite symptoms to hypothyroidism, including tachycardia (reviewed in (5, 38)), weight loss with reduced cholesterol levels (reviewed in (5, 39, 45)), and heat intolerance (reviewed in (41)). Depending on the individual situation, hyperthyroidism is treated with a thyreostatic drug (e.g. inhibition of hormone synthesis, iodide uptake or TH secretion, and radioactive iodine therapy). How THs lead to the above mentioned symptoms, especially regarding thermogenesis and cardiovascular function, will be more discussed in the following chapters.

1.3. Cardiovascular system

The cardiovascular system, also known as the circulatory system, consists of the heart, blood, and blood vessels. This one-way and highly carefully orchestrated system acts in synchrony with the pulmonary system. Therefore, it is not only involved in the transport of the hormones produced by the endocrine system but also essential for oxygen and nutrient supply. The functionality of these systems relies on the heart's ability to operate properly. The heart is a strong muscle that consists of four chambers (right atrium, right ventricle, left atrium, and left ventricle). The blood flow is unidirectional, starting with the blood entrance to the right atrium, which is then pumped down to the right ventricle. Afterwards, the blood enters the pulmonary circulation resulting in the return of the oxygen-rich blood to the heart into the left atrium. The blood is then pushed down into the left ventricle and enters the systemic circulation via the aorta. The right atrium not only presents the point of entry, but also harbors the sinoatrial (SA) node myocytes, which fire off electrical impulses to stimulate contraction and initiating a heartbeat; therefore, they are also called cardiac pacemaker cells. The SA node was first discovered in 1907 and has since then sparked the interest of many research topics (46). The depolarization of the SA node influences intracellular calcium (Ca^{2+}) levels, which triggers an action potential and results in muscle contraction. The Ca^{2+} molecule is a regulator of the interactions between the myosin head and the actin filament, thereby generating force and ultimately resulting in contraction (47). There are three cardiac myosin heavy chain genes, *MYH6*, *MYH7* and *MYH7B*, resulting in alpha myosin heavy chain (α-MHC), β-MHC and myosin-7B, respectively. The *Myh6* is predominantly expressed in the atrial region, whereas *Myh7* is mainly expressed in the ventricle. However, in the rodent adult heart *Myh6* is the dominant gene expressed in both the atrial and ventricular chamber (48). The primary underlying mechanisms controlling the rate of SA node depolarization, resulting in Ca^{2+} level changes is still under debate (see (49)). For a long time, the main player in heart beat initiation was thought to be an ion current (also called funny current, I_f) mediated by hyperpolarization-activated cyclic nucleotide-gated (HCN) channels (50, 51). The HCN channels consist of three members (HCN1, HCN2, and HCN4), where HCN4 covers 70-80% of SA node I_f (52). This current is a mixed inward Na^+ and K^+ current, that can be activated by cyclic adenosine monophosphate (cAMP), and has been handled as "the pacemaker current" (reviewed in (53)). Studies suggested that I_f is responsible for processing diastolic depolarization, in which the membrane depolarizes towards the threshold for firing action potential by activating voltage-gated Ca^{2+} channels. The following repolarization is covered by a variety of voltage-dependent K^+ channels (transient outward, fast delayed rectifier, and slow delayed rectifier K^+ currents) so that the whole process can start again. Recently, a complementary hypothesis has been presented in which the electrical events causing the heart beat are based on a "coupled clock system" (54). In this scenario, the HCN channels are part of a network named the "membrane clock" as the events are occurring at the cell membrane. The other part is called the "Ca^{2+} clock" and includes

the intracellular Ca^{2+} release from a major intracellular store, the sarcoendoplasmic reticulum (SR). First, the cytosolic Ca^{2+} concentration increases gradually through spontaneous local Ca^{2+} releases from the SR. Then, almost at the end of the diastole the whole cell Ca^{2+} transient increases through a Ca^{2+} release from SR-based Ca^{2+} release channels, the ryanodine receptors (RYRs), which is also known as a "Ca^{2+} spark" (55). The Ca^{2+} ions diffuse out and are then able to interact with the contractile machinery (myosin and actin complexes), which promotes cell shortening and results in generating the force to pump blood. At the end of the action potential, the cytoplasmic Ca^{2+} is transported back to the SR mainly via the SR Ca^{2+} adenosine triphosphatase (SERCA) and to a lesser account by the sarcolemmal sodium-calcium exchanger (NCX), so that the cells return to resting diastolic levels (56). The former one is regulated by the transmembrane phosphoprotein, phospholamban (PLN). When PLN is phosphorylated the interaction with SERCA is prevented, which results in an increased activity of the pump promoting Ca^{2+} uptake back to the SR (57, 58). NCX is activated by the exposure to intracellular Ca^{2+} but the activity can also be regulated by posttranslational modifications (59). A simplified overview of cellular actions in a cardiomyocyte is illustrated in **Figure 3**. In humans, one complete cardiac cycle lasts for ~0.8 seconds, whereas a mouse completes a cardiac cycle in 0.09 seconds. The sole spontaneous depolarization rate of SA myocytes is also known as intrinsic heart rate. Additional to the described heart's intrinsic ability to regulate its electrical activity, the autonomic nervous system can also directly influence the electrical impulses throughout the heart, which will be described be in the following chapter.

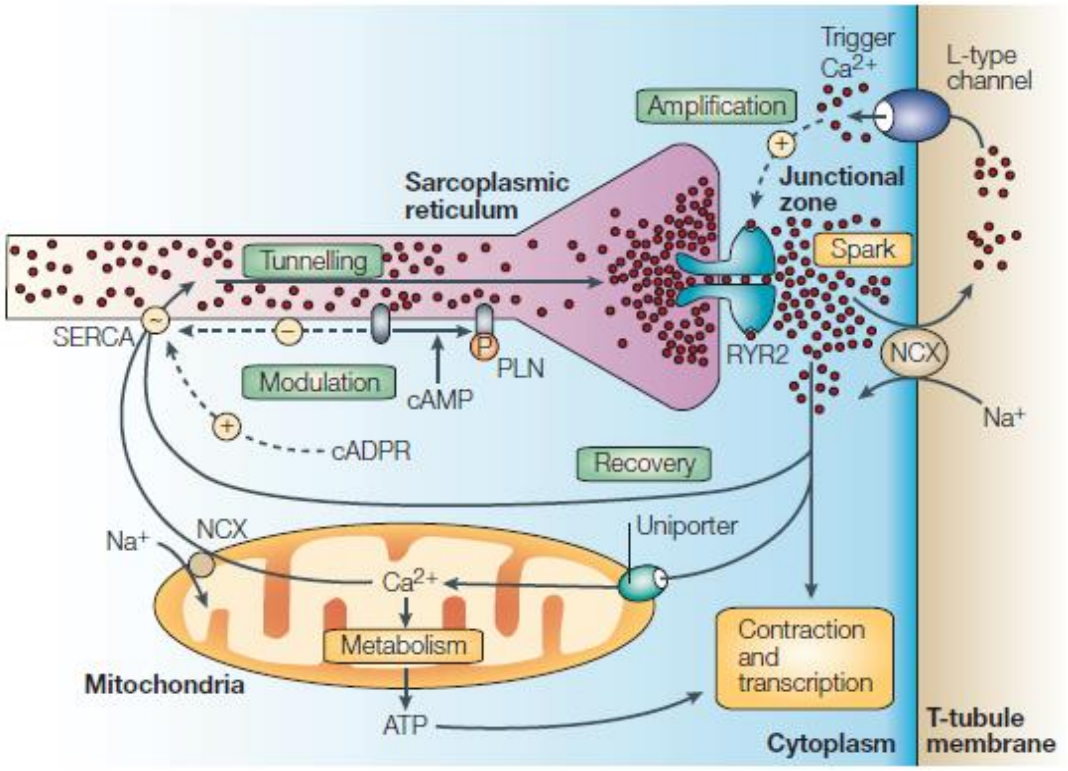

Figure 3: Calcium actions in the cardiac myocyte (60).
The calcium signaling consists of several direct (solid arrows) and indirect (dashed arrows) actions: amplification, recovery, modulation, and tunneling. First upon depolarization, the L-type channel opens up to allow the entry of Ca^{2+} (red circles) into the cytoplasm leading to an initial small Ca^{2+} 'sparklet'. Once inside Ca^{2+} stimulates RYR2, which results in a strong Ca^{2+} release from the SR. This spark is

formed through amplification of the first initial sparklet. As a next step Ca^{2+} binds to myosin resulting in the interaction of myosin and actin, and ultimately induces contraction. This is followed by the recovery phase, in which Ca^{2+} is pumped out of the cell via the NCX, into the SR via SERCA and also a small proportion is pumped into the mitochondria for ATP production. Within the SR, the Ca^{2+} is channeled back to the junctional zone in a process called tunneling. Several modulations are possible including by cAMP, which is involved in the reversible phosphorylation of PLN and RYR2 and also by cyclic ADPR, which enhances the Ca^{2+} uptake back to the SR.
ADP, adenosine diphosphate; ATP, adenosine triphosphate; Ca^{2+}, calcium; cADPR, cyclic ADP ribose; cAMP, cyclic AMP; NCX, Na^{+}/Ca^{2+} exchanger; P, phosphorylation; PLN, phospholamban; RYR2, ryanodine receptor 2; SERCA, sarcoendoplasmic reticulum Ca^{2+} adenosine triphosphatase; SR, sarcoendoplasmic reticulum.

1.3.1. Autonomic nervous system

The autonomic nervous system regulates the body's unconscious actions and is subdivided into the SNS and the PSNS, which arise from different origins; however, the central coordination takes place at supraspinal levels, namely hypothalamic as well as extra-hypothalamic nuclei. The cardiac parasympathetic nervous control arises from vagal nuclei in the brainstem and consists of numerous nerves from the spinal cord reaching different target organs. The cranial nerve X or also known as vagus nerve is responsible for transmitting the signal to the heart. At the parasympathetic nerve terminals the neurotransmitter acetylcholine is released, which binds to muscarinic receptors. Activation of these receptors leads to several downstream effects resulting in an overall decrease of heart rate, force of atrial contraction, rate of relaxation, and conduction rate of the SA and atrioventricular nodes. On the other hand, the SNS operates through a series of inter-connected neurons, which arise from the spinal cord and are also called presynaptic neurons. These neurons release acetylcholine at the synapses, which binds and activates nicotinic receptors on the peripheral sympathetic neurons (postsynaptic neurons). In response to this stimulus, these neurons release noradrenaline (norepinephrine, NE), binding and activating the alpha adrenergic receptors (α-ARs) as well as the beta ARs (β-ARs), which are essential for cardiovascular modulation (61). The three known β-ARs are expressed in cardiac myocytes and have been shown to play a role *in vivo* (reviewed in (62, 63)). The activation of the SNS results, contrary to the PSNS, in increases in heart rate, force of contraction, rate of relaxation, and conduction rate of the SA and atrioventricular nodes. Even though actions of the PSNS and the SNS are opposite to each other, they still work reciprocally. In humans the parasympathetic tone is predominant, whereas in mice it was generally accepted that under resting conditions the cardiac sympathetic tone is predominant over the vagal tone (reviewed in (64)). However, recent studies suggested that the cardiac vagal tone dominates the autonomic control of resting heart rate when housing conditions are taken into account (65), which would be more comparable to a human-like physiological state and therefore, serve as a better model for translational research.

1.4. Thermogenesis

During evolution the acquisition of endothermy, the dissipation of energy by producing heat endogenously, also termed thermogenesis, occurred, which is one of the most important events. This ability enabled mammals to maintain their body temperatures of 30 – 37 degree Celsius (°C) even at ambient temperatures below thermoneutrality allowing the exploration of new environments and adapting to different niches (66). There are two different forms of thermogenesis, the obligatory and facultative (adaptive) thermogenesis. The former one is defined as the heat produced from all metabolic reactions necessary to maintain vital organ function (67). For a narrow range of ambient temperatures, namely the thermoneutral zone, this energy is sufficient to maintain body temperature without any other thermoregulatory mechanisms. For most of wildtype (WT) mouse species the thermoneutral zone is around 30°C (68). However, when the ambient temperature drops below the thermoneutral zone additional heat-conservation mechanisms are required to maintain body temperature. This includes taking a curled posture to minimize the surface area to avoid heat loss, as well as vasoconstriction and skin cooling (reviewed in (67, 69)). As these mechanisms have limitations, facultative thermogenesis is also induced. This form of thermogenesis is divided into shivering and non-shivering thermogenesis (NST), each coming with unique characteristics and the interaction is carefully orchestrated. The former one involves involuntary muscle contractions resulting in the hydrolysis of adenosine triphosphate (ATP), thereby releasing energy instead of mechanical work. However, this form of thermogenesis requires large amounts of energy and is therefore not suitable for long lasting cold periods and severe cold (reviewed in (67)). Therefore, the NST comes into play, which relies on biochemical and not on contractile processes (reviewed in (70)). The main site of NST in mammals is the brown adipose tissue (reviewed in (71)); however, first evidence that the muscle could act as an additional NST site has recently been presented (72). Furthermore, it has been suggested that browning of white adipocytes resulting in brown-in white (brite) adipocytes also contributes to thermogenesis but this is still under debate (reviewed in (73-75)). In the following chapter, the NST in brown adipose tissue will be explained more in detail as THs play an essential role in its activation.

1.4.1. Brown adipose tissue

The brown adipose tissue (BAT) has been first identified in the marmot (76) and then the identification in mammals and human newborns followed. In rodents, BAT is predominantly localized in the shoulder-neck region and the interscapular BAT (iBAT) has been mostly used for rodent studies. Revolutionary, in 2007 Nedergaard et al summarized several human studies, which used the glucose uptake (2-[^{18}F]-fluoro-2-desoxy-glucose) in tissues in combination with positron emission tomography settings to search for tumors and speculated on the presence of BAT in human adults mainly in the neck and supraclavicular area (77). These observations have been confirmed by the discovery of BAT in human adults in 2009 by three publications simultaneously (78-80). Since then, research has focused on BAT as a possible target to fight obesity based on its unique characteristics, which will be described more in detail below.

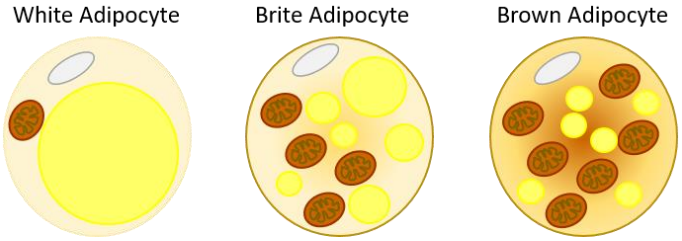

Figure 4: Different types of adipocytes (Modified from (81)).
Left: white adipocyte with one lipid droplet and low density of mitochondria; middle: brite adipocyte as an intermediate phenotype between white and brown adipocytes; right: brown adipocyte with multilocular lipid droplets and high density of mitochondria.

In general, BAT is one of the three types of fat that have been described (**Figure 4**). The other main adipose tissue depot is the white adipose tissue (WAT), which plays a central role in energy homeostasis as it functions as energy storage. Histologically white adipocytes are characterized by one main lipid droplet, where triglycerides are stored, and only few mitochondria (82). In contrast to that, the brown adipocytes have multilocular lipid droplets, and high density of mitochondria, which leads to their brownish appearances (83). The third cell type is the brite adipocyte (73). These cells share some of the characteristics of brown adipocytes, such as the comparable morphology and the expression of the uncoupling protein 1 (UCP1), but the cells are localized in WAT depots (84). Furthermore, there is no consensus regarding the origin and function of these cells as several possibilities have been described (reviewed in (85)).

The BAT is highly vascularized as well as densely innervated and thus cells are tightly connected to sympathetic nerve endings (86). Mitochondria play a key role in NST because they are the sites where the heat is primarily generated. Furthermore, they express UCP1, which is a proton transporter and resides at the inner mitochondrial membrane (87). UCP1 uncouples the respiratory chain from ATP production by transporting protons from the mitochondrial intermembrane space back into the mitochondrial matrix and bypassing the ATP-synthase, which is part of the oxidative

phosphorylation complexes (OXPHOS) (**Figure 5**). These transported protons are released in the form of heat instead of ATP (88). Induction of NST occurs *in vivo* by the release of NE from the SNS to activate BAT (reviewed by (89)). As shown in **Figure 5**, NE binds to β3-ARs and initiates the Gs-protein coupled signaling cascade resulting through the activation of the adenylyl cyclase in an increase in cAMP. This increase then activates on one hand protein kinase A leading to enhanced lipolysis, the release of free fatty acids, and activation of UCP1 (90). On the other hand, cAMP increases DIO2 activity and thereby stimulates the intracellular conversion of T4 to T3 (91). By interacting with their respective receptors, T3 and cAMP synergistically induce *Ucp1* gene transcription, which eventually leads to UCP1 protein and thermogenesis. This shows that THs influence thermogenesis in a direct but also in an indirect manner, which will be more explained (Chapter 1.5.2. Thyroid hormones and thermogenesis).

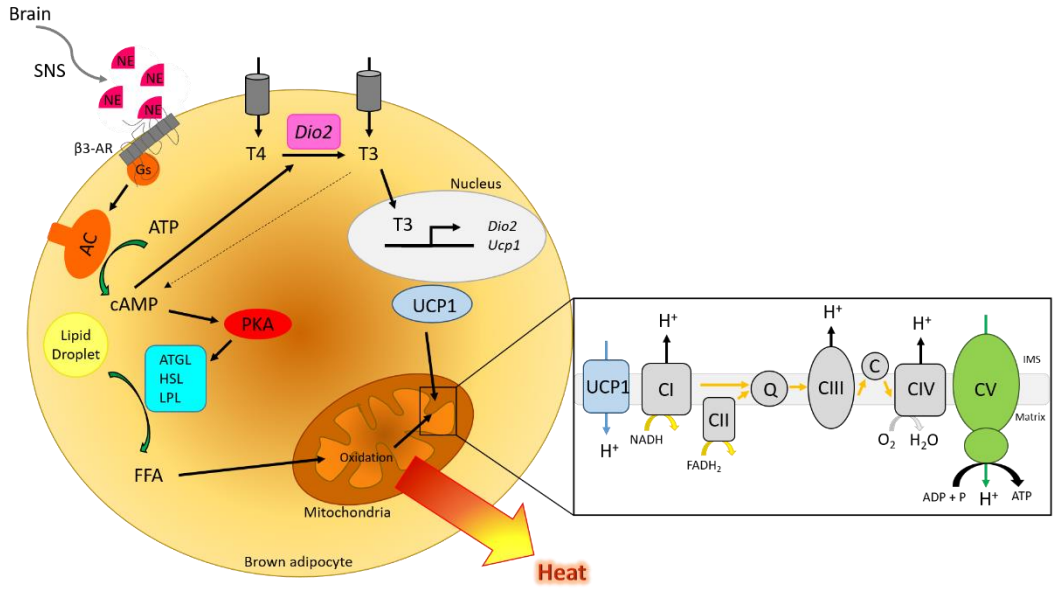

Figure 5: Schematic illustration of the function of brown adipose tissue thermogenesis (Modified from (92, 93)).
Sympathetic activation of Adrb3 through NE results in increasing concentrations of cAMP, which in turn stimulates both *Dio2*, resulting in an increased conversion of T4 to T3, and PKA, thereby activating lipolysis. These actions lead to increased OXPHOS activation and results eventually in heat production. The TH T3 induces *Dio2* and *Ucp1* gene expression, as well as cAMP production.
AC, adenylyl cyclase; ADP, adenosine diphosphate; ATGL, adipose triglyceride lipase; ATP, adenosine triphosphate; C, cytochrome C; cAMP, cyclic adenosine monophosphate; CI, Complex I, NADH, ubiquinone oxidoreductase subunit B8; CII, Complex II, succinate dehydrogenase subunit; CIII, Complex III, ubiquinol-cytochrome c reductase core protein 2; CIV, Complex IV, Cytochrome C Oxidase core subunit 1; CV, Complex V, F1-F0 ATP synthase subunit; *Dio2*, iodothyronine deiodinase type II; $FADH_2$, flavine-adenine dinucleotide; FFA, free fatty acids; Gs, subunit of the heterotrimeric G protein that stimulates cAMP-dependent pathways; HSL, hormone sensitive lipase; IMS, intermembrane space; LPL, lipoprotein lipase; NADH, nicotinamide adenine dinucleotide; NE, norepinephrine; OXPHOS, oxidative phosphorylation; PKA, protein kinase A; Q, electron transfer flavoprotein-Q oxidoreductase; SNS, sympathetic nervous system; T3, 3,3',5-triiodothyronine; T4, 3,3',5,5'-tetraiodothyronine; UCP1, uncoupling protein 1; β3-AR, adrenergic receptor beta 3.

1.5. Peripheral versus central effects of thyroid hormones

THs play important roles among others in thermoregulation (reviewed in (67)) and the cardiovascular system (reviewed in (94)). For a long time, it was accepted that THs act mainly directly on peripheral tissues through the presence of nuclear TRs. This was defined as classical or peripheral view (reviewed in (67)). But recently evidence was presented that challenged this classical view indicating that THs act centrally and thereby, regulates peripheral tissues (95, 96). The underlying concepts and details regarding the cardiovascular system and thermogenesis are presented in the following paragraphs.

1.5.1. Thyroid hormones and the cardiovascular system

The heart is one of the most responsive organs to THs and reacts therefore especially sensitive to thyroid dysfunction. As already mentioned the classical view is based on the direct interaction of THs with TRs on the level of the target tissue, which also applies for the heart. Substantially, T3 is the relevant form of THs for the heart, as the conversion of T4 to T3 does not sufficiently occur in rodent cardiac myocytes (97, 98). First, T3 is transported into the cardiac myocyte, where it enters the nucleus and binds to TRs resulting in the up- or downregulation of T3 responsive genes regulating a broad spectrum of the cardiac characteristics (97). These effects are predominantly mediated through the TRα1 isoform, as the ratio of TRα1 to TRβ messenger ribonucleic acid (mRNA) is three-to-one (99, 100). This is also evident in mice lacking TRα1 as they have a decreased heart rate (101). A simplified illustration of the effects downstream of TRα1 is depicted in **Figure 6**. More in detail, the presence of T3 leads to an upregulation of α-MHC (*MYH6*) and simultaneously to a downregulation of β-MHC (*MYH7*) leading to an increased speed of contraction (102, 103). Another crucial contribution to the contractile status is covered by changes in cytosolic Ca^{2+} levels. Here, T3 leads to the upregulation of SERCA2 and downregulation of PLN resulting in increased cycling of cytosolic Ca^{2+} levels (104). Through the regulation of these genes, T3 directly increases cardiac contractility (reviewed in (105)). Furthermore, gene expression levels of *Hcn2* are positively regulated by T3 resulting in an intrinsic positive effect on the heart rate (106). Universally, T3 has been shown to increase blood pressure and volume, stroke volume and cardiac output (reviewed in (107)). It also has a direct effect on vascular smooth muscle cells, which promotes relaxation (108). Besides these effects through receptor activity, T3 also has non-genomic actions by either influencing both plasma-ion transporters and voltage-gated potassium channels (109) or through TRs located in the cytoplasm (reviewed in (15)). Modulation of the former results in intracellular changes of Ca^{2+} and potassium, which in turn can increase contractility and heart rate (110). The latter is based on the presence of TRα in the cytoplasm, which activates downstream signaling pathways regarding the cell cycle and

thereby, playing a role in ventricular hypertrophy (111). In addition to these genomic and non-genomic actions of T3 on cardiac myocytes, recently our group presented evidence of a central contribution of THs in modulating blood pressure and heart rate (96). The effects are mediated through a novel population of parvalbuminergic neurons in the anterior hypothalamic area. These neurons rely on functional TR signaling for correct development (112). Furthermore, stereotaxic ablation of these neurons resulted in hypertension and temperature-dependent tachycardia (96). These experiments show that the autonomic nervous system responds to THs and thereby, influences cardiovascular properties.

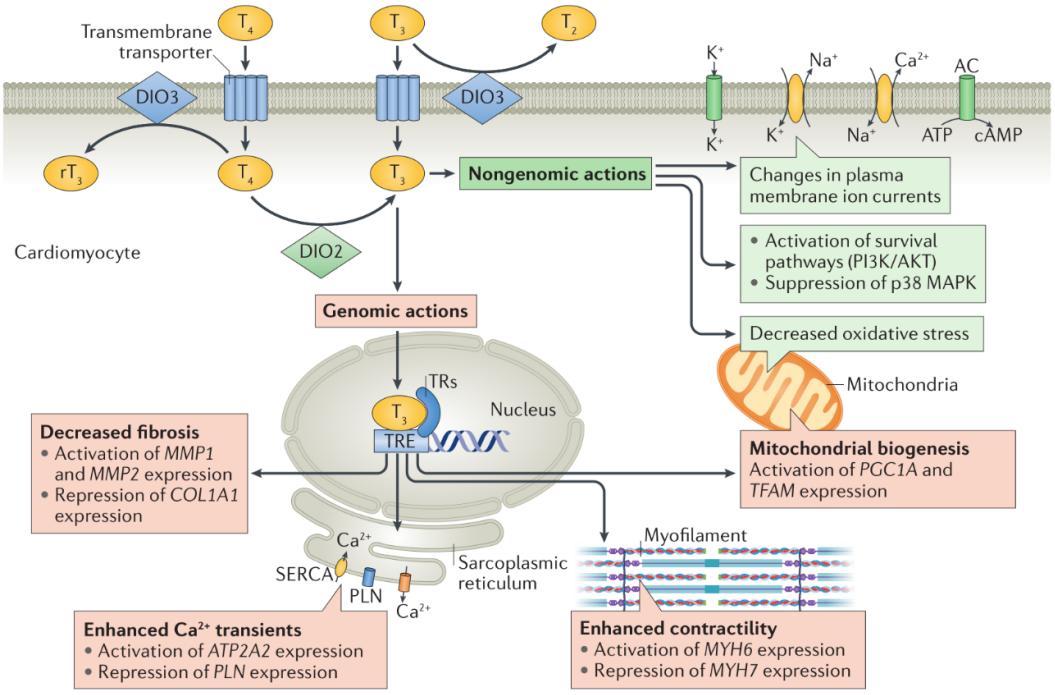

Figure 6: Overview of genomic and non-genomic effects of THs on the human cardiomyocyte (113).
T3 is transported into the cardiomyocyte through thyroid hormone transporters and it can also be produced by the cell by conversion of T4 by DIO2. Afterwards, T3 enters the nucleus, which is known as genomic action as it results in the transcription of several target genes. The non-genomic actions include the regulation of voltage-gated K+ channels, Na^+/K^+ ATPase, and the Na^+/Ca^{2+} exchanger.
AC, adenylyl cyclase; AKT, serine/threonine-protein kinase; ATP, adenosine triphosphate; *ATP2A2*, sarcoendoplasmic reticulum calcium ATPase 2; Ca^{2+}, calcium ion; cAMP, cyclic adenosine monophosphate; *COL1A1*, Collagen, type I, alpha 1; DIO2/3, iodothyronine deiodinase type 2/3; K^+, potassium ion; MAPK, mitogen-activated protein kinase; *MMP1/2*, matrix metallopeptidase 1/2; *MYH6*, myosin, heavy polypeptide 6, cardiac muscle, alpha; *MYH7*, myosin, heavy polypeptide 7, cardiac muscle, beta; Na^+, sodium ion; *PGC1A*, peroxisome proliferator-activated receptor gamma coactivator 1-alpha; PI3K, phosphatidylinositol 3-kinase; *PLN*, phospholamban; rT3, reverse T3; T2 , diiodothyronine; T3, triiodothyronine; T4, thyroxine; *TFAM*, mitochondrial transcriptional factor A; TR, thyroid hormone receptor; TRE, thyroid hormone-response element.

1.5.2. Thyroid hormones and thermogenesis

Regarding thermogenesis, the classical view is based on direct activation through TRs in the thermogenic tissues. This is supported by the presence of a large number of nuclear α1 and β1 TRs in mature brown adipocytes (114). The two receptor types play differential roles in which TRα1 is required for normal adrenergic responsiveness (101) and the TRβ1 isoform mediates the T3-induced *Ucp1* gene expression (115). The activation of BAT by the SNS is actually an indirect central action, which raises the question whether THs have a direct effect on the brain and thereby directly modulating BAT function. This sparked the interest and in the last few years' research focused on the central role of THs. The first evidence that TRα1 signaling might be implicated in the BAT activation through the CNS was found in TRα1 mutant mice, which showed high BAT thermogenesis (116). These findings were recently rediscovered when supporting evidence was presented showing a homeostatic link between the central adenosine monophosphate-activated protein kinase (AMPK) and iBAT function (117). In particular, the activation of iBAT occurred through initiation of *de novo* lipogenesis in the hypothalamus while inhibiting AMPK (95, 118). These experiments are in favor of the central view as they mimic the effects of whole-body hyperthyroidism (reviewed in (92)). Recently, our group could show that the central body temperature setpoint is modulated by THs. More in detail, in the situation of hyperthyroidism the setpoint is positively modified, which results in an increase in defended body temperature (119). These data reveal a complex interplay between the central and peripheral actions of THs. However, this is not fully understood yet because it would require a model with different TH levels in brain and periphery. Fortunately, the discovery of thyroid hormone transporters and the therewith establishment of mouse models have opened up new experimental approaches. These mouse models are deficient in thyroid hormone transporters, which results in a unique tissue-specific TH state.

1.6. Thyroid hormone transporter

As THs are lipophilic molecules, it has been assumed for a long time that the transport of THs across the plasma membrane occurs by passive diffusion. However, the first evidence published about an active energy-dependent transport of THs into cells was in 1954, but only years later several studies confirmed the saturable and energy-dependent transport of T3 and T4 into cells (reviewed in (120)). These findings sparked the interest and after several decades of intensive research, it is now proven that THs cross the cell membrane via proteins known as TH transporters (THTs). It is also undebatable, that THTs are present at the blood-brain-barrier (BBB), with the BBB being functional by embryonic day 15.5 in mice and by 18 weeks of gestation in humans and thereby, highlighting the requisite of THTs (121). Furthermore, the BBB is probably the

primary route for THs entering the CNS in adult rodents (122), whereas the blood-cerebrospinal fluid barrier (BCSFB) might be preferred during fetal and early postnatal stages (123).

The existence of THTs fueled the interest and studies in thyroid research, which even gained more importance after the discovery of inactivating mutations in the gene encoding the monocarboxylate transporter 8 (MCT8), which is responsible for the Allan-Herndon-Dudley Syndrome (AHDS) (124-126). To date, about 16 human transporters have been identified to transport THs or metabolites thereof, but the contribution of every transporter regarding tissue TH homeostasis *in vivo* has to be clarified. These THTs mainly consists of members of the MCT family (solute carrier (SLC) 16, reviewed in (127)), the organic anion transporting polypeptide (OATP) superfamily (reviewed in (128)), and the heterodimeric L-type amino acid transporter (LAT) family (reviewed in (129)).

MCT family

This family is encoded by the *SLC16* gene with 14 identified members so far, which all belong to the major facilitator superfamily (MFS) characterized by 12 transmembrane domains organized in two symmetrical bundles to allow for rotary movement (reviewed in (130)). The first ones, MCT1-4, are involved in the transport of monocarboxylate metabolites, including pyruvate, L-lactate and ketone bodies, which are involved in energy metabolism (reviewed in (131)). The only members found to be involved in TH transport are MCT8 and MCT10, encoded by *SLC16A2* and *SLC16A10*, respectively (132, 133). More in detail, the *SLC16A2* gene consists of 6 exons and 5 introns (134) and two translational starting sites (TLSs) have been identified in humans, whereas rodents have only one TLS corresponding to the downstream TLS in human *SLC16A2* (135). Furthermore, MCT10 was first described as T-type amino acid transporter 1 as it also accepts aromatic amino acids such as phenylalanine, tryptophan, and tyrosine as substrates (136, 137). MCT8 transports specifically the L-enantiomers of THs and facilitates the cellular uptake as well as efflux of THs (133). T3 is equally well transported by MCT8 and MCT10, but MCT10 is less effective with T4 as a substrate (133). Both transporters, *MCT8* and *MCT10*, are widely distributed and co-expressed in various human tissues including kidney, liver, thyroid gland, muscle, and intestines (6). Notably, *Mct10* expression levels in the murine brain are low and restricted to certain areas and subsets of cells (138, 139). In contrast to that, *Mct8* is more widely expressed in the murine brain including different neuronal populations of the cerebral and cerebellar cortex, hypothalamus, striatum, and hippocampus, but also in capillary endothelial cells, choroid plexus structures, and tanycytes (140-142). Furthermore, MCT8 protein expression was detected in all barriers relevant for TH uptake from early developmental stages into adulthood, whereas a developmental decline of MCT8 expression has been observed in neuronal cell populations (143). Regarding the human adult brain, protein expression levels of MCT8 were detected in endothelial cells of the BBB, whereas astrocytes, pericytes, and neurons did not display MCT8 expression (143). However, MCT8 protein expression could be detected in

neuronal progenitor cells of human organoids as well as in neuronal populations in fetal brain tissues (gestational week 14 – 38) (143, 144). These expression data show that MCT8 is present in all brain barriers, and especially in the BBB, underlying the importance of MCT8 in the transport of THs into the brain. However, consequential of the different tissue distribution patterns it is unlikely that the absence of one transporter can be fully compensated by the other one.

OATP superfamily

This superfamily consists of more than 300 members which are multi-specific transporters as they accept a broad range of substrates, including bile acids, steroid hormones, prostaglandins and several drugs (reviewed in (128)). Several transporters (e.g. OATP1A4 and OATP1B2 (145, 146)) promote the uptake of iodothyronines *in vitro*, but so far only the OATP 1C1 (OATP1C1) transporter has been proven to contribute to the TH transport *in vivo*. The OATP1C1 transporter also belongs to the MFS and has the highest affinity for T4 and reverse T3 as substrates (147, 148). Furthermore, OATP1C1 is the only human member of the OATP superfamily with rat and mouse orthologues (148). Therefore, it is quite intriguing that as though OATP1C1 has been described as a brain-specific transporter, it shows a species-specific expression pattern. In humans, *OATP1C1* is highly expressed in the cerebral cortex, amygdala, hippocampus, and putamen (148). Additionally, during development (from gestational week 14 to 38) the protein was found in epithelial cells of the choroid plexus, which are part of the BCSFB (144). Furthermore, only weak OATP1C1 expression has been detected in the capillary vessels of the BBB (140, 144). This is radically different in the rodent brain, where most importantly OATP1C1 is present in capillary endothelial cells of the BBB but also in astrocytes and epithelial cells of BCSFB (141, 149). Supporting these species differences, OATP1C1 has been found in the zebrafish but not in the primate brain (150, 151). This suggests, that in rodents TH transport into the brain relies on the functionality of MCT8 and OATP1C1, whereas the human CNS cannot compensate the loss of MCT8 by the presence of OATP1C1. Besides the expression of *Oatp1c1* in the rodent brain, it has also been detected in the rat placenta (152), the human and rat eye (153), and murine satellite cells of skeletal muscle (154).

LAT family

These transporters comprise a heterogeneous family of proteins that primarily transports neutral (branched chain and aromatic) amino acids (e.g. L-leucine, L-isoleucine, L-tyrosine, and L-tryptophan) across the cell membrane independently of sodium (155). Contrary to other transporters, the first two members, LAT1 and LAT2, are composed of a heavy chain (CD98) and different light chains (SLC7A5 and SLC7A8, respectively). The heavy chain is required for targeting the transporter to the cell membrane, whereas the light chains comprise the functional transporter (156, 157). Several other members of this family were additionally discovered (LAT3-5), but only LAT1 and LAT2 have been identified to transport T3 and T4 (158, 159). The

expression of *Lat1* and *Lat2* in humans and rodents have been described for several tissues, including the brain, placenta, kidney, intestine, ovary, testis, and more (155, 160, 161). Despite the TH transport *in vitro*, the *in vivo* contribution of LAT1 and LAT2 needs to be clarified.

1.7. Thyroid hormone transporter deficiency in human and animal models

In 2004, the first patients with intellectual disability and abnormal serum TH concentrations were reported, which were associated to mutations in the *SLC16A2* gene, encoding the MCT8 transporter (124, 125). Afterwards, it was realized that the described neurological phenotype of MCT8 deficiency is similar to patients described by Allan, Herndon, and Dudley in 1944 (162) and thereby, named the Allan-Herndon-Dudley syndrome (126). The *SLC16A2* gene is located on the human chromosome Xq13.2 and to date at least 132 families with 320 affected individuals with a broad spectrum of different mutations have been reported (Orphanet, Allan-Herndon-Dudley syndrome, OMIM 300523; reviewed in (163, 164)). Based on the location and characteristics of the mutation, the effects range from large deletions, frameshift deletions, single amino acid deletions or insertions to single amino acid substitution. Depending on the degree of damage, the pathogenic mechanisms of MCT8 mutations have been subdivided into three categories: first, the transporter kinetics are limited but no changes in expression levels; second, interference with protein stability and last, the most severe form with full inactivation of MCT8 (reviewed in (164)). Therefore, the clinical phenotype is quite divers in addition to unspecific signs and symptoms, making it even more challenging for diagnosis. In general, the clinical phenotype consists of two main characteristics: first, the neurological phenotype with severe intellectual disability and second, the abnormal serum TH fingerprint (high plasma T3, low total T4 and free T4, normal – mildly elevated TSH levels) leading to thyrotoxicosis in peripheral tissues (124, 125). The neurological phenotype develops due to insufficient TH supply during critical developmental periods; however, it remains unknown at which exact stage brain development is interrupted as newborns show no obvious abnormalities. During the first year of life, affected children show signs of developmental delay and feeding problems. Furthermore, patients have psychomotor symptoms including congenital hypotonia and muscle hypoplasia, which progress to spasticity and dystonia (124, 125, 165). As a result, most patients have a poor head control, are unable to walk, and become wheelchair-bound. One common key hallmark is the intellectual impairment with an IQ <20-34 accompanied by rudimentary communication skills and absence of speech development. Other clinical characteristics include dysmorphic features (elongated face, abnormal anatomy of the ears, synophrys, and prominence of lower lip (**Figure 7**)), loss of body weight and muscle mass, increased perspiration and presence of seizures (124-126, 162, 165).

Figure 7: Appearance of four affected males from four generations of one family (126).
(A) 1-year old boy (generation IV) with normal face.
(B) 14-years old male (generation III) with an elongated and myopathic face.
(C) 28-years old male (generation III) with synophrys and prominence of lower lip.
(D) 39-years old male (generation II) with an elongated face and open mouth.

Brain magnetic resonance imaging revealed delayed myelination as another significant characteristic of AHDS patients (166). Extensive studying with profiling tissue THTs and investigating animal models, helped to unravel the functions of MCT8 in tissue TH homeostasis. It has become clear, that MCT8 is present in neurons of the paraventricular nucleus and therefore, plays a pivotal role in the controlling of the negative feedback-loop of the HPT axis by transporting T3 (141). As MCT8 is the most significant THT at the BBB in humans, its absence resulted in an almost completely diminished T3 transport into the brain, leading ultimately in a pronounced TH-deficient state (124, 125). Contrary, the high serum T3 levels result in tissue-specific thyrotoxicosis for tissues that do not solely rely on MCT8 as THT. This includes the liver (increased *Dio1* expression levels and reduced serum cholesterol concentrations (167) as well as the kidneys (increased TH content and elevation of *Dio1* expression levels (168, 169). Furthermore, the skeletal muscle is affected by the high serum T3 levels (increased muscle T3 content, and changes in T3-regulated gene expression levels of MHCs (154, 170)). These insights were mainly gained from the generated *Mct8* knockout (ko) mice. More in detail, these mice replicated the abnormal serum TH status seen in the AHDS patients, but surprisingly they did not develop the severe neurological features (142, 167, 171). Detailed investigation of TH transport with radioactive labelled T3 and T4 of the *Mct8* ko mice revealed strongly diminished uptake of T3 into the brain, whereas the uptake of T4 was unaffected. Furthermore, DIO2, which is negatively regulated by T3, and DIO3, which is positively regulated by T3, were up- and

downregulated, respectively (171). These changes most likely present a compensatory mechanism and as a consequence the brain T4 and T3 content were only mildly reduced (171). Furthermore, *Mct8* is highly expressed in the follicular cells of the thyroid gland and it had been speculated, that the TH production may be constantly stimulated due to the high serum T3 levels. Indeed, *Mct8* ko mice presented an enlarged thyroid gland with larger follicles and an enhanced efflux of T3 upon pharmacological TSH stimulation. The disrupted T4 efflux may lead to a partial retention in the thyrocytes, increasing the T4 to T3 turnover and thereby eventually contributing to the abnormal serum TH profile (172-174). Additionally, the higher hepatic T3 content stimulates *Dio1* enzymatic activity resulting in an increased turnover of T4 to T3 leading to hepatic thyrotoxicosis (167). However, liver-specific inactivation of *Dio1* in combination with *Mct8* ko could not rescue the abnormal serum TH profile (175). Nevertheless, as the *Mct8* ko mice do not replicate fully the clinical phenotype in humans, these discrepancies might be due to an additional THT present in mice. As the transport of T4 into the brain is not interrupted in the absence of MCT8, a transporter which preferentially accepts T4 as a substrate and is present at the BBB could compensate for the absence of MCT8. After T4 enters the brain it can be locally converted to T3 by DIO2, and indeed, DIO2 enzymatic activities are upregulated in the *Mct8* ko mice (171). A potential candidate is the OATP1C1, which is present in vascular endothelial cells of the BBB in the rodent CNS in contrast to the human situation, where OATP1C1 is not present at the BBB (140, 149, 176). In order to test OATP1C1 as potential candidate, single *Oatp1c1* ko mice were generated, which presented unchanged serum TH profile but significantly decreased T4 content in the brain (176). Subsequently, mice with combined inactivation of *Mct8* and *Oatp1c1* were generated (*Mct8*/*Oatp1c1* double knockout (*M/O* dko)). Faithfully, these mice exhibited the same serum TH changes as the *Mct8* ko mice, including elevated T3, reduced T4 level and even more reduced TSH levels (168). More remarkably, T4 transport into the brain was almost completely abolished in the *M/O* dko mice, which lead to strongly reduced T3 and T4 content in the brain (168). Histological investigation of the CNS revealed similarities between the *M/O* dko mice and the AHDS patients, including delayed cerebellar development, disrupted maturation of the GABAergic system, and sustained hypomyelination (168). Moreover, pronounced locomotor impairments, abnormal gait and reduced muscle strength have been detected in the *M/O* dko mice by using a series of motor balancing and coordination tests (168). Taken everything into account, the *M/O* dko mice represent the most suitable mouse model for human AHDS to date.

This mouse model is also relevant for testing possible therapeutic approaches as the combination of the hypothyroid brain in the presence of the hyperthyroid periphery has been proven to be difficult to overcome. Therefore, a simple TH replacement therapy is not able to ensure thyromimetic action in the brain. Based on this complexity, a therapeutic approach needs to be identified in which either THs or a TH analogue is transported into the brain independent of MCT8 but is still able to activate TR. Classical thyroid drugs have been tested and even though they were able to normalize the serum TH levels, they had no beneficial effects on neurocognitive

development (177, 178). More promising effects have been seen with the T3-analogue TA3, which is a naturally occurring TH metabolite and most importantly, its cellular uptake is MCT8-independent (179). TA3 has a short half-life of about 6 hours in humans and it is a TR agonist with a three to six fold higher binding affinity to TRβ than to TRα (180-182). Additional studies are required to further investigate the outcomes of TA3 treatment.

1.8. Aim of this project

THs enter almost all cells via THTs and exert tissue-specific actions. It was generally accepted that THs act predominantly on the peripheral tissues. Thereby, they initiate downstream actions and in case of thyroid dysfunction contribute to disease development. This route of action was defined as classical or peripheral view. During the last decades the central and peripheral effects of THs have received more attention and evidence was presented that THs also act centrally and thereby regulate peripheral tissues, namely the iBAT and the cardiovascular system (95, 96). These experiments challenged the classical view; however, they are based on direct central modulation, which bypasses regulatory check points such as the BBB.

The aim of the present study was to dissect the peripheral contributions of TH action versus its central effects under physiological conditions *in vivo* for the symptoms occurring in hyperthyroidism, with a focus on thermoregulation and cardiovascular function.

Therefore, the *M/O* dko mouse as a unique model for central hypothyroidism and peripheral hyperthyroidism as well as one mouse model with systemic hyperthyroidism was used. The present study aims to address the following research questions:

1. How does a hypothyroid brain in the presence of the hyperthyroid periphery affect the thermoregulatory and cardiovascular system?

2. Which of the thermoregulatory and cardiovascular effects can be attributed to the central or peripheral effects of THs?

3. Which side effects could possibly develop by pharmacological intervention with TA3?

2. Materials and Methods

2.1. Materials

The following tables list the kits (Table 1), drugs and reagents (Table 2), consumables (Table 3), buffer recipes (Table 4), laboratory equipment (Table 5), and software (Table 6) used for experiments.

Table 1: Kits used for experiments.

Kit	**Catalog #**	**Supplier**
cAMP ELISA	RPN 225	GE Healthcare, USA
Molecular Biology RevertAid strand cDNA Kit	K1622	Thermo Fisher Scientific, USA
RNeasy Kits: Mini, Fibrous and Lipid Tissue	74106 74704 74804	Qiagen, Germany
TGX (Tris-Glycine eXtended) Stain-Free™ FastCast™ Acrylamide Kit, 12 %	161-0185	Bio-Rad Laboratories, USA
Total T3 ELISA	DNOV053	NovaTec Immundiagnostica GmbH, Germany
Total T4 ELISA	EIA-1781	DRG Instruments GmbH, Germany

Table 2: Drugs and reagents used for experiments.

Drugs/Reagents	**Catalog #**	**Supplier**
β-Mercaptoethanol	M3148	Sigma-Aldrich, USA
3,3',5-Triiodo-L-Thyronine sodium salt (T3)	T6397	Sigma Aldrich, USA
3,3',5-Triiodothyroacetic acid (Triac, TA3)	T7650	Sigma-Aldrich, USA
Agarose Powder	2267.4	Carl Roth GmbH & CO KG, Germany
Ammonium Peroxydisulfate	9592.3	Carl Roth GmbH & CO KG, Germany
Bicinchoninic Acid solution	B-9643	Sigma-Aldrich, USA
Bovine Serum Albumin (BSA)	A7906	Sigma-Aldrich, USA

Bromophenol Blue	B0126	Sigma-Aldrich, USA
Calcium Chloride Dihydrate ($CaCl_2$ $2H_2O$)	HN04.2	Th. Geyer GmbH, Germany
Carprofen (Rimadyl®)	Vnr462986	Pfizer, USA
Chloroform (Trichloromethane)	C2432	Honeywell, Sigma-Aldrich, USA
Clarity Western ECL Substrate	1705060	Bio-Rad, USA
Collagenase, type I (Clostridium histolyticum)	LS004194	Worthington Biochemical Corporation, USA
cOmplete Ultra Tablets Mini	5892791001	Roche Diagnostics, Switzerland
Copper Sulfate Pentahydrate	7758-99-8	Merck, Germany
DEPC-treated Water	AM9906	Thermo Fisher Scientific, USA
D-Glucose	G7021	Sigma-Aldrich, USA
Diethyl Ether Rotipuran >99% pro analysi	3942.1	Carl Roth GmbH & CO KG, Germany
Disodium Hydrogen Phosphate (Na_2HPO_4)	P030.1	Th. Geyer GmbH, Germany
DMEM, high glucose, HEPES, no phenol red (Lipolysis Buffer)	21063029	Thermo Fisher Scientific, USA
dNTP Mix (10 mM)	R0191	Thermo Fisher Scientific, USA
DreamTaq Buffer	B65	Thermo Fisher Scientific, USA
DreamTaq DNA Polymerase 500 U	EP0702	Thermo Fisher Scientific, USA
Ethanol 99% (extra pure)	5054.4	Th. Geyer GmbH, Germany
Ethanol (denatured)	24194	Sigma-Aldrich, USA
Ethylenediaminetetraacetic Acid (EDTA)- Solution	A3145,0500	AppliChem, Germany
Free Glycerol Reagent	F6428	Sigma-Aldrich, USA
Glycerol 0.5 %	2006,1000	GERBU Biotechnik GmbH, Germany
Glycerol Standard Reagent 2.5 mg/mL equivalent triolein concentration	G7793	Sigma-Aldrich, USA
Glycine	G8898	Sigma-Aldrich, USA
Hydrochloric Acid	K025.1	Carl Roth GmbH & CO KG, Germany
Isoflurane	TU061220	Zoetis, USA
Isopropanol 99%	17024	Th. Geyer GmbH, Germany
Lugol Solution	L6146	Sigma-Aldrich, USA

Magnesium Chloride	KK36.2	Carl Roth GmbH & CO KG, Germany
Methanol >99%	8388.5	Carl Roth GmbH & CO KG, Germany
Milk Powder	T145.3	Carl Roth GmbH & CO KG, Germany
Molecular Biology Water (AccuGENE™)	BE51200	Lonza, Switzerland
Nonidet P40 Substitute Solution	11754599001	Sigma-Aldrich, USA
PageRuler™ Plus Prestained Protein Ladder	26619	Thermo Fisher Scientific, USA
Paraformaldehyde Powder, 95%	158127	Sigma-Aldrich, USA
PeraSafe (Powder for Transmitter Sterilization)	7712	DuPont, UK
Phenylephrine Hydrochloride	P6126	Sigma-Aldrich, USA
Phenylmethylsulfonyl Fluoride (PMSF) Solution, 0.1 M in ethanol	93482	Sigma-Aldrich, USA
Potassium Chloride (KCl)	P017.1	Carl Roth GmbH & CO KG, Germany
Potassium Dihydrogen Phosphate (KH_2PO_4)	P018.2	Carl Roth GmbH & CO KG, Germany
Proteinase K, Liquid (20mg/mL)	25530049	Thermo Fisher Scientific, USA
Restore™ PLUS Western Blot Stripping Buffer	46430	Thermo Fisher Scientific, USA
RNase ZAP™	R2020	Th. Geyer GmbH, Germany
Saline (0.9 %)		Berlin-Chemie AG, Germany
Scopolamine Methylbromide	S8502	Sigma-Aldrich, USA
Sodium Dodecylsulfate Solution 10%	A0676,1000	AppliChem, Germany
Sodium Hydrogen Carbonate	6885.2	Carl Roth GmbH & CO KG, Germany
Sodium Chloride (NaCl)	9265.2	Carl Roth GmbH & CO KG, Germany
Sodium Deoxycholate ($C_{24}H_{39}NaO_4$)	A1531.0025	AppliChem, Germany
Sodium Fluoride Solution (NaF)	919	Sigma-Aldrich, USA
Sodium Hydroxide (NaOH)	6771.3	Carl Roth GmbH & CO KG, Germany

Sodium Orthovanadate, activated (Na_3VO_4)	450243	Sigma-Aldrich, USA
Standard Diet	1324	Altromin, Germany
Standard DNA Ladder (100 bp)	MWD100	NIPPON Genetics EUROPE GmbH, Germany
Sulfuric Acid 2N	X873.1	Carl Roth GmbH & CO KG, Germany
SYBR green PCR Master Mix (+ROX) FastStart Universal	04913914001	Sigma-Aldrich, USA
SYBR™ Safe DNA Gel Stain	S33102	Thermo Fisher Scientific, USA
TBE Buffer 10x pH 8,3	106177	Th. Geyer GmbH, Germany
Tetramethylethylenediamine (TEMED)	2367.1	Carl Roth GmbH & CO KG, Germany
Timolol Maleate Salt	T6394	Sigma-Aldrich, USA
Trichloroacetic Acid	T9159	Sigma Aldrich, USA
Tris	AE15.2	Carl Roth GmbH & CO KG, Germany
Tris-EDTA (TE) Buffer	T9285	Sigma-Aldrich, USA
Tween®-20	P1379	Sigma-Aldrich, USA

Table 3: Consumables used for experiments.

Consumables	**Catalog #**	**Supplier**
96 PCR Plate half skirt flat	72.1979.102	Sarstedt AG, Germany
Absorbable suture, coated vicryl	V369	Ethicon, USA
Alcohol Pads	9160612	Braun, Germany
Bepanthen Eye Ointment		Bayer, Germany
Ceramic beads (1.4 mm, 325 g)	432-0356	VWR International, USA
Eppendorf Tubes 5.0 mL	30119401	Eppendorf, Germany
Filter tip (10 µL, 100 µL, 1000 µL)	701114210, 70760212, 70762211	Sarstedt AG, Germany
Filtropur S 0.2 (Syringe Filters 0,2µm)	831826001	Sarstedt AG, Germany
Immobilon®-P Transfer Membrane Pore Size 0.45 µm	IPVH00010	Merck Millipore, USA
Micro Tube 1.5 mL SafeSeal	72.706.400	Sarstedt AG, Germany

Micro Tube 2 mL SafeSeal	72.695.500	Sarstedt AG, Germany
Multiwell Plate 24-well	734-0949	VWR International, USA
Non-absorbable suture, Perma-Hand Silk	681H	Ethicon, USA
Surgibond	ZG2-TR10	SMI A.G., Belgium
Suture Clips Michel (7.5 mm x 1.75 mm)	22-620-007	Allgaier Instrumente GmbH, Germany
Tube 15 mL	62.554.002	Sarstedt AG, Germany
Tube 50 mL	62.559.001	Sarstedt AG, Germany
Western Blotting Filter Paper	8860	Thermo Scientific, USA

Table 4: Buffer recipes used for experiments.

Buffer	**Final concentration**	**Substance**
Genotyping Buffer	100 mM	Tris (pH 8.5)
	0.5 mM	EDTA
	0.2%	SDS
	200 mM	NaCl
Lugol Reaction Mix	30 parts	KCl (25% w/v)
	0.5 parts	Lugol Reagent
	0.2 parts	HCl (5M)
Lysis Buffer	50 mM	Tris-HCl (pH 7.4)
	150 mM	NaCl
	1% v/v	Nonidet P40
	0.25% w/v	$C_{24}H_{39}NaO_4$
	1 mM	EDTA
	1 Tablet	cOmplete Ultra Tablets Mini
	1 mM	PMSF
	1 mM	activated Na_3VO_4
	1 mM	NaF
Phosphate Buffered Saline (PBS, 10x) pH = 7.4	27 mM	KCl
	17.6 mM	KH_2PO_4
	188.8 mM	Na_2HPO_4
	1370 mM	NaCl
Resolving Gel (for 1 Gel with TGX Stain-Free™ FastCast™ Acrylamide Kit)	1 part	Resolver 1 (ready-to-use solution, Kit)
	1 part	Resolver 2 (ready-to-use solution, Kit)
	0.5 %	Ammonium Peroxydisulfate (10 %)
	0.08 %	TEMED

Running Buffer	0.25 M	Tris
	1.92 M	Glycin
	1% (w/v)	SDS
Sample Buffer (4x Lämmli Buffer)	50 % (v/v)	Glycerol
	10 % (w/v)	SDS
	312.5 mM	Tris-HCl (pH 6.8)
	1 spatula	Bromphenol Blue
	→ before use: add 1 part β-Mercaptoethanol to 4 parts buffer	
Stacking Gel (for 1 Gel with TGX Stain-Free™ FastCast™ Acrylamide Kit))	1 part	Stacker 1 (ready-to-use solution, Kit)
	1 part	Stacker 2 (ready-to-use solution, Kit)
	0.5 %	APS (10%)
	0.15 %	TEMED
TBS (tris-buffered saline, 10x, pH 7.4)	100 mM	Tris-HCl
	1.5 M	NaCl
TBS-T (TBS-Tween20, 1x)	1 part	TBS (10x)
	9 parts	distilled water
	0.1 %	Tween-20
Transfer Buffer	0.025 M	Tris
	0.192 M	Glycine
	20 %	Methanol

Table 5: Laboratory equipment used for experiments.

Device	**Supplier**
Anaesthesia Unit 410	High Precision Instruments, Univentor, Malta
Animal Clipper (GT415)	Braun, Germany
Blood Pressure Device	Model SC-100, Hatteras Instrument Incorporated, USA
Blotting chamber	Bio-Rad, USA
Cannula (0.45*25mm; Gr.18)	Sterican, Braun
Centrifuge 4°C (5430R)	Eppendorf, Germany
Centrifuge room temperature (RT; 5430)	Eppendorf, Germany
ChemiDoc™	Touch Imaging System, Bio-Rad Laboratories, USA
Eppendorf Research (R) Plus (0.5-10, 10-100, 100-1000)	Eppendorf, Germany
Gel Chamber (Horizon)	Thermo Fisher Scientific, USA

Green Line individually ventilated cage Sealsafe cage system GM500	Tecniplast, Italy
Heating Pad (Thermolux)	Witte + Sutor GmbH, Germany
Incubator Hera Cell	Thermo Fisher Scientific, USA
Infrared Camera T355	Compact-Infrared-Thermal-Imaging-Camera FLIR systems; Sweden
Microplate Spectrophotometer (Plate:Take3)	Epoch, BioTek Instruments, USA
Mini-Centrifuge (C1301P-230)	Labnet, USA
qPCR machine (QuantStudio 5, A28134)	Thermo Fisher Scientific, USA
Radio transmitters (G2-HR E-Mitter)	Respironics, USA
Receivers (ER-4000)	Energizer Respironics, USA
Rectal Thermometer Probe (BAT-12)	Physitemp Inc., USA
Roller (RSTR05)	Phoenix Instrument, Germany
Scale (Gemeinsame Tierhaltung)	Smart weigh Instrument CO., China
Scale (SE 203-LR)	VWR International, USA
SPECTROstar Nano Microplate Reader	BMG Labtech, Germany
Surgical instruments	Fine Science Tools, Canada
Syringes (Injekt-F)	Braun, Germany
Temperature control unit HB 101/2	Panlab, Harvard Apparatus, USA
Thermal cycler (PTG-200)	Bio-Rad, USA
Thermomixer compact	Eppendorf, Germany
Tissue Grinder 2 mL (D8938*), 7 mL (D9063*)	Geyer Th. GmbH, Germany
Tissue Homogenizer (Bead Mill 24)	Fisherbrand, USA
Transient hot bridge instrument	Linsei System THB, Gammadata Instruments, Sweden
Vortex PV-1	Grant Instruments, UK
Water Bath	Techtum Lab, Sweden
Western Blot Equipment	Bio-Rad, USA

Table 6: Software used for experiments.

Software	Supplier
FLIR Tools 5.3.15268.1001	FLIR Systems Termisk Systemteknik, Sweden
GraphPad Prism 5 and 7	GraphPad Software Inc, USA
ImageLab™ Software	Bio-Rad Laboratories, USA
Microsoft Office 2013	Microsoft, USA
Quantstudio Applied	Biosystems Thermo Fisher Scientific, USA
VitalView Data Acquisition System	Mini Mitter Respironics, USA

2.2. Animal husbandry and experimental set ups

For all studies, mice were kept in individual ventilated cages (IVC) on a constant 12-hour light/dark cycle with an ambient temperature of 22 ±1 °C and were continuously allowed free access to food (standard rodent diet) and water.

At the time of sacrifice, blood and tissues were collected, weighed, frozen on dry ice and stored at -80°C until further usage. The blood was immediately stored on ice for at least 30 minutes and then centrifuged twice (4°C, 1,000xg, 10 min). After each centrifugation step, the supernatant was transferred to a new tube and stored at -20°C until further usage.

All procedures were approved by the Ministerium für Energiewende, Landwirtschaft, Umwelt, Natur und Digitalisierung, Schleswig-Holstein, Germany (V243-70506/2015(63-5.15) and V241-34882/2017(87-7/17)).

2.3. Part A: Dissecting central from peripheral TH actions using *M/O* dko mice

All genotypes (*Oatp1c1*$^{floxed/floxed}$, *Mct8* ko, *Oatp1c1* ko and *Mct8/Oatp1c1* dko mice) were generated, bred, and obtained from Prof. Dr. Heike Heuer. The generation of these genotypes has been described in more detail before (168, 171, 176). In this part, the *Oatp1c1*$^{floxed/floxed}$ are hereafter referred as WT animals.

2.3.1. Genotyping

Genotypes of mice were analyzed by isolating DNA from ear snips or tail pieces at weaning and at the end of the respective studies by performing polymerase chain reaction (PCR) and DNA gel electrophoresis. For the DNA isolation, tail or ear snips were incubated overnight in 500 µL genotyping buffer and 5 µL proteinase K (100µg/ml) at 55°C and 450 rpm (covered with aluminum foil) to neutralize the charge of the nucleic acid backbone and to digest proteins, respectively. Then, the samples were centrifuged (5 min, 18000 xg, RT) and the supernatant was

transferred to a fresh tube which was filled with 500 µL isopropanol for DNA precipitation. Afterwards, the samples were centrifuged (30 min, 18000 xg, RT) to pellet the sample, then the supernatant was discarded, the pellet washed with 100 µL 80% ethanol to remove the amount of salt and centrifuged (30 min, 18000 xg, RT) again. The supernatant was discarded and the air-dried pellet was re-suspended in 100 µL 1/10 TE (in nuclease-free water) at 55°C by shaking for 30-60 min and used together with the relevant primer pairs (**Table 7**) for PCR analysis as indicated in **Table 8** and **Table 9** to exponentially amplify the desired DNA sequence. The PCR consists of four main steps: first, the denaturation of the double-stranded DNA; second, the annealing of the desired primers; third, the Taq polymerase synthesizes a new DNA strand by using the dNTPs in the mixture; and the last step includes the repetition of this cycle and cooling the reaction for termination. The PCR product was visualized on a 1% agarose gel with SYBR safe, which is a highly sensitive stain to visualize DNA and it is a less hazardous alternative to ethidium bromide. The expected band sizes are listed in **Table 10**.

Table 7: Primer sequences used for genotypes.

Genotypes	**Primer Names**	**Primer sequence 5´-3´**
Mct8	*Mct8*-com-for	TGTGAGTATATTCACTGACCGTTTG
	Mct8-WT-rev	CAATTCAATGGTCAAAGCAGGACTG
	Mct8-KO-rev	GGGCCAGCTCATTCCTCCCACTCAT
Oatp1c1	*Oatp1c1*-com-for	CACTGCCCTGTCCTGTAGGT
	Oatp1c1-WT-rev	CATCGCTTGATGAGTGGTCTTG
	Oatp1c1-KO-rev	ACCATGTGGTTGTTGGGAAT

Table 8: One PCR reaction per primer pair was performed according to the following instructions.

Substance	**Volume**
Primer 1 (*Oatp1c1*-com-for or *Mct8*-com-for)	1 µL
Primer 2 (*Oatp1c1*-WT-rev or *Mct8*-WT-rev)	1 µL
Primer 3 (*Oatp1c1*-KO-rev or *Mct8*-KO-rev)	1 µL
dNTPs	1 µL
Taq Buffer (10x)	1 µL
DreamTaq DNA Polymerase	0.5 µL
Nuclease-free water	3.5 µL
Genomic Tail/Ear DNA	1 µL
Total volume	10 µL

Table 9: PCR cycles for genotyping.

Program *Mct8*			**Program *Oatp1c1***		
Temp. (°C)	Time (min)		Temp. (°C)	Time (min)	
95	3		95	3	
95	0.45		95	0.45	
58	0.45	35x	58	0.45	35x
72	0.8		72	0.8	
72	10		72	10	
4	Forever		4	forever	

Table 10: Expected size of bands.

	Mct8	***Oatp1c1***
WT (*Oatp1c1*$^{floxed/floxed}$)		800
KO	650bp	550

2.4. Part B: Further dissection of central versus peripheral TH action by induction of systemic hyperthyroidism

WT C57/Bl6NCr mice were purchased from Charles River Laboratories GmbH (USA) and used at the ages of 3-6 months for the experiments. Systemic hyperthyroidism was induced with 3,3',5-Triiodo-L-Thyronine (T3) in drinking water containing 0.01% BSA and different doses of T3 (185 ng/mL, 150 ng/mL, 120 ng/mL) for 14 days, to reach an uptake of app. 800 ng T3. Total T3 and total T4 ELISA (Section 2.13) were performed and only animals with 1-3 µg/dL of serum total T4 were included in the analysis. Parts of the *in vivo* studies were performed with the help of Dr. Lisbeth Harder during my maternal leave.

2.5. Part C: Investigation of the safety of TA3 administration in WT mice

WT C57/Bl6NCr mice were purchased from Charles River Laboratories GmbH (USA) and used at the ages of 3-4 months for the experiments. Animals were injected with 3,3',5-triiodothyroacetic acid (TA3), which was dissolved at a concentration of 4 mg/ml in 1 M NaOH and stored at -20°C. At the time of experiment, the stock solution was diluted in saline and animals were injected intraperitoneally (i.p.) with a final concentration of 400 ng/g body weight of the TA3 (stock solution: 4 mg/mL and working solution 0.086 mg/mL). Negative control animals were injected with saline. All animals were injected daily between 10 AM – 1PM.

2.6. Radio transmitter implantation

An implantable telemetry system with transmitters and receivers was used for recording heart rate, body temperature, and activity in freely moving and conscious mice. The operational procedure was performed as previously described (96, 183): The mice were placed on a heating pad, anesthetized using 4% isoflurane and air flow of 400 mL/min in the chamber and kept at approximately 2% isoflurane at 200 mL/min flow-rate during the surgery. To control for depth of anesthesia, the toe-pinch-reflex was used and to avoid drying of the eyes, eye cream was applied. Next, i.p. injection of pain medication (5 mg/kg Carprofen in sterile 1x PBS) was given and body temperature was monitored by rectal temperature probe. The belly was shaved to avoid later inflammation of the wound. The first vertical incision in the top skin was performed from the sternum over the belly, which was then followed by a vertical incision on the white line (Linea alba) of the cavity and then the sterilized transmitter was implanted into the abdominal cavity. The lower skin was closed and sutured with absorbable suture and the electrodes were sutured below the skin to the lower left chest (positive electrode) and right shoulder (negative electrode) using non-absorbable suture, allowing to record the generated electrical potentials. The top skin was closed with non-absorbable suture and if necessary, it was additionally closed with a tissue adhesive (Surgibond®). The mice were allowed to wake up in their cage on a heated platform and on the next day they received pain medication (5 mg/kg Carprofen in sterile 1x PBS). Animals recovered for seven days prior to baseline recordings and were kept in individual cages that were placed directly on top of the respective receiver. The receiver provides an electrical field that powers the respective transmitter, which in turn observes the electrical activity and the heart rate is calculated with the assumption that every electrical pulse leads to a cardiac contraction cycle. At the end, PeraSafe powder was used as a disinfectant for the radio transmitter.

2.7. Autonomic nervous system (ANS) investigation

2.7.1. Layout of ANS investigation

After one week of recovery, the mice were weighed in the morning and then the baseline was recorded for 72 hours starting at noon. On the fourth day, mice were injected with saline (i.p., 5 µL/g body weight). On the following day, the mice were first injected with scopolamine methylbromide (i.p., 0.1 mg/kg body weight) and then 40-42 minutes later with timolol maleate salt (i.p., 1 mg/kg body weight). For animals with induced hyperthyroidism, baseline measurements were performed on day 9-12, with the saline injection on day 12 and scopolamine methylbromide and timolol maleate injections on day 13 of treatment.

2.7.2. Baseline calculations

Baseline was recorded every minute for 72 hours without any disturbances of the mice. The mean for every 30 minutes and subsequently the mean for all three days per mouse was calculated. Lastly, the values for every genotype/condition were averaged.

2.7.3. Maximum heart rate determination

Mice were injected i.p. with saline and then the highest absolute heart rate in beats per minute (bpm) achieved within 20 minutes after injection was taken. The values were averaged for each genotype/treatment group.

2.7.4. Calculation of the contribution of the PSNS and SNS

For blocking the PSNS, scopolamine methylbromide was injected at time point zero, which was followed after 40-42 min with a timolol maleate salt injection to block the SNS.

For the calculation of the contributions of the PSNS and SNS:

1. Median of the two minutes before the first injection (scopolamine methylbromide) ≈ Median baseline
2. Median of the minutes 21 after the first injection (scopolamine methylbromide) up to the second injection (timolol maleate salt) ≈ Median scopolamine
3. Median of the minutes 21 after the second injection (timolol maleate salt) up to two hours after the second injection (timolol maleate salt) ≈ Median timolol
4. ΔPSNS = Median scopolamine – Median baseline
5. ΔSNS = Median timolol – Median scopolamine

2.7.5. Calculation of heart rate distribution

The heart rate values (bpm) obtained during the baseline recordings for 72 hours (a value every minute) were plotted in GraphPad Prism. Then, for every animal the frequency distribution in a histogram were calculated according to the settings in **Table 11**. These distribution values were then analyzed with a two-way analysis of variance (ANOVA) with Holm-Sidak's multiple comparisons test.

Table 11: Settings used for calculation of frequency distribution.

Create	**Frequency distribution**
Tabulate	Relative frequencies as fraction
Bin range	100 – 800 bpm
Bin width	20 bpm
Replicates	Bin each replicate

2.8. Infrared thermography

Infrared thermography allows to detect infrared energy and converting it into an electronic signal, without any contact to the animals. This electronic signal is then processed to generate a thermal image visualizing differences in temperature fields. Therefore, it is an essential tool to investigate thermoregulation in the animals. To study body temperature, heat production and heat loss, pictures were taken from the inner ear, iBAT area and tail surface, respectively. Pictures were performed during the light phase and at RT. During monitoring, the animals were allowed to move freely on the cage grid, except for tail surface pictures at 32°C and 38°C, where the animals were placed onto a heated platform for 10 minutes before taking the pictures. For the cold exposure experiment, animals were kept at 10°C for 16 hours and then the photos were taken. During each session, three pictures of the selected area per mouse were taken and the highest maximum temperature of the desired area was chosen using the infrared analysis software FLIR Tools. Statistical analysis was performed using a two-way ANOVA with post-hoc Bonferroni test (Part A), a paired (Part B) or unpaired (Part C) Student's t test with Welch's correction. The infrared pictures of the WT, *Mct8* ko, *Oatp1c1* ko and *M/O* dko mice were performed by Dr. Lisbeth Harder and Dr. Jiesi Chen (group of Prof. Heike Heuer) in Düsseldorf, Germany. Infrared images of animals with induced hyperthyroidism were taken on days 7-9 of treatment and for animals with TA3 treatment on days 12-14 of treatment.

2.9. Blood pressure determination

A non-invasive tail-cuff system was used for blood pressure measurement recording pulse, mean arterial pressure, systolic and diastolic parameters. This system is comparable to the blood pressure measurement in humans, as the blood flow is restricted by a cuff. However, the sensor assembly contains a bright red LED, which passes through the tail and is then monitored by a sensing device (a very sensitive photodiode) to recognize variations in the light intensity. These variations occur due to changes in the blood flow with each heartbeat. Finally, this pulse is then

converted into a digital signal. As the sensor is very sensitive to movements, the mouse was restrained on a 100 F (38°C) preheated platform. The tail was inserted through the tail cuff and placed into its slot under the top half of the sensor. Finally, the tail was secured with masking tape. Before starting the measurement, the mouse was also allowed to adapt for 3 minutes. One measurement included 15 cycles and only if more than 5 cycles per mouse were successful the values were used for calculation, but the measurement was not repeated and only performed once per mouse per day. The detailed setting parameters are presented in **Table 12**. In general, 2 days of training sessions were performed, which were followed by 3 days of measurement. For the animals with TA3 treatment, there was a training session on day eleven of treatment, followed by the three days (Days 12-14) of measurement. For analysis, only diastolic values below 40 mmHg were excluded. The mean for every mouse of the three session was calculated, which was then used to calculate the mean for each genotype. Statistical analysis was performed using two-way ANOVA with post-hoc Bonferroni test (Part A) or unpaired Student's t-test with Welch's correction (Part C).

Table 12: Settings for blood pressure measurement.

Operating Mode	Platform
Preliminary Cycles	0
Measurement Cycles	15
Movement Detection	No
Min. Pulse Amplitude	5%
No. of consecutive Peaks	70
Ignore Peaks Smaller than	0.5%
Max. Pressure	242 mmHg
Pulse Time Out	30s
Measurement Time	30s
Time between Measurements	2.5 s
Systolic Threshold	20%
Diastolic Threshold	50%
Systolic criterion	Signal below threshold 90%
Systolic criterion	Time below 0.5 s
Diastolic Criterion	Signal below threshold 90%
Diastolic Criterion	Time below 0.5s
Platform Temperature	100F
Single Operation	

2.10. Thermal hot bridge analysis

Skin samples still containing fur were dissected from the interscapular area of WT, *Mct8* ko, *Oatp1c1* ko, and *M/O* dko mice and analyzed using a transient hot bridge instrument. A Kapton insulated sensor generated heat, which was transferred to the skin sample and the resulting change in temperature was used by the software to calculate heat conductivity (the ability to transfer thermal energy in form of heat), diffusivity (indication of the rate at which a temperature change migrates through the fur), and heat capacity (is defined as the amount of energy that is needed to increase 1°C per g). Statistical analysis was performed using a two-way ANOVA with post-hoc Bonferroni test (Part A).

2.11. RNA isolation, cDNA synthesis and quantitative real-time PCR (qPCR)

QPCR was used as a quantitative measurement of gene expression levels in different tissues and conditions. First, ribonucleic acid (RNA) isolation was performed on dry-ice frozen tissue using RNeasy Lipid Tissue Kit for iBAT, inguinal WAT (iWAT), and pituitary; the RNeasy Mini Kit was used for liver samples, whole heart and brain homogenate, and the RNeasy Fibrous Tissue Mini Kit for M. soleus, M. gastrocnemius, aorta, and tail artery according to the manufacturer's instructions. The RNA concentrations were determined in 2 µL sample and water as blank and measured with the BioTek Epoch spectrophotometer.

The following complementary DNA (cDNA) synthesis was performed using the Molecular Biology RevertAid strand cDNA Kit and anchored oligo (dT)18 primers. The cDNA was then finally diluted in nuclease-free water to achieve a final concentration of 1.25 – 5 ng/µl depending on the available amounts of obtained RNA from isolation. Consistent concentrations were used among the same tissues to allow comparison of Part A and B.

QPCR measurement was performed using the SYBR green PCR master mix (**Table 13**) following a two-step protocol with 40 cycles and 60°C for annealing and extension (**Table 14**). At the end, a melting curve was performed to confirm the specificity of the primers. To correct for primer efficiency standard curves were performed. This efficiency was calculated for each individual gene using the slope of the standard curve and the following equation: $E = 10^{(-1/slope)}$. All primer sequences are listed in **Table 15** and for analysis the software Quantstudio Applied Biosystems was used. Gene expression levels were normalized to the housekeeping genes. For every tissue three housekeeping genes were measured and the ones with less variety were chosen. This decision was determined using an algorithm encoded by the software NormFinder (184). The following housekeeping genes were used (brain: mean of *Cyclophilin* and hypoxanthine-guanine phosphoribosyltransferase (*Hprt*); iBAT: *Hprt*; iWAT: mean of *Cyclophilin* and *ribosomal protein, large, P0, 36B4* (*Rplp0*); heart (Part A+B): *60S ribosomal protein L32* (*Rpl32*);

heart (Part C): mean of *Cyclophilin* and *Rpl32*; liver (Part A+B): mean of *Cyclophilin* and *Hprt*; liver (Part C): mean of *Hprt* and glyceraldehyde-3-phosphate dehydrogenase (*Gapdh*);
M. gastrocnemius: mean of *Hprt* and *Gapdh*; M. soleus: mean of *Cyclophilin* and *Hprt*; pituitary: mean of *Cyclophilin* and *Hprt*; WT tissues: mean of *Cyclophilin* and *β-actin*). The same housekeeping primers were used for Part A and B to ensure comparability, but differed for Part C.

With the qPCR measurement the threshold cycle (Ct) value is determined, which is defined as the number of cycles that are required to produce a constant fluorescence signal. As the amplification of PCR products results in a sigmoidal curve, the Ct measure is taken in the exponential phase where the curve is linear. As the samples are pipetted in duplicates, first these values were averaged. Then, the difference of the target gene mean Ct value and the mean Ct value of the housekeeping genes are calculated, resulting in ΔCt (ΔCt = mean Ct $_{\text{target gene}}$ − mean Ct $_{\text{housekeeping gene}}$). As a next step, the gene expression is adjusted to the primer efficiency using this equation: gene expression $=E^{-\Delta Ct}$. To compare and visualize different genotypes/treatment conditions the single values of gene expression levels were divided by the mean of the control group to normalize the expression levels. Statistical analysis was performed using a two-way ANOVA with post-hoc Bonferroni test (Part A) or unpaired Student's t test with Welch's correction (Part B + C).

Table 13: Protocol for qPCR preparation.

Substance	**Volume (µL)**
FastStart Universal SYBR green master (+ROX)	10
Primer mix (0.5 µM of forward and reverse primer)	2
cDNA	4
Nuclease-free water	4
Total Volume	20

Table 14: Protocol for qPCR measurement.

Temperature (°C)	**Time (min)**	
50	02:00	
95	10:00	
95	00:15	x 40
60	01:00	
Melting curve		

Table 15: Primer sequences used for qPCR measurements.

Abbreviation	**Gene**	**Sequence 5 → 3 (Forward/Reverse)**
Acaca	Acetyl-Coenzyme A Carboxylase α	GTCCCCAGGGATGAACCAATA GCCATGCTCAACCAAAGTAGC
Adrb1	Adrenergic Receptor beta 1	CTCATCGTGGTGGGTAACGTG ACACACAGCACATCTACCGAA
Adrb2	Adrenergic Receptor beta 2	GGGAACGACAGCGACTTCTT GCCAGGAGCATAACCGACAT
Adrb3	Adrenergic Receptor beta 3	AGAAACGGCTCTCTGGCTTTG TGGTTATGGTCTGTAGTCTCGG
a-MHC	Myosin, heavy polypeptide 6, cardiac muscle, alpha	GCCCAGTACCTCCGAAAGTC GCCTTAACATACTCCTCCTTGTC
Atp2a2	Calcium-Transporting ATPase Sarcoplasmic Reticulum Type, Slow Twitch Skeletal Muscle Isoform	TCCGCTACCTCATCTCATCC CAGGTCTGGAGGATTGAACC
Chrm2	Cholinergic Receptor Muscarinic 2	CAAGATCCAGAATGGCAAGG GACAGACGTGGAGTCATTGG
Cidea	Cell Death-Inducing DNA Fragmentation Factor alpha Subunit-like Effector A	TGACATTCATGGGATTGCAGA GGCCAGTTGTGATGACTAAGA
Cs	Citrate Synthase	GGACAATTTTCCAACCAATCTGC TCGGTTCATTCCCTCTGCATA
Cyclophilin	Peptidylprolyl Isomerase D (Cyclophilin D)	TCACAACAGTTCCGACTCCTC ACCTCTACATTTTCAAGCGTCC
Dio1	Iodothyronine Deiodinase Type I	GCTGAAGCGGCTTGTGATATT GTTGTCAGGGGCGAATCGG
Dio2	Iodothyronine Deiodinase Type II	ATGGGACTCCTCAGCGTAGAC ACTCTCCGCGAGTGGACTT
Dio3	Iodothyronine Deiodinase Type III	CACGGCCTTCATGCTCTGG CGGTTGTCGTCTGATACGCA
Gh	Growth Hormone	GCTACAGACTCTCGGACCTC CGGAGCACAGCATTAGAAAACAG
Hcn2	Hyperpolarization Activated Cyclic Nucleotide Gated Potassium And Sodium Channel 2	TCCGCACCGGCATTGTTATT CCGGGATGGATGACACGAAG
Hcn4	Hyperpolarization Activated Cyclic Nucleotide Gated Potassium And Sodium Channel 4	ACCCGCAGAGGATCAAGATGA AATGCGAGTCTCCACTATAAGGA
Hprt	Hypoxanthine-Guanine Phosphoribosyltransferase	GCAGTACAGCCCCAAAATGG AACAAAGTCTGGCCTGTATCCAA
Hr	Hairless	CGGAGACAATCATAGGAAGCAAG

		CCGGTCAGTACCCCTACCT
Kcna1	Potassium Voltage-Gated Channel Subfamily A Member 1	CTGAGCTGAAGGACGACAAG AAGCGGATGACCCTGAGGAT
Klf9	Krueppel-like Factor 9	TTATTGCACGCTGGTCACTATC CTCATCGGGACTCTCCAGAC
Lat1	Large Neutral Amino Acids Transporter Small Subunit 1	ATATCACGCTGCTCAACGGTG GCCGCCTGACTTGGAGATG
Lat2	Large Neutral Amino Acids Transporter Small Subunit 1	TCAGCGCCTGTGGTATCATTG TGATGCCTGTCACGATCCAGA
Ldha	Lactate Dehydrogenase A	CATTGTCAAGTACAGTCCACACT TTCCAATTACTCGGTTTTTGGGA
Lipe	Hormone-Sensitive Lipase	CACCCATAGTCAAGAACCCCTTC TCTACCACTTTCAGCGTCACCG
Lpl	Lipoprotein Lipase	GGTTGCGCGTAGAGAGGATG CTCACGCTCTGACATGCCTTC
Mct10	Monocarboxylate Transporter 10	GAGGTGGAGCTGACGAGGT CATGGACACGAAGAGCACCC
Mct8	Monocarboxylate Transporter 8	CTTGCAGGTCCTCTCATTCC TGAAGAAGCCATCACATAGGC
Me1	Malic Enzyme 1, NADP(+)-dependent, cytosolic	GAAAGAGGTGTTTGCCCATGA AATTGCAGCAACTCCTATGAGG
Mlycd	Malonyl-CoA Decarboxylase	CTGTCGCCTATCCCTGGATTC CCGGTAACCGCTGAGATTTCT
Nppb	Brain Natriuretic Factor	GAGGTCACTCCTATCCTCTGG GCCATTTCCTCCGACTTTTCTC
Oatp1a4	Solute Carrier Organic Anion Transporting Polypeptide 1A4	CAATTCGGTATCCCCACGTCT CTGCACATCCTACACCAATCAT
Oatp1b2	Solute Carrier Organic Anion Transporting Polypeptide 1B2	GCACTGCGATGGATTCAGGAT AGCTTTGGTCGGTGTAGCTTG
Oatp1c1	Solute Carrier Organic Anion Transporting Polypeptide 1C1	GGGCCATCCTTTACAGTCGG ACCCAAGAACACCTTGAGTTTTC
Pck1	Phosphoenolpyruvate Carboxykinase 1, cytosolic	ATCTTTGGTGGCCGTAGACCT GCCAGTGGGCCAGGTATTT
Pklr	Pyruvate Kinase Liver and Red Blood cell	TCAAGGCAGGGATGAACATTG CACGGGTCTGTAGCTGAGTG
Pln	Phospholamban	ACTGTGACGATCACCGAAGC TTCCATTATGCCAGGAAGG
Pnpla2	Adipose Triglyceride Lipase	GGTGACCATCTGCCTTCCAG TGCAGAAGAGACCCAGCAGT
Ppargc1A	Peroxisome Proliferator-activated Receptor γ coactivator 1-α	TTGTCAGGCTGGAGTGTACC CACCATGGTCGTATCAGAGG

Prl	Prolactin	TGGGATCTACTTTGTTTGGTCAC ATGGGCAATTTGGCACCTCA
Rpl32	60S Ribosomal Protein L32	TTAAGCGAAACTGGCGGAAAC TTGTTGCTCCCATAACCGATG
Rplp0	Ribosomal Protein, large, P0, 36B4	TCGGGTCCTAGACCAGTGTTC AGATTCGGGATATGCTGTTGGC
Ryr2	Ryanodine Receptor 2	ACGGCGACCATCCACAAAG CGGGGGAACATTCTTGGAATT
Tfam	Mitochondrial Transcription Factor A	GGAATGTGGAGCGTGCTAAAA ACAAGACTGATAGACGAGGGG
Th	Tyrosine Hydroxylase	GCTGGAGGATGTGTCTCACT GAGGAGGCATGACGGATGTA
Thrsp	Thyroid Hormone Responsive Gene Spot 14	AAGGTGGCTGGCAACGAAA GGGTCAGGTGGGTAAGGATG
Tshb	Thyroid Stimulating Hormone Subunit beta	GGGCAAGCAGCATCCTTTTG GTGTCATACAATACCCAGCACAG
Ucp1	Uncoupling Protein 1	ACTCAGGATTGGCCTCTACG CCACACCTCCAGTCATTAAGC
xCT	Cystine/Glutamate Transporter	GGCACCGTCATCGGATCAG CTCCACAGGCAGACCAGAAAA
β-actin	Beta actin	GGCTGTATTCCCCTCCATCG CCAGTTGGTAACAATGCCATGT
β-MHC	Myosin, heavy polypeptide 7, cardiac muscle, beta	GGAATCCTTTGGAAATGCGAAGA GCCCCAACAATATAGCCAGTTAC

2.12. Protein isolation, western blot, and analysis

Protein isolation was performed on dry-ice frozen tissue by homogenizing iBAT tissues samples (10-15 mg) in 250 µL lysis buffer or M. soleus tissue samples (6-10 mg) in 100 µL lysis buffer. Protein concentration was determined using the bicinchoninic acid solution and 4% copper sulfate, and measured at 562 nm in the SPECTROstar Nano Microplate Reader. The optical densities were then used to calculate protein concentrations using the standard curve with the following equation: Protein [mg/ml] = $\frac{(optical\ density\ of\ sample - blank) - slope}{y - intercept}$. Electrophoresis was performed using 20 µg protein (not pre-heated at 98°C) on a 12% SDS Gel (TGX Stain-free cast gels prepared as described in **Table 4**) and afterwards, the gel was activated in the ChemiDoc™ to activate a unique compound, which reacts with tryptophan residues in the protein sample to develop UV light inducible fluorescence detection ((185); settings: Stain free blot with 60 seconds exposure time). Then, the proteins were transferred onto a polyvinylidene difluoride membrane

for 1 hour at 100 V. Afterwards, total protein was measured using ChemiDoc™ without any staining steps (settings: stain free blot with automatic exposure intense bands). Then, the blots were blocked for 1 hour in 5% milk in TBS-T to minimize unspecific binding sites and afterwards, incubated with primary antibodies (**Table 16**) overnight at 4°C. Afterwards, membranes were washed six times for 10 min with TBS-T, incubated with the corresponding secondary antibodies, which is conjugated to the horseradish peroxidase (HRP) enzyme (**Table 16**), for 1 hour at RT and washed again six times for 10 min with TBS-T. The HRP enzyme releases light by acting on the substrate luminol. To enhance the signal by increasing the amount of light emitted, the Clarity Western ECL Substrate was added and chemiluminescence was recorded using ChemiDoc™. After each detection, the blots were stripped with Restore PLUS Western Blot Stripping Buffer for 20 min at RT. Afterwards, the blots were washed three times for 5 min with 1x TBS-T, blocked for 1 h in 5% milk in TBS-T and then either used or stored at 4°C. The quantification of band intensities was performed using ImageLab™ Software. As several blots were necessary to detect all samples, either one identical sample or group was used for every single blot. The intensity values were fist normalized to either β-actin (Part A + B) or total protein content (Part C) and then normalized to this identical sample/group. Lastly, the different groups/treatment conditions were averaged and normalized to the control group. Statistical analysis was performed using a two-way ANOVA with post-hoc Bonferroni test (Part A) or unpaired Student's t-test with Welch's correction (Part B + C).

Table 16: Primary (1) and secondary (2) antibodies used for western blot analysis.

	Antibody	**Species**	**Dilution**	**Catalog #**	**Supplier**
(1)	β- actin	mouse	1:10.000	A1978	Sigma
	UCP-1	rabbit	1:10.000		(186)
	OxPhos	mouse	1:2.000	45-8099	Thermo Scientific
	Serca2	rabbit	1:1.000	4388	Cell Signaling Technology
(2)	Anti-rabbit	goat	1:5.000	P0448	DAKO, Denmark
	Anti-mouse	goat	1:5.000	P0447	DAKO, Denmark

2.13. Enzyme-linked immunosorbent assay (ELISA)

The ELISA is a fast and convenient way to quantify soluble proteins. There are several possible ELISA principles, but the basic one is based on antigen attachment to the surface of a microtiter plate and application of a matching antibody-enzyme-complex. The final detection method includes a color change based on the enzyme linked to the antibody.

2.13.1. Total T4 ELISA for mouse serum analysis

Serum levels of total T4 (tT4; free T4 and protein-bound T4) were measured using a commercially available ELISA kit (**Table 1**) and performed according to manufacturer's instruction. In this ELISA, the T4 in the serum competes with the conjugate solution (T4 labeled with HRP and also containing 8-anilino-1-naphtalene sulfonic acid to inhibit binding of T4 to serum proteins) for the T4-antibody in the coated microtiter well. After several washing steps, to remove unbound-labeled T4, tetramethylbenzidine (TMB) is added, which acts as a hydrogen donor for the reaction catalyzed by HRP resulting in a blue color. This reaction is stopped by sulfuric acid leading to a color change from blue to yellow. The color intensity is lastly measured with the SPECTROstar Nano Microplate Reader and the formed color is proportional to the amount of enzyme and is inversely related to the tT4 in the sample. Statistical analysis was performed using unpaired Student's t-test with Welch's correction (Part A - C).

2.13.2. Total T3 ELISA for mouse serum analysis

Serum levels of total T3 (tT3; free T4 and protein-bound T3) were measured using a commercially available ELISA kit (**Table 1**) and performed according to manufacturer's instruction. This ELISA is similar to the serum tT4 ELISA described above. Here, the T3 in the sample competes as well with the HRP-labeled T3 for the anti-T3 antibody sites. This immune complex is then visualized with TMB, the reaction is stopped with sulfuric acid and measured with the SPECTROstar Nano Microplate Reader. The final measured intensity is inversely proportional to the amount of tT3 in the sample. Statistical analysis was performed using unpaired Student's t-test with Welch's correction (Part A - C)

2.13.3. ELISA for cAMP levels in iBAT tissue samples

Intracellular cAMP levels in iBAT tissue samples were measured using a commercially available ELISA kit (**Table 1**) and performed according to manufacturer's instruction. First, dry-ice frozen iBAT tissue samples were homogenized with trichloroacetic acid, which is used for precipitating proteins from dilute solutions. After centrifugation, the supernatant is washed with water-saturated diethyl ether to remove trichloroacetic acid from the aqueous solution. Lastly, the aqueous solution was dried under a stream of nitrogen and the pellet is dissolved in the kit's assay buffer right before the ELISA. The cAMP ELISA also relies on the competition between the cAMP in the sample and the HRP-labeled cAMP. Furthermore, also TMB is added and the reaction is stopped with sulfuric acid. The only difference is the microplate containing donkey anti rabbit antibodies, which requires the addition of antiserum (anti-cAMP antibodies) to allow for the binding of either labeled or unlabeled cAMP. The optical density was measured at the SPECTROstar Nano Microplate Reader. The first step in the analysis is to calculate the percent

bound for each standard/sample by using the following equation: $\%B/B0 = \frac{(Standard\ or\ sample\ OD - NSB\ OD) * 100}{(zero\ Standard\ OD - NSB\ OD)}$ with OD: optical density and NSB: non-specific binding. The values are then interpolated using the standard curve and adjusted to the applied tissue weight. Statistical analysis was performed using a two-way ANOVA with post-hoc Bonferroni test (Part A) or unpaired Student's t-test with Welch's correction (Part B).

2.14. Glycogen determination in liver tissue

Glycogen content determination on dry-ice frozen liver tissue samples was performed as described previously (187). Briefly, liver tissue samples were homogenized in trichloroacetic acid to precipitate proteins and nucleic acid, whereas the glycogen remains in solution with other water-soluble compounds. After centrifugation, to remove the participated proteins and nucleic acids, ethanol was added to the supernatant to separate glycogen from the other compounds by precipitation. This precipitation was performed at 4°C for 4 hours, then for 30 min at RT and afterwards, the samples were centrifuged to pellet the precipitated glycogen. Then, the supernatant was discarded and the air-dried pellet re-suspended in Lugol Reaction Mix, allowing the iodine atoms to bind to the glycogen forming a complex which produces a brown-blue color. This color change is then quantified by measuring the optical density at the SPECTROstar Nano Microplate Reader. For calculations, the measurements were normalized against the blank (Lugol reaction mix) and the mean of the OD of triplicates was calculated and normalized to the initial tissue weight. Statistical analysis was performed using a two-way ANOVA with post-hoc Bonferroni test (Part A) or unpaired Student's t-test with Welch's correction (Part B + C).

2.15. Lipolysis in adipose tissue

Glycerol release as an indicator of *ex vivo* lipolysis was measured in pieces of iBAT (2-5 mg), iWAT (10-15 mg) and gonadal WAT (gWAT; 10-15 mg). Tissue samples were incubated for 2 hours in 200 µL pre-warmed lipolysis buffer + 2% BSA at 37°C and 5% CO_2 to stimulate lipolysis. As blank measurement, 200 µL of pre-warmed lipolysis buffer + 2% BSA without any tissue pieces was also incubated. Afterwards, 60 µL of the supernatant or blank was diluted in 40 µL free glycerol reagent in duplicates in a 96 well plate. As control, the standard reagent was used by diluting 5 µL in 95 µL of free glycerol reagent. The free glycerol reagent measures the free endogenous glycerol based on the same coupled enzymatic reactions. The last reaction step results in the production of a quinoneimine dye, which can be measured using the SPECTROstar Nano Microplate Reader. The increase in absorbance is directly proportional to the free glycerol concentration of the sample. For calculations, the mean of the OD duplicates was first normalized against the blank, then against the used volume of standard and to the volume of lipolysis buffer. Finally, the total glycerol (µg) was normalized against the initial tissue weight (mg). The mean

of all standard values of every single measurement was calculated and used in the single calculations to correct for inter-assay variances. Statistical analysis was performed using a two-way ANOVA with post-hoc Bonferroni test (Part A).

2.16. Statistical analysis

For data analysis Microsoft Office Excel and GraphPad Prism 5 and 7 software were used. Values are shown as mean ± standard error of the mean (S.E.M.). Statistical testing was performed using a two-way ANOVA measurement with Bonferroni post-hoc test, unpaired or paired Student's t-test as stated more in detail in the figure legends. The results of the two-way ANOVA calculations are summarized in Chapter 6.1, 6.2, and 6.3. P values of less than 0.05 were considered significant and values between 0.05 and 0.1 are stated as a tendency. The respective levels of significance and group sizes are stated in the figure legends.

3. Results

To dissect the influence of central versus peripheral TH actions on thermogenesis and cardiovascular function, the consequences of a hypothyroid brain in the presence of a hyperthyroid periphery were investigated (*M/O* dko mice, Part A) and compared to the effects of a mild general thyrotoxicosis where both, brain and periphery, are hyperthyroid (WT + T3 mice, Part B). Moreover, the possible effects of systemic TA3 administration, which is used in clinical trials to treat AHDS patients (188), were studied (Part C).

3.1. Part A: Dissecting central from peripheral TH actions using *M/O* dko mice

As outlined in the introduction, the *M/O* dko mice lack the THTs MCT8 and OATP1C1, which results in elevated serum TH concentrations as well as in a hypothyroid brain (168). Before starting the profiling of the *M/O* dko mice, the expression levels of several transporters in WT mice were analyzed to get an overview which tissue might depend on MCT8 and OATP1C1 as THTs. Therefore, the expression levels of *Mct8*, *Oatp1c1*, and *Mct10* were investigated in the brain, iWAT, gWAT, liver, tail artery, and aorta using qPCR measurements (**Figure 8A**). *Oatp1c1* was only detected in the brain, whereas *Mct10* was found to be expressed in the different adipose tissue depots as well as in the liver. As this thesis focuses on thermoregulation and the cardiovascular system, the iBAT and the heart have been further investigated and the expression of additional THTs (*Lat1*, *Lat2*, *Oatp1b2*, *Oatp1a4*, and cystine/glutamate transporter (*xCT)*) was additionally analyzed. Regarding the heart, *Mct10* was also found to be expressed and to a much lower extent the *Lat 1* and *2* transporter (**Figure 8B**). In case of the iBAT, only *Mct10* was found to be sufficiently expressed to play a possible role in compensating the loss of MCT8 (**Figure 8C**).

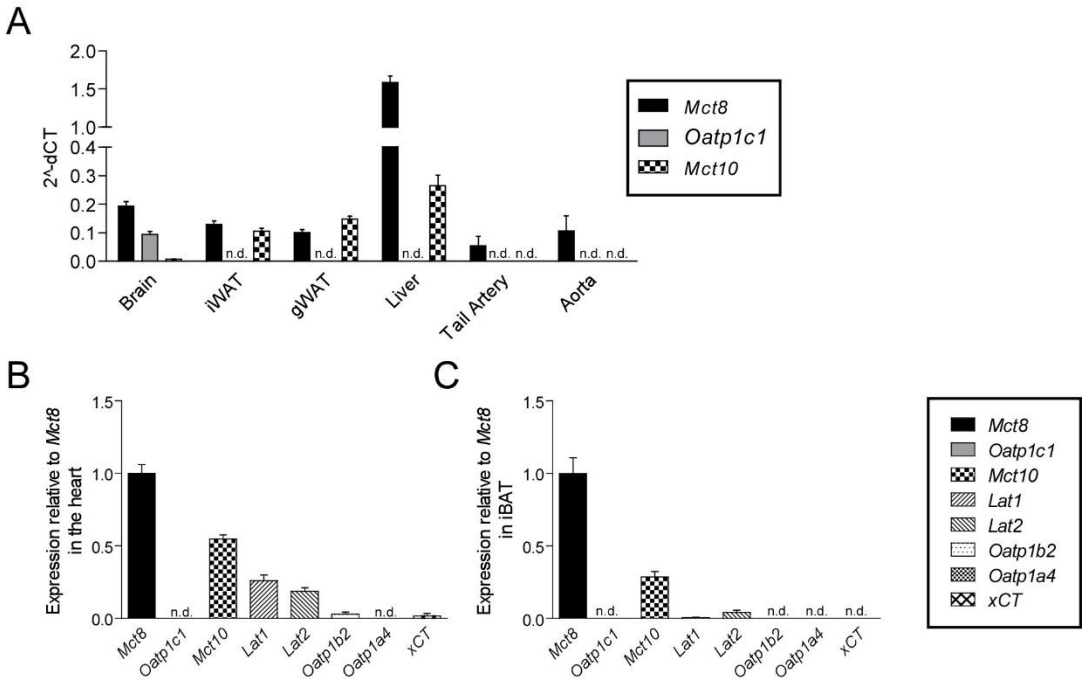

Figure 8: Transporter evaluation in WT mouse tissues (Modified from (189)).
(A) Gene expression levels of THTs in WT mouse tissues normalized to *Cyclophilin* and *β-actin* (n=5).
(B) Cardiac gene expression levels in WT mouse tissue normalized to *Cyclophilin* and *β-actin* (n=5).
(C) iBAT gene expression levels in WT mouse tissue normalized to *Cyclophilin* and *β-actin* (n=5).
All values are shown as mean ± S.E.M. dCT, delta threshold cycle; *Lat1/2*, large neutral amino acid transporter 1/2; *Mct8/10*, monocarboxylate transporter 8/10; n.d., not detectable; *Oatp1a4*, organic anion transporting polypeptide 1A4; *Oatp1b2*, organic anion transporting polypeptide 1B2; *Oatp1c1*, organic anion transporting polypeptide 1C1; THTs, thyroid hormone transporters; *xCT*, cystine/glutamate transporter; WT, wildtype.

The aim of Part A of this thesis was to analyze the consequences of a hypothyroid brain in the presence of a hyperthyroid periphery regarding general metabolic parameters such as weight, food consumption, and activity, as well as thermogenic and cardiovascular properties. Therefore, the following mouse models of THT deficiency were studied: WT (white), *Mct8* ko (black), *Oatp1c1* ko (grey), and *Mct8/Oatp1c1* dko (*M/O* dko; squared) (**Figure 9A**). The *Mct8* ko and the *M/O* dko mice have an elevated T3 to T4 ratio but only the *M/O* dko brain has been profoundly hypothyroid for its entire postnatal life (**Figure 20**, (168)). To evaluate the metabolic consequences of *Mct8* and *Oatp1c1* deficiency, body weight and food and water intake were assessed in all genotypes. The *M/O* dko mice showed a tendency for reduced body weight compared to the controls, while the body weight of *Oatp1c1* ko and *Mct8* ko mice was not altered (**Figure 9B**, Supplementary Table 1). Furthermore, the *M/O* dko mice showed an increase in food intake compared to WT, whereas water intake was increased only compared to the *Oatp1c1* ko mice (**Figure 9C+D**, Supplementary Table 1). This increase was not caused by higher locomotor activity, as the twenty-four-hour profile recorded over 72 hours by radio telemetry as well as the

area under the curve (AUC) over a twenty-four-hour time course was comparable in all genotypes (**Figure 9E+F**, Supplementary Table 1).

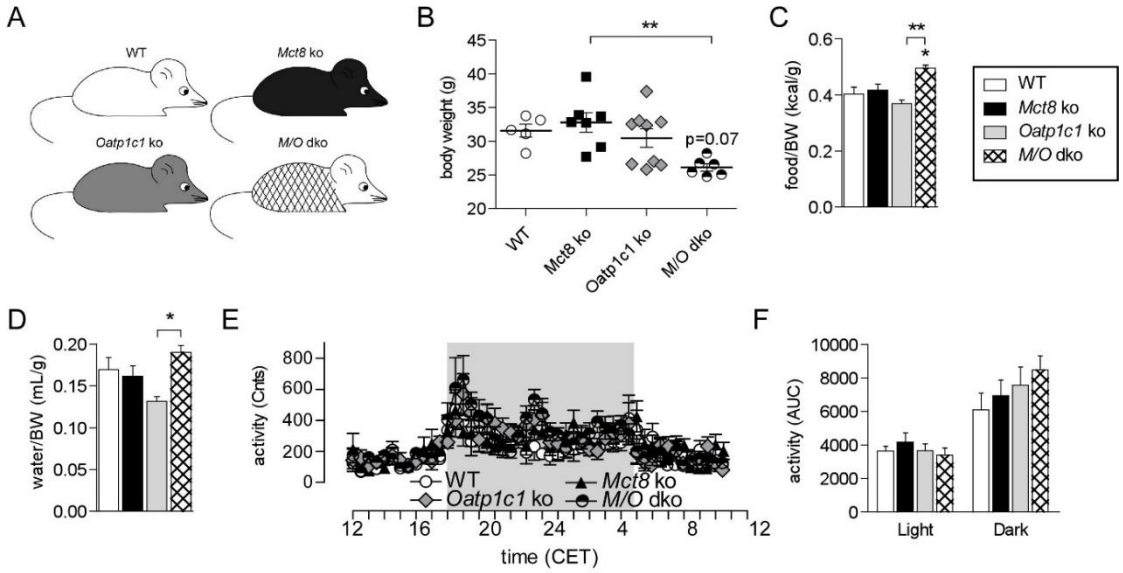

Figure 9: Increase in food intake and trend towards a reduced body weight in M/O dko mice (Modified from (189)).
(A) Schematic overview of the genotypes (WT, *Mct8* ko, *Oatp1c1* ko, and *M/O* dko mice).
(B) Body weight of the different genotypes at the age of 4-5 months.
(C) Average food intake (kcal) normalized to body weight (n=8 for WT, n=7 for *Mct8* ko and *Oatp1c1* ko, and n=5 for *M/O* dko).
(D) Average water consumption (mL) in relation to average body weight (g) (n=8 for WT, n=7 for *Mct8* ko and *Oatp1c1* ko, n=5 for *M/O* dko).
(E) Mean twenty-four-hour profile of activity recorded for 72 hours with radio telemetry in conscious and freely moving animals (n=6 for WT, n=7 for *Mct8* ko, *Oatp1c1* ko and *M/O* dko). Grey background indicates the dark phase.
(F) Area under the curve of the activity profiles separated in light and dark phase (n=6 for WT, n=7 for *Mct8* ko, *Oatp1c1* ko and *M/O* dko).
All values are shown as mean ± S.E.M and analyzed with two-way ANOVA with Bonferroni post-hoc multiple comparisons test with *: $p<0.05$ or **: $p<0.01$ vs. the respective WT/control, or as indicated otherwise (brackets). AUC, area under the curve; BW, body weight; CET, Central European Time; cnts, counts; WT, wildtype.

3.1.1. Are body temperature and thermogenesis altered in *M/O* dko mice?

For monitoring body temperature, 72 consecutive hours were recorded by radio telemetry in freely moving and conscious animals. The twenty-four-hour profile as well as the averaged absolute temperatures separated into the light (inactive) and dark (active) phase revealed no differences in the THT deficient mice (**Figure 10A+B**, Supplementary Table 1). Furthermore, infrared pictures from different body areas were taken. They showed a small albeit not significant difference in iBAT temperature (**Figure 11A+C**, Supplementary Table 1) as an indicator of heat production

but no changes in tail temperature (**Figure 11B+D**, Supplementary Table 1) indicative of heat loss.

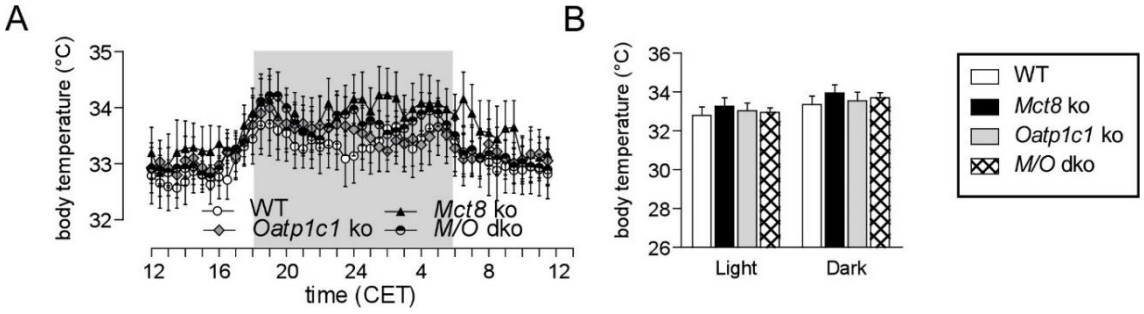

Figure 10: Body temperature of M/O dko mice is not altered (Modified from (189)).
(A) Mean twenty-four-hour profile of body temperature recorded for 72 hours with radio telemetry in conscious and freely moving animals (n=6 for WT, n=7 for *Mct8* ko, *Oatp1c1* ko and *M/O* dko). Grey background indicates the dark phase.
(B) Mean absolute body temperature values of the twenty-four-hour profile recorded for 72 hours of the four genotypes separated in light and dark phase (n=6 for WT, n=7 for Mct8 ko, *Oatp1c1* ko and *M/O* dko).
All values are shown as mean ± S.E.M and analyzed with two-way ANOVA with Bonferroni post-hoc multiple comparisons test. CET, Central European Time; WT, wildtype.

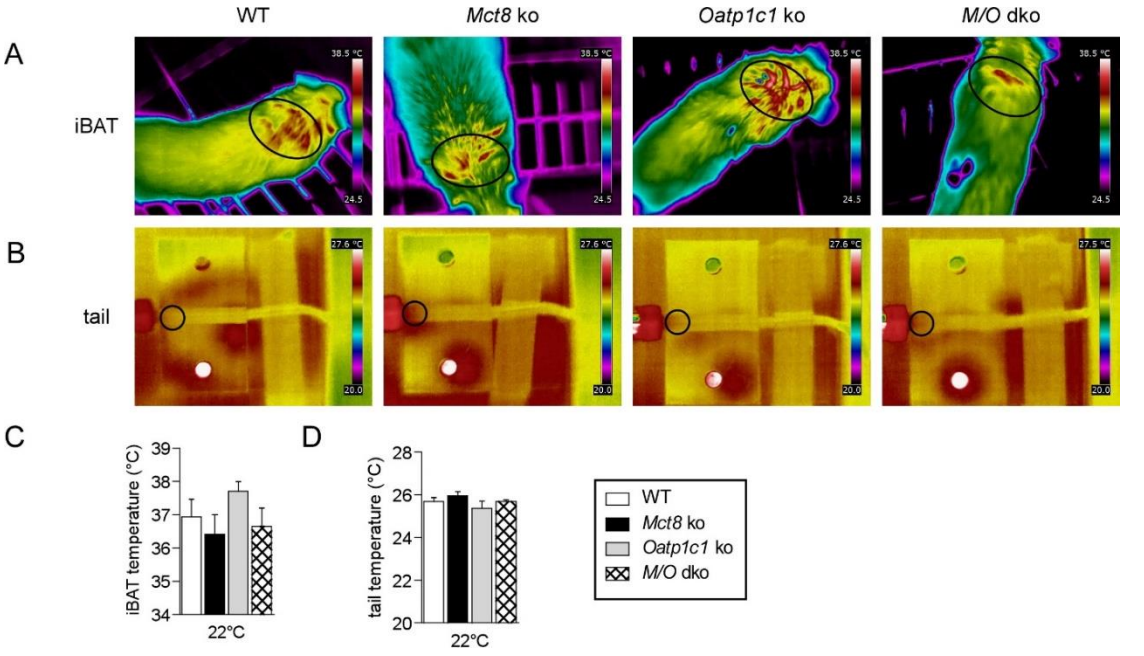

Figure 11: M/O dko mice show no changes in iBAT thermogenesis and tail heat loss at room temperature (22°C) (Modified from (189)).
(A) Representative infrared pictures of iBAT at 22°C.
(B) Representative infrared pictures of the tail at 22°C.
(C) Quantification of average maximum temperature of infrared iBAT images at 22°C (n=5/genotype).
(D) Quantification of average maximum temperature of infrared tail images at 22°C (n=5/genotype).
All values are shown as mean ± S.E.M and analyzed with two-way ANOVA with Bonferroni post-hoc multiple comparisons test. Black circles visualize area of measurement. iBAT, interscapular brown adipose tissue; WT, wildtype.

Additionally, the mice were first cold challenged at 10°C for 16 hours and then infrared pictures were taken at 10°C. After acclimatization to RT and in a second experiment, they were kept at temperatures at 38°C (above thermoneutrality) and at 32°C (around thermoneutrality) for 10 minutes to investigate their body temperature regulatory capability. Interestingly, after the cold challenge the *Oatp1c1* ko mice showed a minor reduction in body temperature, indicating that they were unable to defend their body temperature setpoint and suggesting a mild cold sensitivity (**Figure 12A+C**, Supplementary Table 1). Although core body temperature was decreased, neither iBAT nor tail temperature were changed to respectively increase endogenous heat production or reduce heat loss (**Figure 12B+D+E**, Supplementary Table 1). Whereas, the *Oatp1c1* ko mice displayed a mild cold sensitivity, the *Mct8* ko mice seemed to suffer from heat stress as tail temperature at 32°C was slightly elevated compared to controls (**Figure 12E**, Supplementary Table 1). Furthermore, the investigation of the skin heat conductivity, diffusivity, and capacity using transient hot bridge did not reveal any differences between the genotypes (**Table 17**). This indicates normal skin and fur isolation properties.

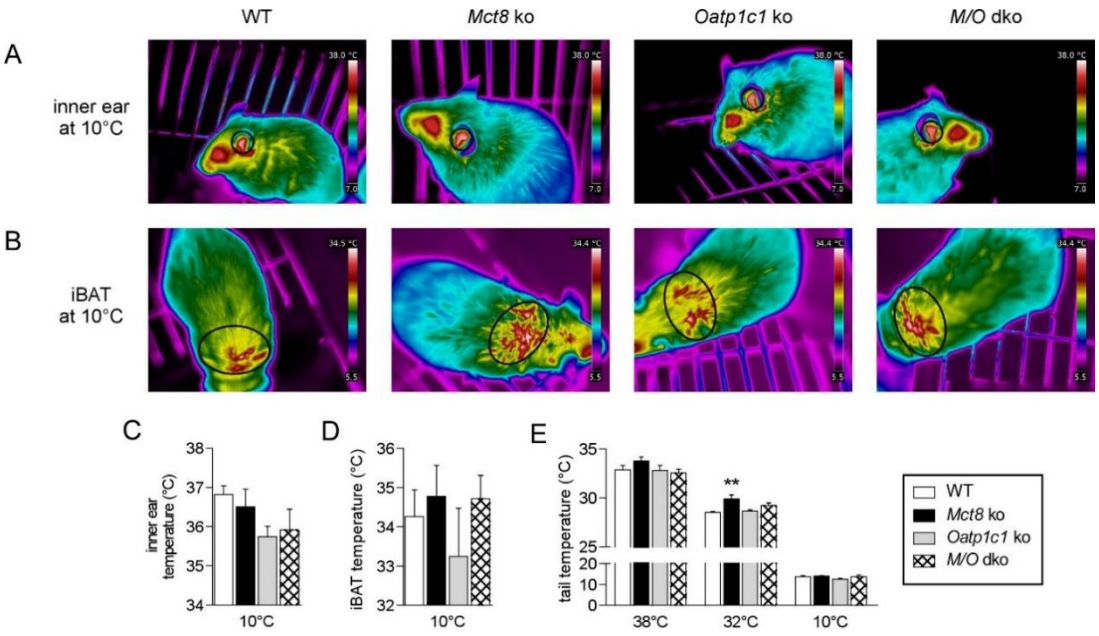

Figure 12: Mild cold sensitivity is observed in Oatp1c1 ko mice, whereas heat stress was present in Mct8 ko mice in response to different ambient temperatures (Modified from (189)).
(A) Representative infrared images of the inner ear temperature after 16 hours at 10°C (cold exposure).
(B) Representative infrared images of the iBAT temperature after 16 hours at 10°C (cold exposure).
(C) Quantification of average maximum temperature of the inner ear temperature after 16 hours at 10°C (cold exposure; n=5/genotype).
(D) Quantification of average maximum temperature of the iBAT temperature after 16 hours at 10°C (cold exposure; n=5/genotype).
(E) Quantification of average maximum temperature of the tail base measured after 10 minutes at 38°C (above thermoneutrality) and at 32°C (around thermoneutrality) and after 16 hours at 10°C (cold exposure; n=5/genotype).
All values are shown as mean ± S.E.M with **: $p<0.01$ vs. the respective WT and analyzed with two-way ANOVA with Bonferroni post-hoc multiple comparisons test. Black circles visualize area of measurement (A+B). iBAT, interscapular brown adipose tissue; WT, wildtype.

Table 17: Basic thermal skin parameters.

	WT	***Mct8* ko**	***Oatp1c1* ko**	***M/O* dko**
Heat Conductivity (W/m*K)	0.38 ± 0.01	0.36 ± 0.02	0.38 ± 0.01	0.36 ± 0.01
Heat Diffusivity (mm^2/s)	0.2 ± 0.01	0.2 ± 0.02	0.2 ± 0.02	0.21 ± 0.02
Heat Capacity (J/g*K)	1.95 ± 0.07	1.94 ± 0.25	1.96 ± 0.25	1.79 ± 0.21

All values are shown as mean ± S.E.M (n=6 for WT, *Oatp1c1* ko, and *M/O* dko; n=7 for *Mct8* ko). All p>0.05 in two-way ANOVA testing.

To have a closer look at body composition, several adipose tissue depots were collected, weighted, and the values normalized to the respective body weight (**Figure 13A**, Supplementary Table 1). No alterations in iBAT and iWAT weight were detected between the genotypes, but gWAT of the *M/O* dko mice was significantly lighter as compared to the *Oatp1c1* ko mice (**Figure 13A**, Supplementary Table 1).

To identify molecular alterations in thermogenesis, gene and protein expression analysis were performed in iBAT, which is the primary thermogenic tissue in mice. All tested genes (iodothyronine deiodinase type II (*Dio2*), uncoupling protein 1 (*Ucp1*), mitochondrial transcription factor A (*Tfam*), and adrenergic receptor beta 3 (*Adrb3*)) were significantly downregulated in *M/O* dko mice, whereas only *Dio2* and *Adrb3* were significantly reduced in *Mct8* ko mice (**Figure 13B**, Supplementary Table 1). Despite the reduction of *Adrb3*, the intracellular iBAT cAMP levels in all genotypes were similar, indicative of no change in the sympathetic input to the iBAT (**Figure 13C**, Supplementary Table 1). To further evaluate the change in *Ucp1* expression on the mRNA level, the protein levels of UCP1 were investigated and found to be unchanged (**Figure 13D**, Supplementary Table 1). Although, *M/O* dko mice showed a strong reduction in *Ucp1* mRNA, UCP1 protein expression were unchanged, which was in line with no significant alterations in iBAT temperature (**Figure 11D**, Supplementary Table 1). Furthermore, the proteins levels of selected oxidative phosphorylation complexes proteins revealed a significant increase in protein levels of complex IV (CIV-MTCO1, Complex IV Cytochrome C Oxidase core subunit 1) in *M/O* dko mice compared to both single ko mice (**Figure 13E**, Supplementary Table 1). Furthermore, genes involved in fatty acid metabolism (acetyl-CoA-carboxylase 1 (*Acaca*), malonyl-CoA decarboxylase (*Mlycd*), citrate synthase (*Cs*) and hormone-sensitive lipase (*Lipe*)) showed an overall reduction in *M/O* dko mice (**Figure 13F**, Supplementary Table 1). The changes for the single ko animals were more subtle. For instance, in the *Mct8* ko animals only a significant reduction of complex III (CIII-UQCRC2, Complex III ubiquinol-cytochrome c reductase core protein 2, **Figure 13E**, Supplementary Table 1) of OXPHOS was detected as well as an increase in peroxisome proliferative-activated receptor gamma coactivator 1-alpha (*Ppargc1A*, **Figure 13F**, Supplementary Table 1). The *Oatp1c1* ko animals showed no changes in OXPHOS protein levels and only an increase *PpargcA1*, *Cs*, and

cell death-inducing DNA fragmentation factor alpha subunit-like effector A *(Cidea)* (**Figure 13E+F**, Supplementary Table 1). As mRNA expression levels do not always reflect the protein activity, the glycerol release in the different adipose tissues was measured as indication of lipolytic activity. The *M/O* dko mice had significant higher glycerol release in iBAT compared to the *Mct8* ko mice and in iWAT compared to the controls and both single ko mice (**Figure 13G**, Supplementary Table 1).

Overall, the thermogenic profile analysis of iBAT revealed minor modifications in *Mct8* ko mice, which were more pronounced in the *M/O* dko mice.

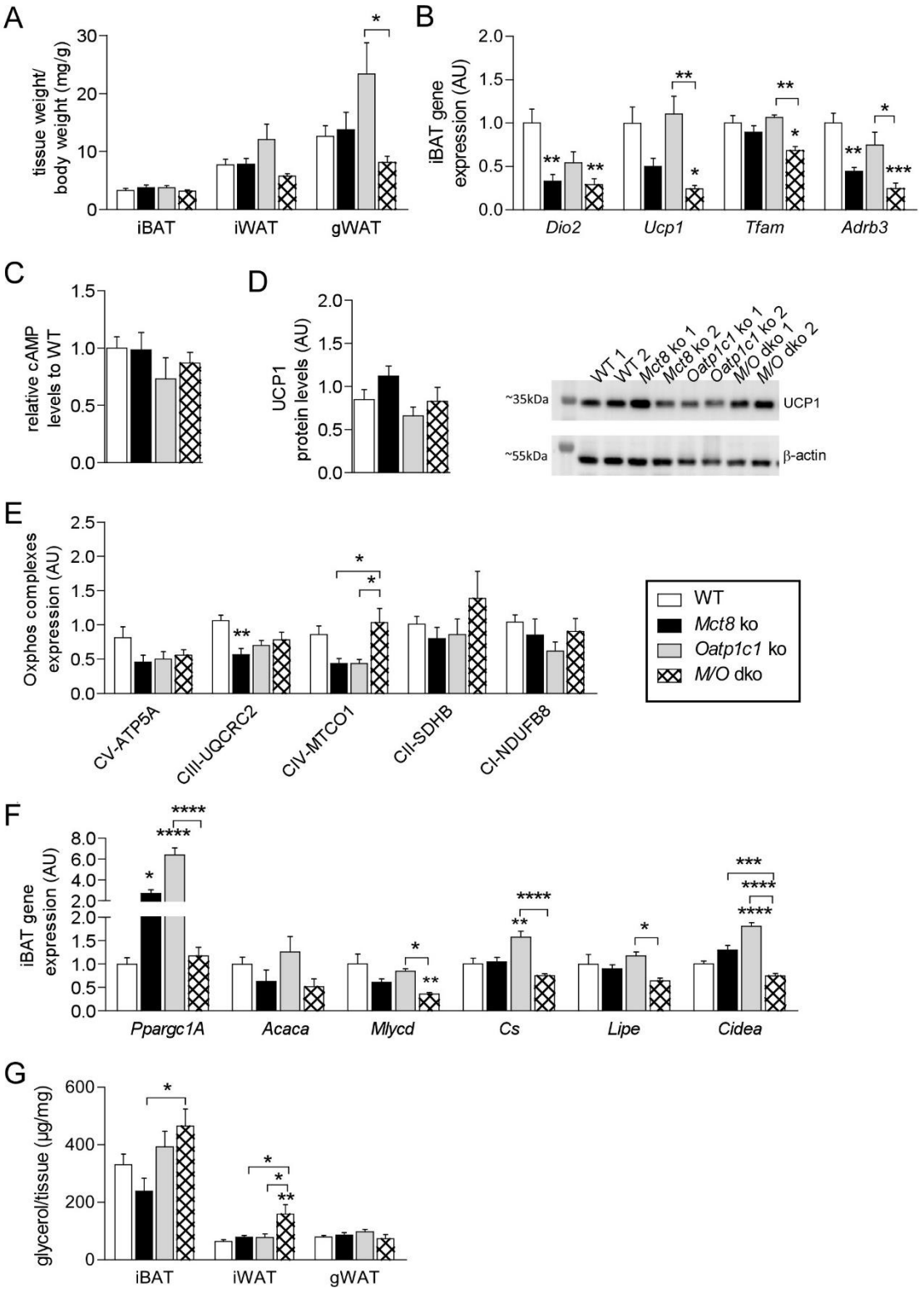

Figure 13: Distinct differences on mRNA level are observed in iBAT of M/O dko mice (Modified from (189)).

(A) Tissue weight (mg) in relation to body weight (g) of adipose tissue depots (n=7 for WT, *Mct8* ko, *M/O* dko, and n=9 for *Oatp1c1* ko).

(B) Expression levels of genes in iBAT normalized against *Hprt* (n=6/genotype).

(C) Intracellular cAMP levels in iBAT normalized to WT animals (n=5/genotype).

(D) Quantification of UCP1 protein levels normalized to β-actin in iBAT and a representative western blot image (n=6/genotype).

(E) Quantification of proteins representing the different OXPHOS complexes (CI- CV) normalized to β-

actin in iBAT (n=6/genotype).
(F) Expression levels of genes in iBAT normalized against *Hprt* (n=6/genotype).
(G) Basal lipolysis in adipose tissue depots (n=7 for WT, *Mct8* ko and *M/O* dko, n=9 for *Oatp1c1* ko).
All values are shown as mean ± S.E.M and analyzed with two-way ANOVA with Bonferroni post-hoc multiple comparisons test *: p<0.05; **: p<0.01; ***: p<0.001; ****: p<0.0001 vs. the respective WT, or as otherwise indicated (brackets). *Acaca*, acetyl-CoA carboxylase 1; *Adrb3*, adrenergic receptor beta 3; AU, arbitrary units; cAMP, cyclic adenosine monophosphate; *Cidea*, cell death-inducing DNA fragmentation factor alpha subunit-like effector A; CIII-UQCRC2, Complex III ubiquinol-cytochrome c reductase core protein 2; CII-SDHB, Complex II succinate dehydrogenase subunit; CI-NDUFB8, NADH ubiquinone oxidoreductase subunit B8; CIV-MTCO1, Complex IV Cytochrome C Oxidase core subunit 1; *Cs*, citrate synthase; CV-ATP5A, Complex V F1-F0 ATP synthase subunit; *Dio2*, iodothyronine deiodinase type II; gWAT, gonadal white adipose tissue; *Hprt*, hypoxanthine-guanine phosphoribosyltransferase; iBAT, interscapular brown adipose tissue; iWAT, inguinal white adipose tissue; *Lipe*, hormone-sensitive lipase; *Mlycd*, malonyl-CoA decarboxylase; OXPHOS, oxidative phosphorylation; *Ppargc1A*, peroxisome proliferative-activated receptor gamma coactivator 1-alpha; *Tfam*, mitochondrial transcription factor A; *Ucp1*, uncoupling protein 1; WT, wildtype.

To extend the thermogenic analysis iWAT, which is also capable of thermogenesis, was also investigated. The gene expression analysis revealed a significant increase in *Dio2* in *Mct8* ko mice but no consistent changes in *Ucp1*, *Cidea*, *Ppargc1A*, and *Mlycd* mRNA expression levels (**Figure 14A**, Supplementary Table 1). Furthermore, no changes were observed in genes involved in iWAT fatty acid metabolism (adipose triglyceride lipase (*Pnpla2*), *Lipe*, lipoprotein lipase (*Lpl*)) and *Adrb3* (**Figure 14B**, Supplementary Table 1). Taken together, these data indicate only minor alterations in the thermogenic and metabolic activity of the iWAT.

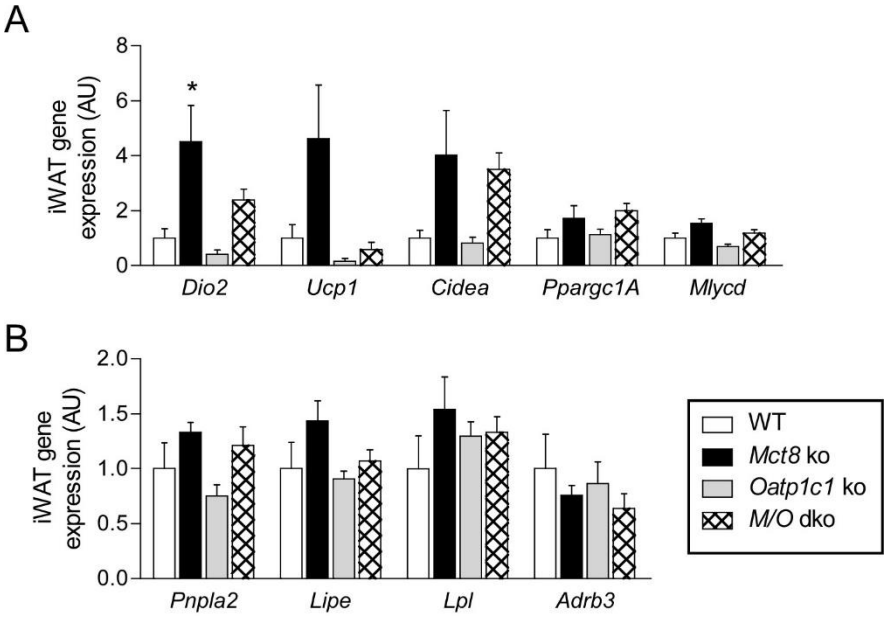

Figure 14: Only minor alterations between the different genotypes are observed in iWAT (Modified from (189)).
(A) Expression levels of genes in iWAT normalized against the mean of *Cyclophilin* and *Rplp0* (n=5 for WT, n=6 for *Mct8* ko, *Oatp1c1* ko and *M/O* dko).
(B) Expression levels of genes in iWAT normalized against the mean of *Cyclophilin* and *Rplp0* (n=5 for WT, n=6 for *Mct8* ko, *Oatp1c1* ko and *M/O* dko).
All values are shown as mean ± S.E.M *: p<0.05 vs. the respective WT and analyzed with two-way

ANOVA with Bonferroni post-hoc multiple comparisons test. *Adrb3*, adrenergic receptor beta; AU, arbitrary units; *Cidea*, cell death-inducing DNA fragmentation factor alpha subunit-like effector A; *Dio2*, iodothyronine deiodinase type II; *Lipe*, hormone-sensitive lipase; *Lpl*, lipoprotein lipase; *Mlycd*, malonyl-CoA-decarboxylase; *Pnpla2*, adipose triglyceride lipase; *Ppargc1A*, peroxisome proliferator-activated receptor gamma coactivator 1-alpha; *Rplp0*, ribosomal protein, large, P0; *Ucp1*, uncoupling protein 1; WT, wildtype.

Taken together, although minor changes in body temperature regulation of *Mct8* ko and *Oatp1c1* ko were detected, the presented data suggest no major alterations in body temperature regulation of the THT deficient animals due to the hypothyroid status of the brain.

3.1.2. What is the metabolic condition of *M/O* dko livers?

The liver is also a well-known target organ of THs, which can be directly (190) and centrally (191) regulated. Consistent with previous reports, expression levels of hepatic iodothyronine deiodinase type I (*Dio1*) and thyroid hormone responsive gene (*Thrsp*) were significantly upregulated in the *M/O* dko mice, whereas only *Thrsp* was increased in the *Mct8* ko mice (**Figure 15A,** Supplementary Table 1). Furthermore, in the *Mct8* ko mice another T3 sensitive gene, the malic enzyme (*Me1*; (192, 193)), was upregulated as well. This confirms the known hepatic hyperthyroid state in these animals (168, 171, 174). Gene expression analysis exposed distinct alterations, which seem to be independent of the hepatic TH status. For instance, in the *Oatp1c1* ko mice pyruvate kinase (*Pklr*) was increased and lactate dehydrogenase (*Ldha*) was decreased, which could indicate a switch from gluconeogenesis to glycolysis (**Figure 15A**, Supplementary Table 1). However, none of the tested T3 sensitive genes were upregulated in the *Oatp1c1* ko mice and also *Acaca*, a gene belonging to fatty acid synthesis, was unchanged in these mice (**Figure 15A**,Supplementary Table 1). Furthermore, regarding the *M/O* dko mice, only *Ldha* was downregulated but *Pklr* and phosphoenolpyruvate carboxykinase 1 (*Pck1*) were unchanged, which was accompanied by similar glycogen content in all genotypes (**Figure 15A+B**, Supplementary Table 1).

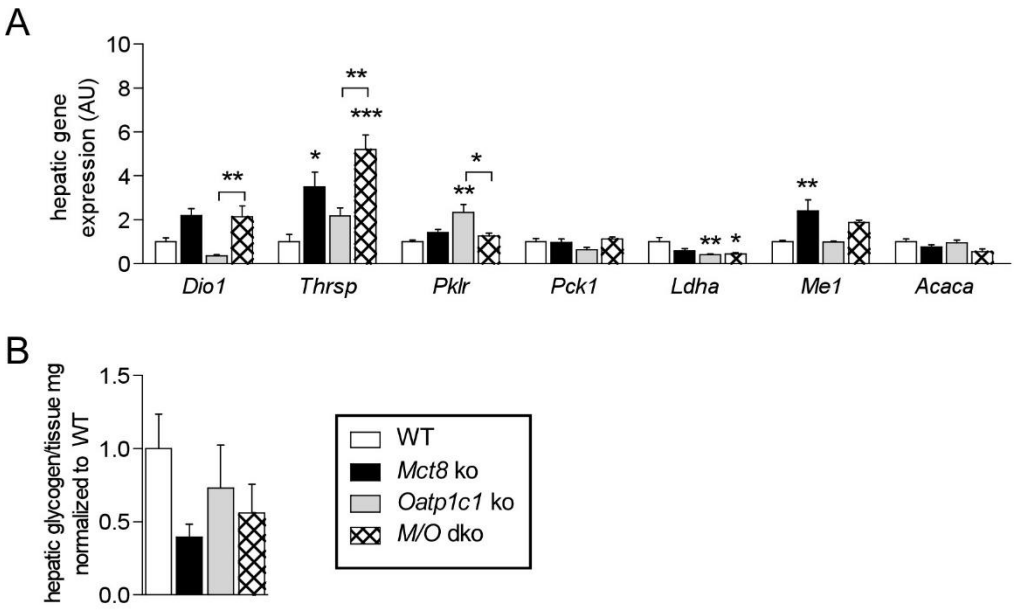

Figure 15: Hyperthyroid state of the liver in the M/O dko mice but no major alterations in metabolic genes (Modified from (189)).
(A) Expression levels of genes in liver normalized against the mean of *Cyclophilin* and *Hprt* (n=5 for WT, n=6 for *Mct8* ko, *Oatp1c1* ko and *M/O* dko).
(B) Hepatic glycogen content relative to WT animals (n=6/genotype).
All values are shown as mean ± S.E.M and analyzed with two-way ANOVA with Bonferroni post-hoc multiple comparisons test with *: $p<0.05$; **: $p<0.01$; ***: $p<0.001$ vs. the respective WT, or as otherwise indicated (brackets). *Acaca*, acetyl-CoA carboxylase 1; AU, arbitrary units; *Dio1*, iodothyronine deiodinase type I; *Hprt*, hypoxanthine-guanine phosphoribosyltransferase; *Ldha*, lactate dehydrogenase; *Me1*, malic enzyme; *Pck1*, phosphoenolpyruvate carboxykinase 1; *Pklr*, pyruvate kinase; *Thrsp*, thyroid hormone responsive gene spot 14; WT, wildtype.

3.1.3. How does the cardiovascular system respond to the central hypothyroidism in the *M/O* dko mice?

As the cardiovascular system heavily depends on THs for many functions (reviewed in (94, 194, 195)), a detailed cardiovascular analysis was performed. Surprisingly, the *M/O* dko mice did not develop cardiac hypertrophy (**Figure 16A**, Supplementary Table 1), although this would have been expected as a result of the elevated serum T3 levels (196). Genes involved in pathological (brain natriuretic peptide (*Nppb*)) or physiological cardiac hypertrophy (calcium transporting ATPase (*Atp2a2*) and the ratio of α-/β- MHC) were not altered either (**Figure 19A**, Supplementary Table 1). To test for changes in heart rate, radio transmitters were implanted in the abdominal cavity of the animals and their heart rate was recorded for 72 consecutive hours. During the whole experimental procedure, animals were allowed to move freely in their home cage to avoid confounding effects of stress on the heart rate. Surprisingly, there was no sign of tachycardia, as the heart rate was comparable throughout the day. Furthermore, the AUC of the

twenty-four-hour profile separated into the light and dark phase revealed no increase in heart rate (**Figure 16B+C**, Supplementary Table 1).

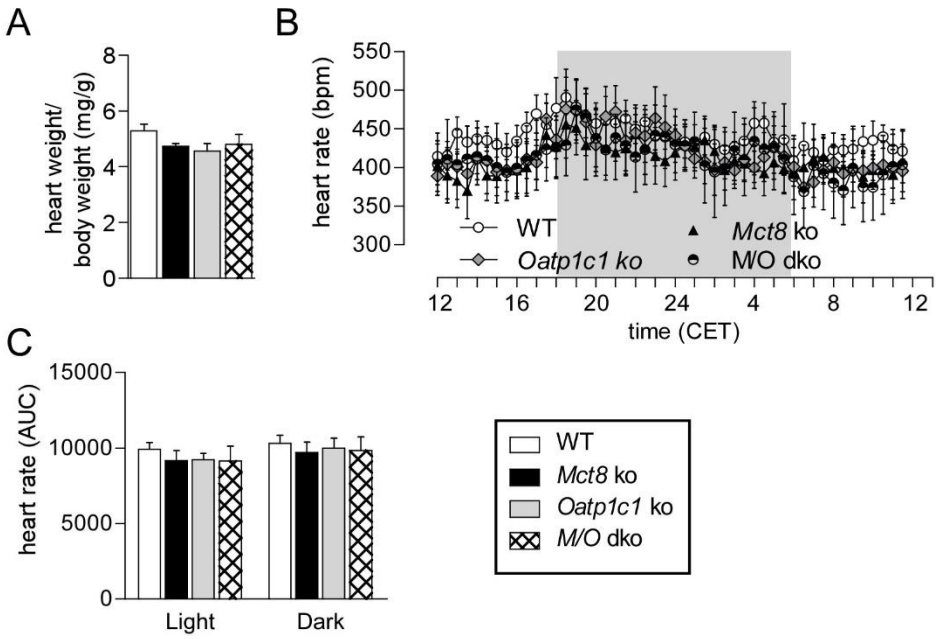

Figure 16: No signs of cardiac thyrotoxicosis in the M/O dko mice (Modified from (189)).
(A) Heart weight (mg) in relation to body weight (g) (n=7 for WT, *Mct8* ko, and *M/O* dko and n=5 for *Oatp1c1* ko).
(B) Mean twenty-four-hour profile of heart rate (bpm) recorded for 72 hours with radio telemetry in conscious and freely moving animals (n=6 for WT, n=7 for *Mct8* ko, *Oatp1c1* ko and *M/O* dko). Grey background indicates the dark phase.
(C) Area under the curve of the twenty-four-hour heart rate profiles separated in light and dark phase (n=6 for WT, n=7 for *Mct8* ko, *Oatp1c1* ko and *M/O* dko).
All values are shown as mean ± S.E.M and analyzed with two-way ANOVA with Bonferroni post-hoc multiple comparisons test. AUC, area under the curve; bpm, beats per minute; CET, Central European Time; WT, wildtype.

Although, no changes in average heart rate could be detected between the four genotypes the heart rate frequency distribution was calculated to identify acute changes in the autonomic control. For the calculation, the heart rate telemetry data over the 72 hours with values of every minute was used. It revealed significant changed frequency percentages during the light and dark phase exclusively in the *M/O* dko mice (**Figure 17A**, Supplementary Table 2). More in detail, it was an overall broader distribution with increased lower (180 and 200 bpm) and higher (400 and 420 bpm) frequencies, while the medium (360 and 380 bpm) heart rate frequencies were reduced. Impressively, these increases in heart rate (=tachycardic episodes) correlated with bursts in locomotor activity, while reduction of heart rate (=bradycardic episodes) occurred at rest (**Figure 17B**, Supplementary Table 2). This phenomenon was only observed in the *M/O* dko mice and not

in the *Mct8* ko mice, suggesting that it is the consequence of the central hypothyroid brain but not the elevated peripheral T3 levels.

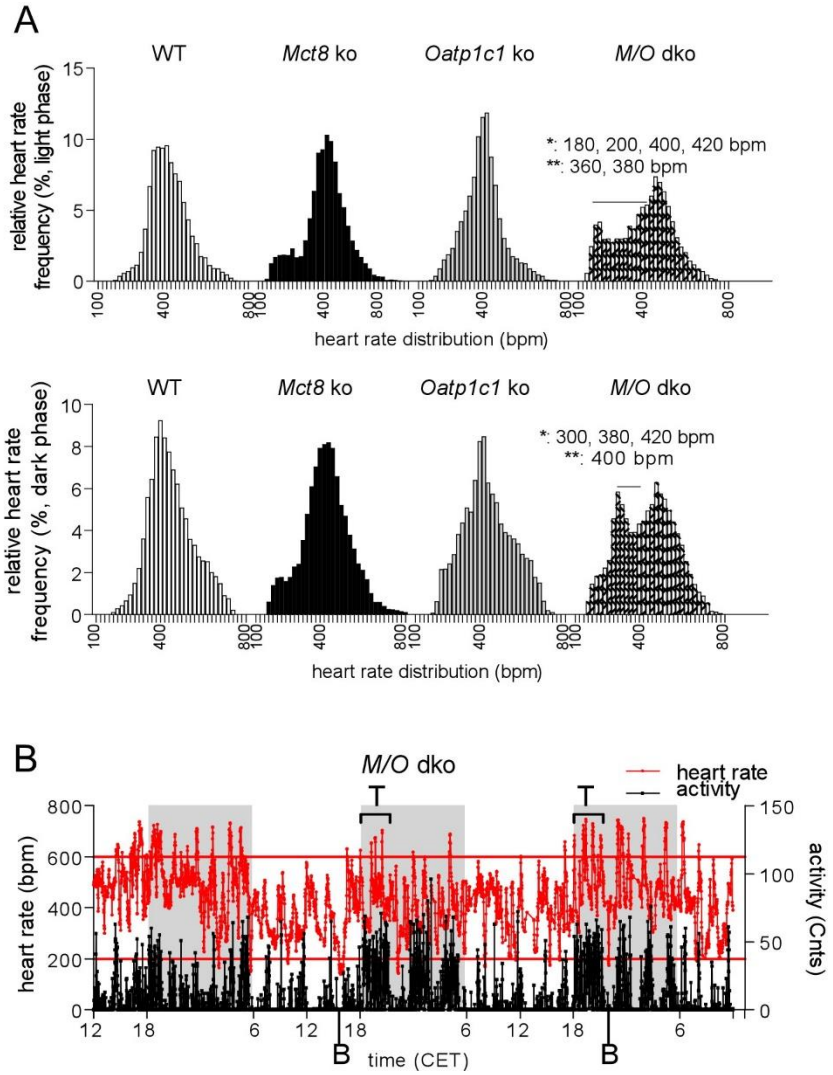

Figure 17: Heart rate frequency distribution is severely altered in the M/O dko mice (Modified from (189)).

(A) Heart rate distribution during the light (upper panel) and dark (lower panel) phase in percentage of the relative heart rate frequency (calculated in 20 bpm intervals). All values are shown as sum of the percentage of the certain heart rate frequency of all animals per genotype and analyzed with two-way ANOVA with Holm-Sidak's multiple comparisons test. $p<0.05$ (* WT vs. *M/O dko*) and $p<0.01$ (** WT vs. *M/O* dko) (n=6 for WT, n=7 for *Mct8* ko, *Oatp1c1* ko and *M/O* dko).

(B) Heart rate plotted against activity level of one representative *M/O* dko mouse over 72 hours. Grey background indicates the dark phase. Red lines indicate the upper and the lower limits of heart rate found in WT controls.

Bpm, beats per minute; CET, Central European Time; cnts, counts; WT, wildtype.

For further analysis of the autonomic system the following experiments were performed: First, to test the stress response and to evaluate the maximum heart rate, saline was injected. Here, no significant changes were observed (**Figure 18A**, Supplementary Table 1). Secondly, two pharmacological blockers, scopolamine methylbromide and timolol maleate, were injected successively to block the PSNS and SNS, respectively. The contributions of the PSNS and SNS were calculated and there was no difference in the distinct input to the heart in this acute condition

(**Figure 18B**, Supplementary Table 1). The intrinsic heart rate, which reflects the heart rate at the completely denervated state, was also not different between the genotypes (**Figure 18C**, Supplementary Table 1), suggesting no intrinsic defect caused by the lack of MCT8 and OATP1C1 transporters.

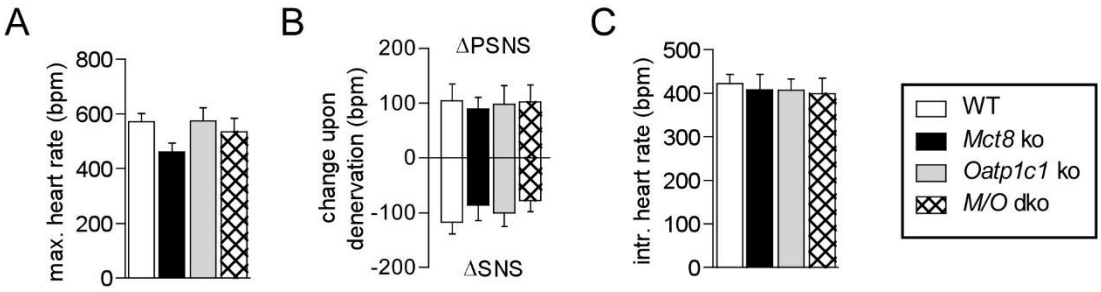

Figure 18: No change in autonomic nervous system regulation in M/O dko mice (Modified from (189)).
(A) Maximum heart rate (bpm) after saline injection (n=6 for WT, n=7 for *Mct8* ko and *Oatp1c1* ko and n=8 for *M/O* dko).
(B) Change in heart rate upon pharmacological denervation of the PSNS with scopolamine methylbromide and the SNS with timolol maleate (n=6 for WT, n=7 for *Mct8* ko and *Oatp1c1* ko and n=8 for *M/O* dko).
(C) Intrinsic heart rate after full pharmacological denervation (n=6 for WT, n=7 for *Mct8* ko and *Oatp1c1* ko, and n=8 for *M/O* dko).
All values are shown as mean ± S.E.M and analyzed with two-way ANOVA with Bonferroni post-hoc multiple comparisons test. Bpm, beats per minute; PSNS, parasympathetic nervous system; SNS, sympathetic nervous system; WT, wildtype; Δ, delta.

To better characterize the molecular fingerprint of the heart, several genes were tested that are regulated by THs and known to be involved in the regulation of cardiac properties; namely, pacemaking activities (hyperpolarization-activated cyclic nucleotide gated potassium and sodium channel 2 and 4 (*Hcn2* and *Hcn4*), cardiac contractility (ratio of α-MHC to β-MHC) and regulators of the intracellular Ca^{2+} concentration (*Atp2a2*, and phospholamban (*Pln*)). Furthermore, the expression level of potassium voltage-gated channel subfamily A member 1 (*Kcna1*), which is positively regulated by T3 (8), was analyzed. However, the tested genes were not significantly altered between the genotypes (**Figure 19A**, Supplementary Table 1). Furthermore, blood pressure, which was assessed by a tail cuff system, was comparable among the genotypes (**Figure 19B**, Supplementary Table 1).

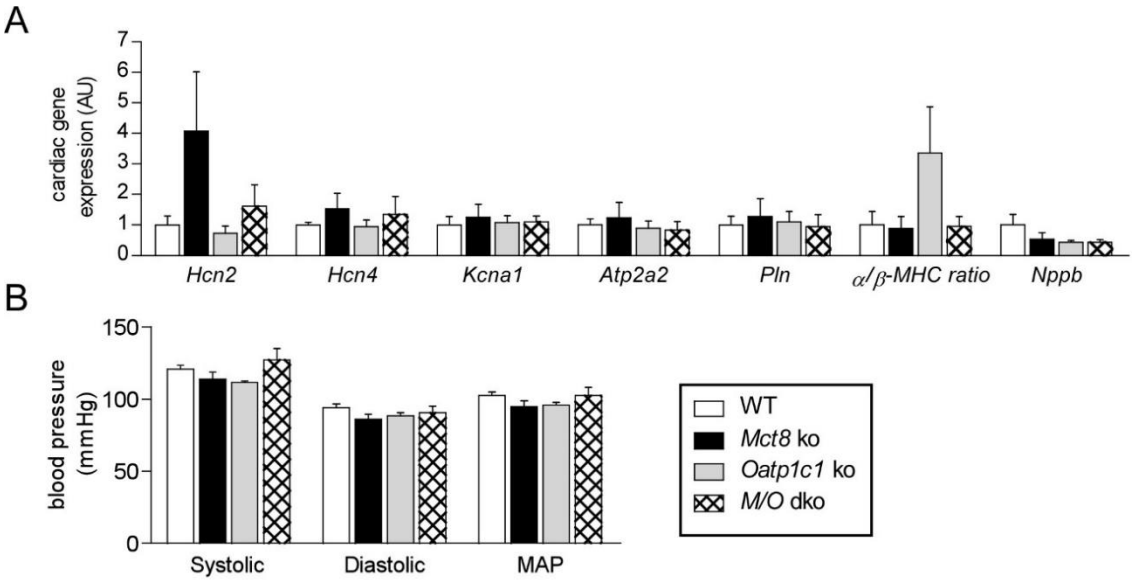

Figure 19: No alterations on molecular level and blood pressure regulation in M/O dko mice (Modified from (189)).
(A) Cardiac gene expression levels normalized to *Rpl32* (n=5 for WT and *Mct8* ko, n=4 for *Oatp1c1* ko and *M/O* dko).
(B) Systolic, diastolic, and mean arterial pressure (MAP) (n=8 for WT, n=7 for *Mct8* ko, n=5 for *Oatp1c1* ko and *M/O* dko).
All values are shown as mean ± S.E.M analyzed with two-way ANOVA with Bonferroni post-hoc multiple comparisons. *Atp2a2*; ATPase, calcium transporting, cardiac muscle, slow twitch; *Hcn2/4*, hyperpolarization-activated cyclic nucleotide-gated potassium channel 2/4; *Kcna1*, potassium voltage-gated channel subfamily A member 1; mmHg, millimeter of mercury; *Nppb*, brain natriuretic factor; *Pln*, phospholamban; *Rpl32*, ribosomal protein L32; *α-Myh*, myosin heavy chain 6 cardiac muscle alpha; *β-Myh*, myosin heavy chain 7 cardiac muscle beta.

Taken together, the *M/O* dko mice presented normal body temperature with small albeit not significantly reduced iBAT temperature, which was accompanied with a significant reduction in several thermogenic markers on gene expression level. Regarding the cardiovascular system, no changes in heart weight or heart rate were detected. Remarkably, the heart rate frequency distribution analysis revealed a broader distribution of frequencies with tachycardic bursts during locomotion.

3.2. Part B: Further dissection of central versus peripheral TH action by induction of systemic hyperthyroidism

In the second part of the thesis, the focus was on further dissecting the central versus peripheral action of THs on the cardiovascular system and thermoregulation. In order to test the hypothyroid brain as cause for the previous findings, WT animals were treated with T3 in the drinking water for 14 consecutive days to induce hyperthyroidism peripherally and importantly, also centrally. Throughout this following part, untreated control WT mice (WT -T3; white striped) are compared with T3-treated WT mice (WT + T3; grey striped) (**Figure 20A**). The T3 dose (~800 ng/day) in the drinking water was selected to result in a serum TH profile comparable to the *Mct8* ko and *M/O* dko mice. Measurement of the serum total T3 and total T4 concentrations proved that the rather low T3 dose resulted in an altered profile of THs (**Figure 20B**) and only mice matching the *Mct8* ko and *M/O* dko profiles were used for the following analyses. To verify the hyperthyroid state of the brain three known T3 sensitive genes in the brain were tested: hairless (*Hr*), iodothyronine deiodinase type III (*Dio3*), and krueppel-like factor 9 (*Klf9*) (8). These tested genes were increased after T3 treatment, verifying that this specific dose was enough to reach the brain (**Figure 20C**). As a next step, the metabolic consequences were evaluated by assessing body weight in animals without and with T3 treatment as well as food and water intake before and during the T3 treatment. The body weight did not differ (**Figure 20D**), whereas food as well as water intake were significantly increased after the T3 treatment as published previously (**Figure 20E+F**; (170)). The locomotor activity, which was assessed by radio telemetry over 72 hours and displayed as twenty-four-hour profile and the resultant calculated AUC was comparable before and during the T3 treatment (**Figure 20G+H**), indicating that the increase in food intake was not the consequence of an increase in locomotor activity.

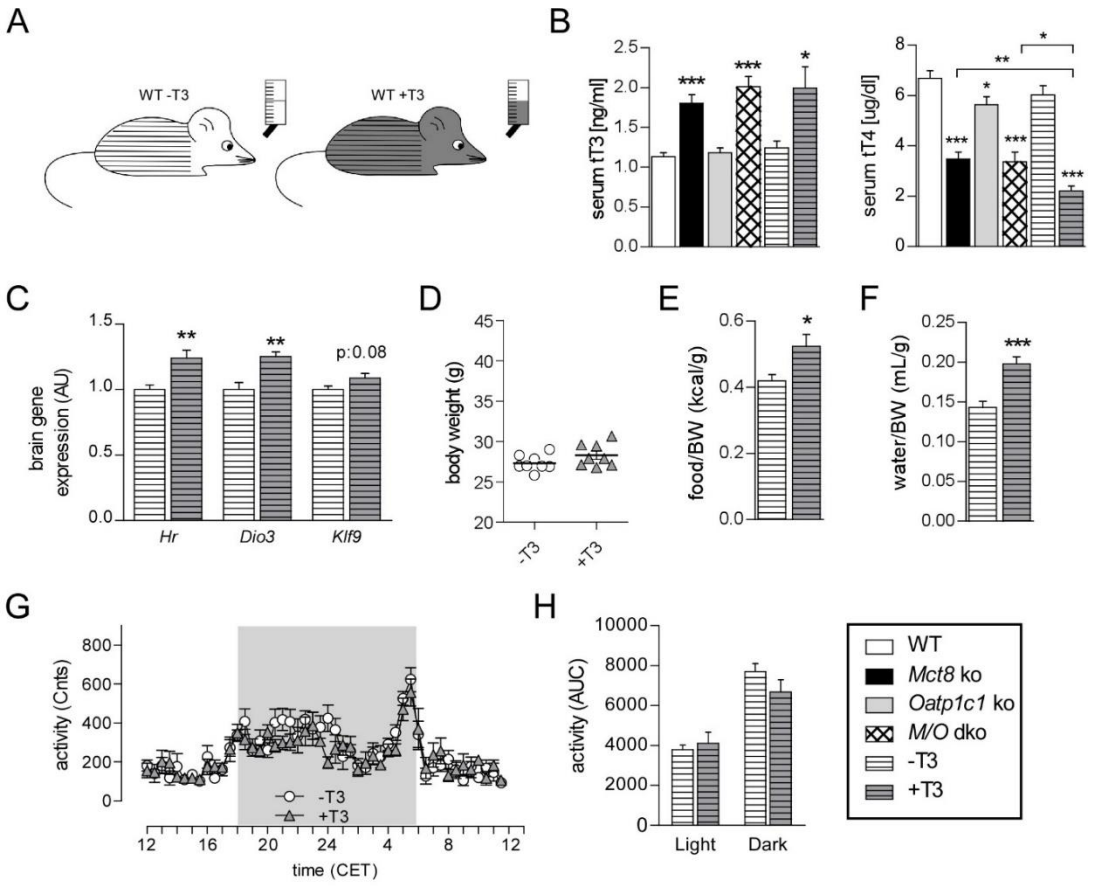

Figure 20: T3 treatment results in a two-fold increase in serum tT3 with increases in T3-responsive genes in the brain and in food intake (Modified from (189)).

(A) Schematic overview of the control (WT -T3, white striped) and the T3-treated mice (WT +T3, grey striped).

(B) Serum total T3 (tT3, left panel) and total T4 (tT4, right panel) concentrations in all animals used in this study (n=7 for WT, *Mct8* ko, *Oatp1c1* ko and *M/O* dko, n=13 for untreated WT (-T3); n=8 for T3-treated (+T3) WT mice).

(C) Gene expression in the brain normalized to the mean of *Cyclophilin* and *Hprt* (n=7 for -T3; n=8 for +T3).

(D) Body weight of animals at the age of 3-4 months.

(E) Mean food intake (kcal) normalized to average body weight (g) before and during T3 treatment (n=6/group).

(F) Mean water consumption (mL) in relation to average body weight (g) before and during T3 treatment (n=6/group)

(G) Mean twenty-four-hour profile of activity recorded for 72 hours with radio telemetry in conscious and freely moving animals before and during T3 treatment (n=6/group). Grey background indicates the dark phase.

(H) Area under the curve of the twenty-four-hour heart rate profiles separated in light and dark (n=6/group).

All values are shown as mean ± S.E.M and analyzed with unpaired Student's t-test with Welch's correction (B-D) or paired Student's t-test (E-G) with *: $p<0.05$, **: $p<0.01$, ***: $p<0.001$ vs. the respective WT/control, or as indicated otherwise (brackets). AU, arbitrary unit; AUC, area under the curve; BW, body weight; CET, Central European Time; cnts, counts; *Dio3*, iodothyronine deiodinase type III; *Hr*, hairless; *Klf9*, krueppel-like factor 9; WT, wildtype.

3.2.1. Does a two-fold increase in serum T3 influence body temperature and thermogenesis?

THs have a major influence on temperature regulation as seen in hyperthyroid humans, who are heat intolerant (reviewed in (67)). To investigate the influence of the two-fold increase in serum T3, body temperature was recorded by radio telemetry and analyzed as described above (Chapter 3.1.1.). The twenty-four-hour profile as well as the averaged absolute temperatures separated into the light (inactive) and dark (active) phase revealed an increase of ~0.6 °C in body temperature during the light phase during T3 treatment (**Figure 21A+B**, Supplementary Table 3, Supplementary Table 4), which is the resting phase of mice. To have a closer look at the underlying cause for this increase in resting body temperature, iBAT thermogenesis as a readout for heat production and tail temperature for heat loss were investigated. The infrared pictures showed no significant difference in iBAT (**Figure 22A+C**) or tail (**Figure 22B+D**) temperatures, respectively.

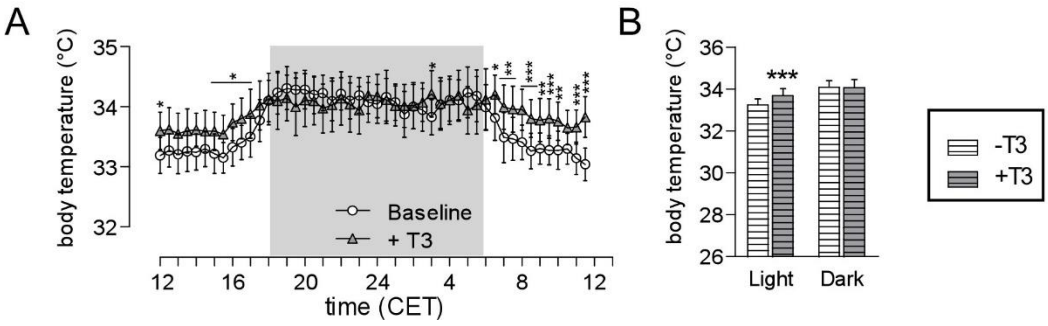

Figure 21: Resting body temperature of T3-treated mice is increased (Modified from (189)).
(A) Mean twenty-four-hour profile on body temperature recorded for 72 hours with radio telemetry in conscious and freely moving animals before and during T3 treatment (n=6/group). Grey background indicates the dark phase.
(B) Mean absolute body temperature values of the twenty-four-hour profile recorded for 72 hours of animals before and during T3 treatment separated in light and dark phase (n=6/group).
All values are shown as mean ± S.E.M and analyzed with two-way repeated measures ANOVA with post-hoc. *: $p<0.05$; **: $p<0.01$; ***: $p<0.001$ for T3 vs. baseline. CET, Central European Time.

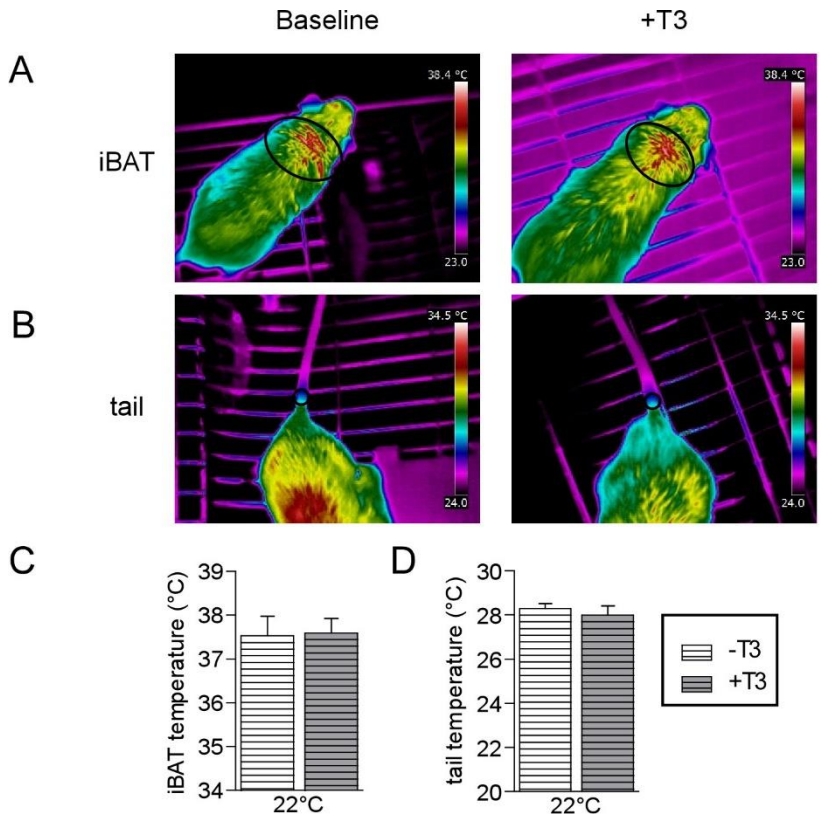

Figure 22: T3-treated mice show no changes in iBAT thermogenesis and heat loss over the tail (Modified from (189)).
(A) Representative infrared pictures of iBAT at 22°C before (Baseline) and after T3 treatment (+T3).
(B) Representative infrared pictures of the tail at 22°C before (Baseline) and after T3 treatment (+T3).
(C) Quantification of average maximum temperature of infrared iBAT images at 22°C before and after T3 treatment (n=6/group).
(D) Quantification of average maximum temperature of infrared tail images at 22°C before and after T3 treatment (n=6/group).
All values are shown as mean ± S.E.M and analyzed with paired Student's t- test. Black circles visualize area of measurement. iBAT, interscapular brown adipose tissue.

As a next step, a more detailed analysis of the thermoregulatory and metabolic properties was performed. First, the distinct adipose tissue depots were collected, weighted and normalized to the respective body weight (**Figure 23A**). The T3-treated animals displayed a significant increase in iBAT weight compared to the controls. This increase could be due to the incorporation of lipid droplets as previously reported (119). However, normalized iWAT and gWAT weights were not altered in response to the T3 treatment (**Figure 23A**).

As the *M/O* dko mice displayed a pronounced reduction in several thermoregulatory markers, the identical molecular analysis was performed in animals without (-T3) and with T3 (+T3) treatment. The tested thermoregulatory genes (*Dio2*, *Ucp1*, and *Tfam*) were unchanged and only a trend towards reduced *Adrb3* transcript levels was detected after the T3 treatment (**Figure 23B**). Nevertheless, the intracellular iBAT cAMP levels were similar (**Figure 23C**). The combined effect of reduced *Adrb3* levels and similar iBAT cAMP levels has also been observed in studies using higher doses of T3 (119). Moreover, protein levels of UCP1 (**Figure 23D**) and OXPHOS

protein complexes (**Figure 23E**) were unchanged. Independent of the unmodified parameters in thermoregulation, genes involved in fatty acid metabolism (*Acaca*, *Mlycd*, and *Cs*) were significantly reduced after the T3 treatment (**Figure 23F**).

Altogether, a trend towards reduced SNS activity can be observed in the iBAT of the T3-treated mice which has also been described previously (119).

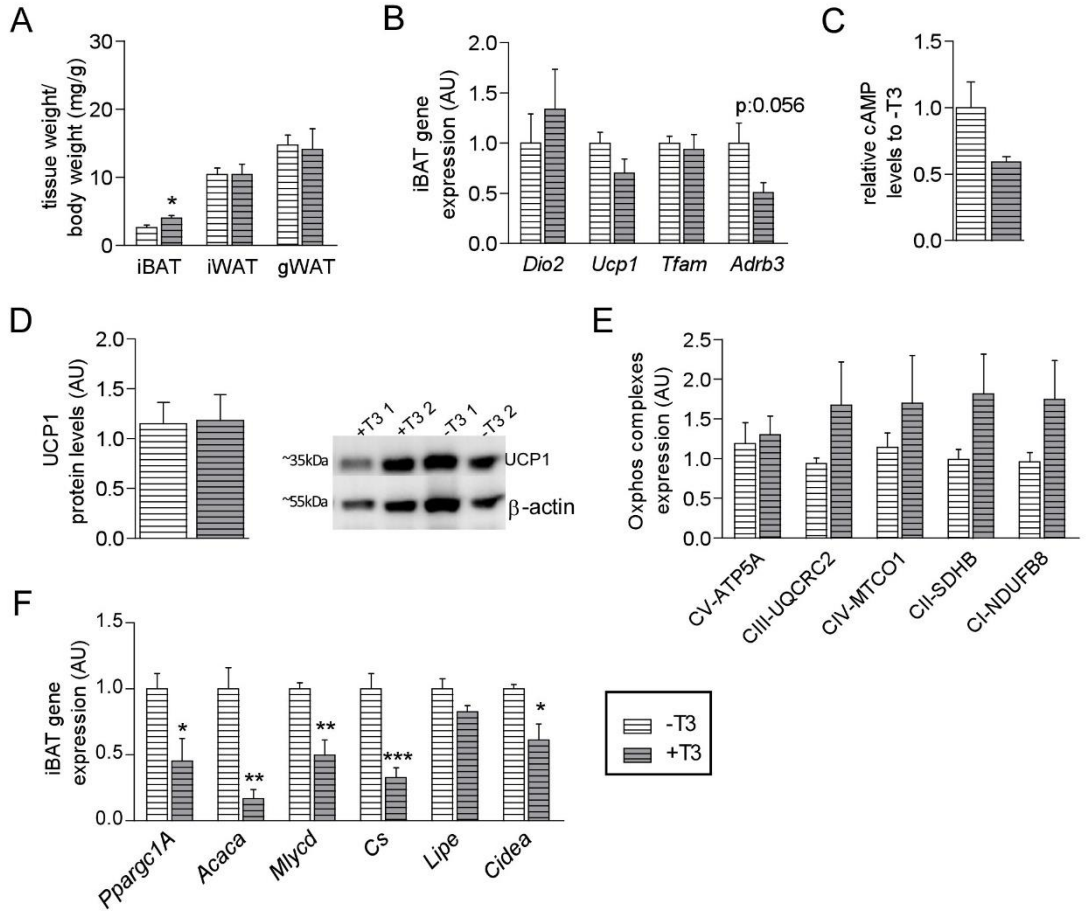

Figure 23: IBAT tissue weight increases and metabolic markers are downregulated on mRNA level after T3 treatment (Modified from (189)).

(A) Tissue weight (mg) in relation to body weight (g) of adipose tissue depots (n=8 for -T3; n=6 for +T3).

(B) Expression levels of genes in iBAT normalized against *Hprt* (n=7 for –T3; n=8 for +T3).

(C) Intracellular cAMP levels in iBAT normalized to animals without (-T3) T3 treatment (n=5 for -T3; n=7 for +T3).

(D) Quantification of UCP1 protein levels normalized to β-actin in iBAT and a representative western blot image (n=6/group).

(E) Quantification of proteins representing the different OXPHOS complexes (CI- CV) normalized to β-actin in iBAT (n=6/group).

(F) Expression levels of genes in iBAT normalized against *Hprt* in animals (n=7 for -T3; n=8 for +T3).

All values are shown as mean ± S.E.M and analyzed with unpaired Student's t-test with Welch's correction *: $p<0.05$; **: $p<0.01$; ***: $p<0.001$ vs. the untreated (-T3) animals. *Acaca*, acetyl-CoA carboxylase 1; *Adrb3*, adrenergic receptor beta 3; AU, arbitrary units; cAMP, cyclic adenosine monophosphate; *Cidea*, cell death-inducing DNA fragmentation factor alpha subunit-like effector A; CIII-UQCRC2, Complex III ubiquinol-cytochrome c reductase core protein 2; CII-SDHB, Complex II succinate dehydrogenase subunit; CI-NDUFB8, NADH ubiquinone oxidoreductase subunit B8; CIV-MTCO1, Complex IV Cytochrome C Oxidase core subunit 1; *Cs*, citrate synthase; CV-ATP5A, Complex V F1-F0 ATP synthase subunit; *Dio2*, iodothyronine deiodinase type II; gWAT, gonadal white adipose

tissue; *Hprt*, hypoxanthine-guanine phosphoribosyltransferase; iBAT, interscapular brown adipose tissue; iWAT, inguinal white adipose tissue; *Lipe*, hormone-sensitive lipase; *Mlycd*, malonyl-CoA-decarboxylase; OXPHOS, oxidative phosphorylation; *Ppargc1A*, peroxisome proliferative-activated receptor gamma coactivator 1-alpha; *Tfam*, mitochondrial transcription factor A; *Ucp1*, uncoupling protein 1.

Another investigated adipose depot was the iWAT, as it is also capable of thermogenesis (e.g. by browning (197) and its function is affected by the TH status. In the hyperthyroid animals, *Dio2* was five-fold elevated and a trend for increased levels of *Cidea* was measured, while the other tested genes (*Ucp1* and *Ppargc1A*) were unaltered (**Figure 24A**). Furthermore, *Mlycd* and *Lpl* were reduced and a trend for reduced *Adrb3* transcript levels after the T3 treatment was detected (**Figure 24A+B**). Taken together, no signs of browning were detected after administration of a low T3 dose.

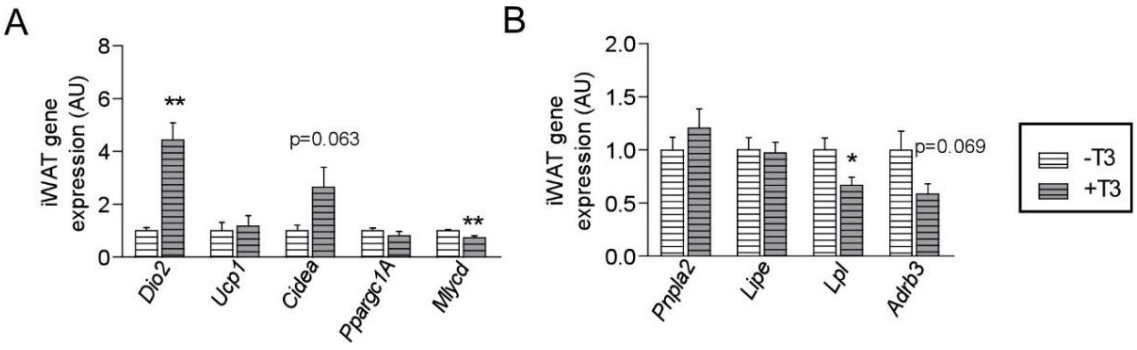

Figure 24: No browning is observed in iWAT after T3 treatment (Modified from (189)).
(A) Expression levels of thermogenic genes in iWAT normalized against the mean of *Cyclophilin* and *Rplp0* (n=7 for -T3; n=8 for +T3).
(B) Expression levels of metabolic genes in iWAT normalized against the mean of *Cyclophilin* and *Rplp0* (n=7 for -T3; n=8 for +T3).
All values are shown as mean ± S.E.M *: $p<0.05$; **: $p<0.01$ vs. the untreated (-T3) animals and analyzed with unpaired Student's t-test with Welch's correction. *Adrb3*, adrenergic receptor beta 3; AU, arbitrary units; *Cidea*, cell death-inducing DNA fragmentation factor alpha subunit-like effector A; *Dio2*, iodothyronine deiodinase type II; iWAT, inguinal white adipose tissue; *Lipe*, hormone-sensitive lipase; *Lpl*, lipoprotein lipase; *Mlycd*, malonyl-CoA-decarboxylase; *Pnpla2*, adipose triglyceride lipase; *Ppargc1A*, peroxisome proliferator-activated receptor gamma coactivator 1-alpha; *Rplp0*, ribosomal protein, large, P0; *Ucp1*, uncoupling protein 1.

3.2.2. Which metabolic changes are observed in the liver after T3 treatment?

As a next step, several TH-responsive and metabolic genes in the liver were tested. The strongly increased transcript levels of *Dio1* and *Thrsp* visualized the hyperthyroid status of the liver, thereby confirming the effectiveness of the T3 treatment (**Figure 25A**). In comparison to the *M/O* dko mice, the T3-treated mice showed increased transcript levels of *Pck1*, the rate-limiting enzyme in gluconeogenesis, which is in accordance with the reduced *Pklr* transcript levels, the enzyme involved in the last step in the glycolysis, pointing towards an increased glucose

production in the liver. *Ldha*, an enzyme that is also involved in gluconeogenesis by providing pyruvate, is as well elevated (**Figure 25A**). Furthermore, the hepatic glycogen content was measured and showed a significant reduction in the T3-treated animals (**Figure 25B**) illustrating the higher glucose demand in these animals and further supporting the altered gene expression levels.

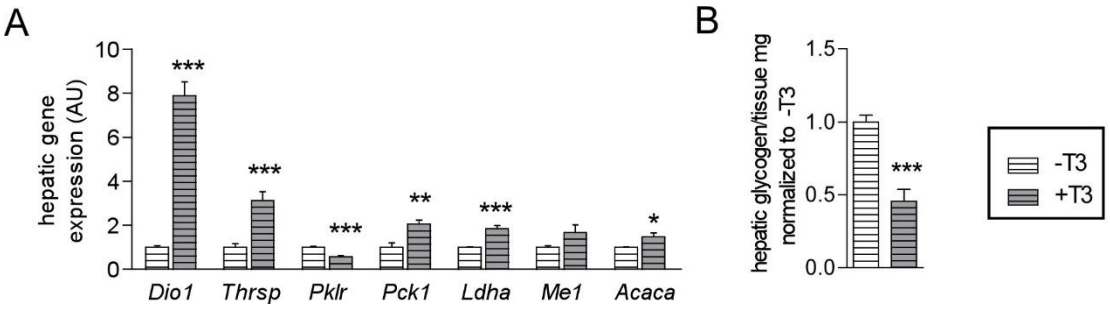

Figure 25: Hyperthyroidism in the liver and reduced hepatic glycogen content after T3 treatment (Modified from (189)).
(A) Expression levels of hepatic genes normalized against the mean of *Cyclophilin* and *Hprt* (n=7 for -T3; n=8 for +T3).
(B) Hepatic glycogen content normalized to animals without (-T3) treatment (n=7 for -T3; n=8 for +T3). All values are shown as mean ± S.E.M and analyzed with unpaired Student's t-test with Welch's correction with *: $p<0.05$; **: $p<0.01$; ***: $p<0.001$ vs. the untreated (-T3) animals. *Acaca*, acetyl-CoA carboxylase 1; AU, arbitrary units; *Dio1*, iodothyronine deiodinase type I; *Hprt*, hypoxanthine-guanine phosphoribosyltransferase; *Ldha*, lactate dehydrogenase; *Me1*, malic enzyme; *Pck1*, phosphoenolpyruvate carboxykinase 1; *Pklr*, pyruvate kinase; *Thrsp*, thyroid hormone responsive gene spot 14.

3.2.3. How does the cardiovascular system react to T3 administration?

The heart weight is the best rough indicator of cardiac hypertrophy and therefore, the mice were sacrificed, the hearts were collected, and weighted. The hyperthyroid animals showed a clear elevation of heart weight in relation to body weight as compared to WT mice (**Figure 26A**) and in contrast to the *M/O* dko mice, which surprisingly showed no signs of cardiac hypertrophy (**Figure 16A**). Unexpectedly, the baseline heart rate, recorded with the radio telemetry for 72 hours in conscious and freely moving animals, as well as the heart rate displayed as AUC and separated into the light and dark phases was unaffected by the T3 treatment (**Figure 26B+C**).

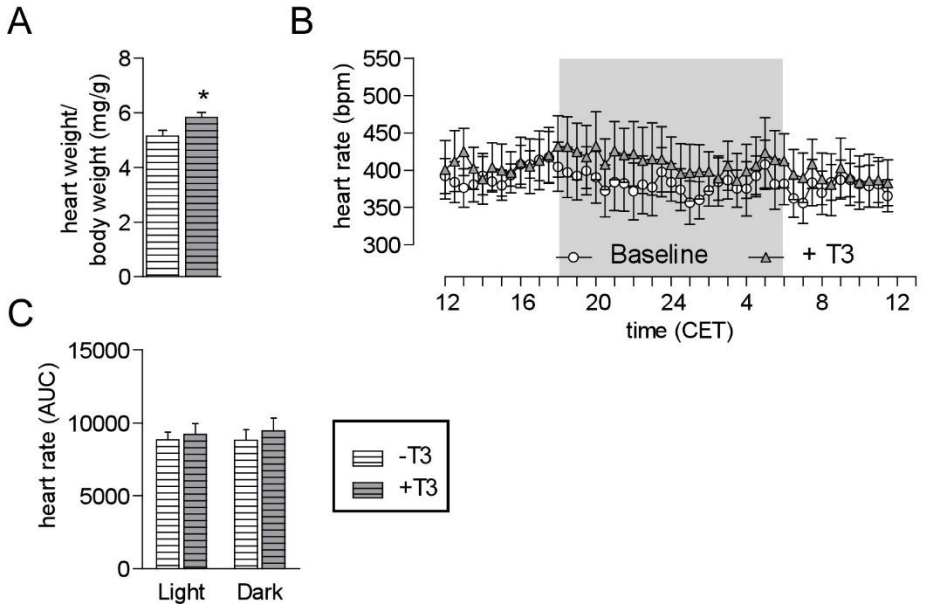

Figure 26: Cardiac hypertrophy but no tachycardia after T3 treatment (Modified from (189)).
(A) Heart weight (mg) in relation to body weight (g) (n=8 for -T3; n=6 for +T3).
(B) Mean twenty-four-hour profile on heart rate (bpm) recorded for 72 hours with radio telemetry in conscious and freely moving animals before and during the T3 treatment (n=6/group). Grey background indicates the dark phase.
(C) Area under the curve of the twenty-four-hour heart rate profiles separated in light and dark phase (n=6/group).
All values are shown as mean ± S.E.M and analyzed with unpaired Student's t-test with Welch's correction (A), two-way ANOVA with Bonferroni post-hoc multiple comparisons test (B) and paired Student's t-test (C). *: $p<0.05$ vs. the untreated (-T3) animals. AUC, area under the curve; bpm, beats per minute; CET, Central European Time.

As the heart rate frequency distribution was severely altered in the *M/O* dko, it was as well investigated in the T3-treated mice. Interestingly, the shifted heart rate frequency distribution was not observed in the T3-treated mice (**Figure 27A,** Supplementary Table 5). Another striking change in the *M/O* dko mice were the tachycardic bursts with bradycardic episodes. This phenomenon was absent in the hyperthyroid animals (**Figure 27B**).

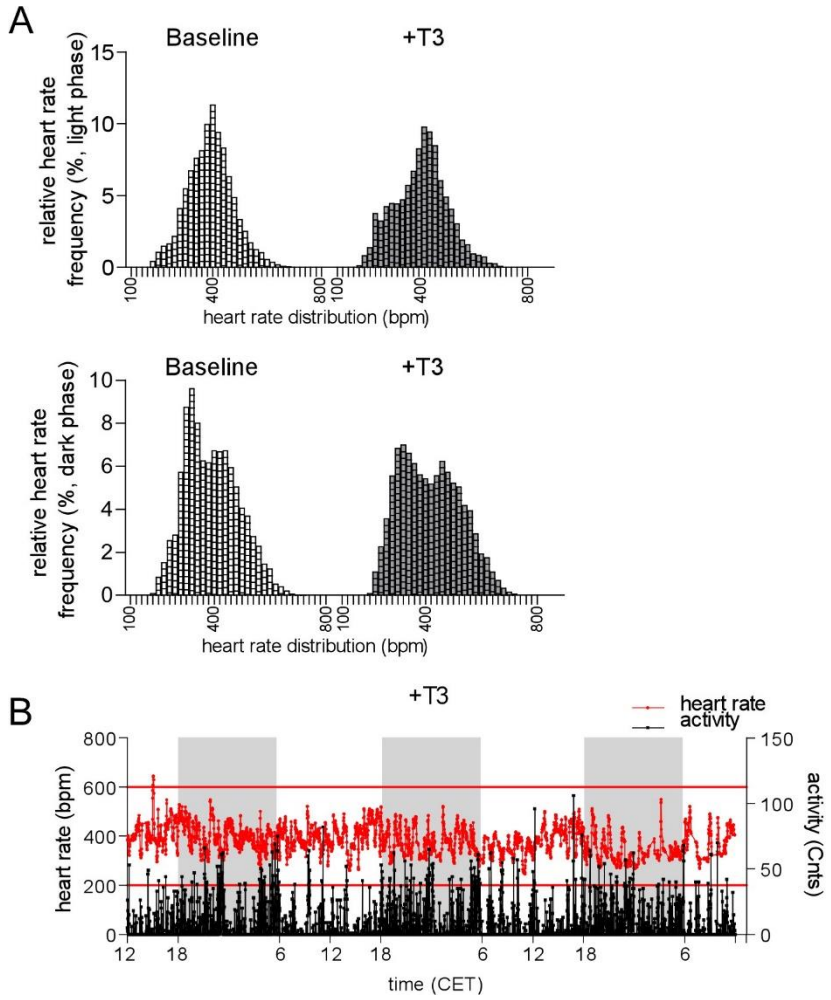

Figure 27: Similar pattern of heart rate frequency after T3 treatment (Modified from (189)).
(A) Heart rate distribution during the light (upper panel) and dark (lower panel) phase in percentage of the relative heart rate frequency (calculated in 20 bpm intervals) before and during T3 treatment. All values are shown as sum of the percentage of the certain heart rate frequency of all animals per genotype and analyzed with two-way ANOVA with Holm-Sidak's multiple comparisons test (n=6/group).
(B) Heart rate plotted against activity level of one representative T3-treated WT mouse over 72 hours. Grey background indicates the dark phase. Red lines indicate the upper and the lower limits of heart rate found in WT controls. Bpm, beats per minute; CET, Central European Time; cnts, counts.

To have a closer look at the PSNS and SNS, first the maximal stress response after a saline injection was tested. The maximal heart rate did not differ before or during the T3 treatment (**Figure 28A**). As a next step, first scopolamine methylbromide, a PSNS blocker, was injected, which was followed by the β-blocker timolol maleate to inhibit the SNS. The analysis revealed a mostly normal working autonomic nervous system with a trend for an increase in SNS (**Figure 28B**). Furthermore, the intrinsic heart rate was significantly increased after the T3 treatment (**Figure 28C**). This could point towards a tissue intrinsic effect due to the hyperthyroidism.

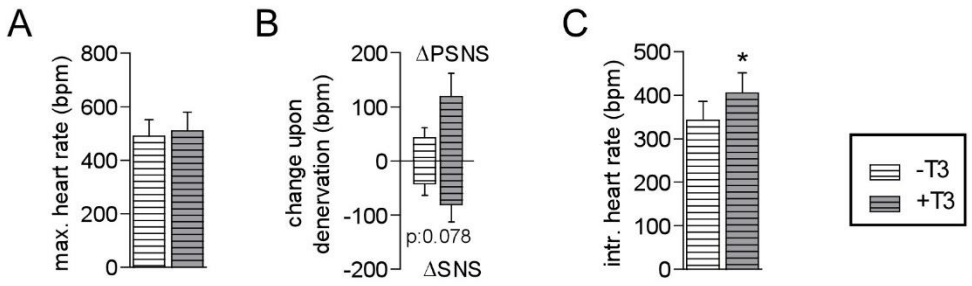

Figure 28: Increased intrinsic heart rate in the presence of unchanged autonomic nervous system input after T3 treatment (Modified from (189)).
(A) Maximum heart rate (bpm) after saline injection before and during T3 treatment (n=6/group).
(B) Change in heart rate upon pharmacological denervation of the PSNS with scopolamine methylbromide and the SNS with timolol maleate before and during T3 treatment (n=5/group).
(C) Intrinsic heart rate after full pharmacological denervation before and during T3 treatment (n=5/group).
All values are shown as mean ± S.E.M and analyzed with paired Student's t-test. *p :<0.05 for T3 vs. baseline. Bpm, beats per minute; PSNS, parasympathetic nervous system; SNS, sympathetic nervous system; Δ, delta.

Lastly, changes on molecular level were investigated by qPCR measurements. A wide range of several TH-responsive and cardiac property genes were investigated. Notably, *Pln*, which is negatively regulated by THs, is in fact downregulated after the T3 treatment (**Figure 29**), implying that this T3 dose is partially able to affect cardiac properties on molecular level. Nevertheless, *Nppb* was also found to be downregulated after the T3 treatment, which is contrary to the first finding, as *Nppb* has been shown to be positively regulated by THs (198, 199). The other tested genes (*Hcn2*, *Hcn4*, *Kcna1*, *Atp2a2*, and α-/β-MHC ratio) were unaffected by the T3 treatment (**Figure 29**).

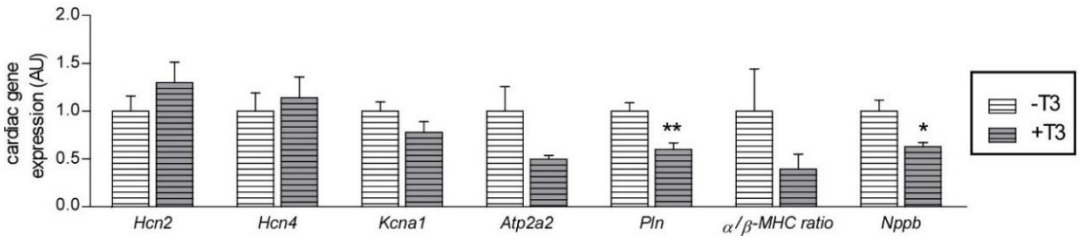

Figure 29: Minor alterations on molecular level in the heart after T3 treatment (Modified from (189)).
Cardiac gene expression levels normalized to *Rpl32* (n=7 for -T3; n=8 for +T3).
All values are shown as mean ± S.E.M and analyzed with unpaired Student's t-test with Welch's correction *: p<0.05, **p<0.01 vs. the untreated (-T3) animals. AU, arbitrary unit; *Atp2a2*; ATPase, calcium transporting, cardiac muscle, slow twitch; *Hcn2/4*, hyperpolarization-activated cyclic nucleotide-gated potassium channel 2/4; *Kcna1*, potassium voltage-gated channel subfamily A member 1; *Nppb*, brain natriuretic factor; *Pln*, phospholamban; *Rpl32*, ribosomal protein L32; *α-MHC*, myosin heavy chain 6 cardiac muscle alpha; *β-MHC*, myosin heavy chain 7 cardiac muscle beta.

In summary, the T3 treatment resulted in an elevation of daytime body temperature with normal iBAT and tail temperature. Furthermore, the T3-treated mice developed cardiac hypertrophy but showed no signs of tachycardia. Also, the intrinsic heart rate was significantly upregulated whereas the heart rate frequency distribution was not altered after 14 days of T3 treatment.

3.3. Part C: Investigation of the safety of TA3 administration in WT mice

TA3 is currently used in clinical trials to treat AHDS patients and to restore TR activity in the brain ((188), ClinicalTrials.gov Identifier NCT02060474 (completed) and NCT02396459 (not yet recruiting)). AHDS patients lack the MCT8 transporter, which in humans is crucial for T3 uptake into the brain. Although, TA3 is a biologically active oxidative deamination metabolite of T3, it reaches the brain through a yet unknown transporter and mechanism. Interestingly, the safety of systemic TA3 drug administration in a healthy control group has not been published so far. Therefore, the aim of this part of the thesis was to evaluate possible effects that are provoked by TA3 administration, which could either worsen or improve the patient's symptoms. In the treatment paradigm, the control mice received daily saline injections (WT -TA3, white patterned) to control for the acute stress response caused by daily injections, whereas the second group received daily TA3 injections (WT +TA3, TA3: 400 ng/g body weight; grey patterned) for 14 consecutive days (**Figure 30A**). This TA3 dose has been used before and was successful in promoting the neural development in *M/O* dko mice (179). After 14 days of treatment, the serum TH levels were investigated and total T3 was found to be unchanged, whereas total T4 was significantly reduced after TA3 treatment, which is in agreement with the literature (**Figure 30B**; (200)). To verify that TA3 reached the brain, expression levels of TH responsive genes in the pituitary were analyzed. Thyroid stimulating hormone subunit beta (*Tshb*) was significantly reduced after TA3 treatment, whereas prolactin (*Prl*) expression was significantly increased (**Figure 30C**). None of the other tested genes, namely the growth hormone (*Gh*), tyrosine hydroxylase (*Th*), and dopamine receptor 2 (*Drd2*) were affected by the TA3 treatment (**Figure 30C**). Throughout this study, metabolic parameters like body weight, and food and water intake were assessed. Neither the TA3 nor the control group showed a difference in body weight gain after treatment at experimental day 14 (**Figure 30D**). Despite this unchanged body weight, the TA3-treated animals consumed more food starting at day seven up to the end (**Figure 30E,** Supplementary Table 6), whereas water intake was comparable (**Figure 30F**).

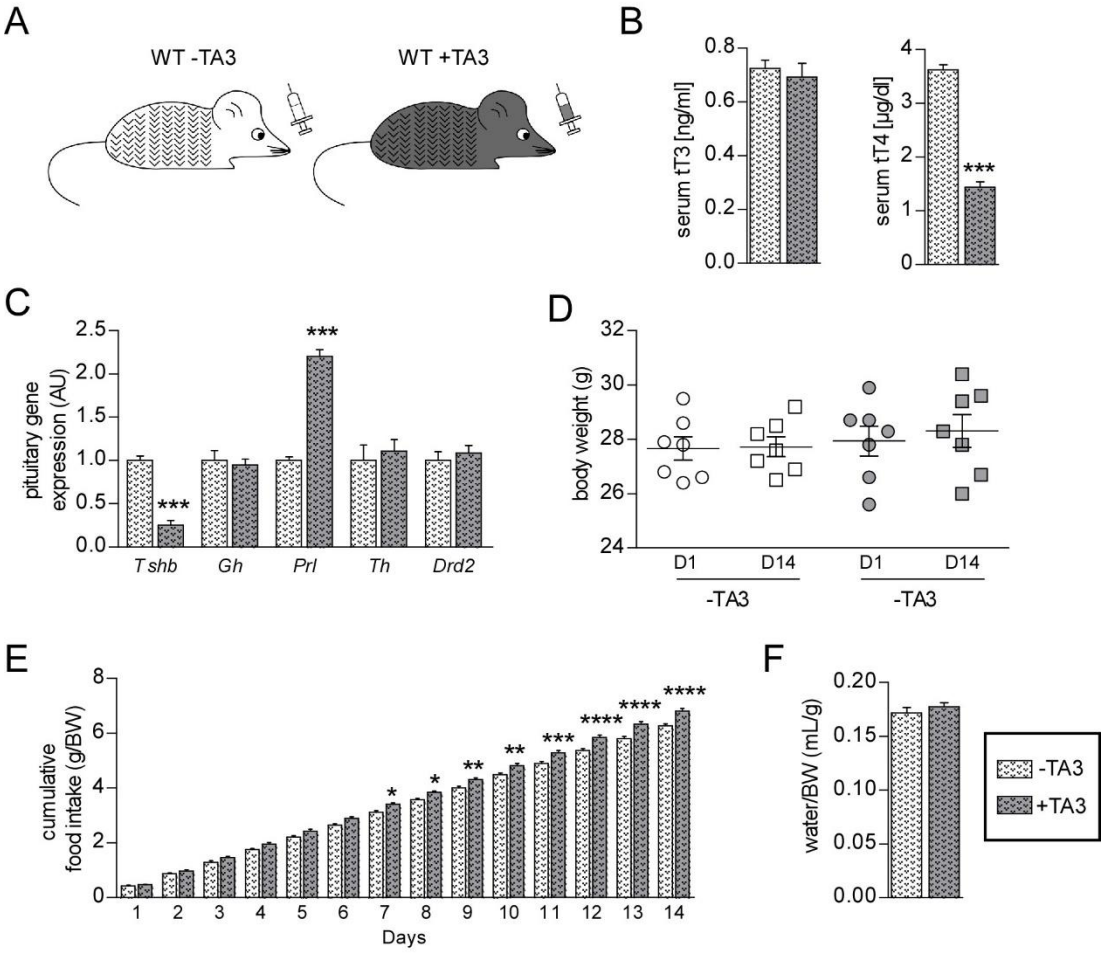

Figure 30: Reduction in serum tT4 and increase in food intake after TA3 treatment.
(A) Schematic overview of the control (WT -TA3, white patterned) and TA3-treated animals (WT +TA3, grey patterned).
(B) Serum total T3 (tT3, left panel) and total T4 (tT4, right panel) concentrations in all animals used in this study (n=7/group).
(C) Pituitary gene expression levels normalized to the mean of *Cyclophilin* and *Hprt* in all animals (n=7/group).
(D) Body weight (g) of animals before (D1) and at the last day of treatment (D14) (n=7/group).
(E) Cumulative food intake (g) in relation to body weight (g) throughout the treatment. Values are shown as sum of the days and analyzed with two-way repeated measures ANOVA and Bonferroni multiple comparisons test (n=7/group).
(F) Average water consumption (mL) in relation to body weight (g) in animals without and with TA3 treatment (n=7/group).
All values are shown as mean ± S.E.M and analyzed with unpaired Student's t-test (A-D, F) *: $p<0.05$; **: $p<0.01$; ***: $p<0.001$; ****: $p<0.0001$ vs. the untreated (-TA3) animals. AU, arbitrary units; BW, body weight; D, day; *Dio2*, iodothyronine deiodinase type II; *Drd2*, dopamine receptor 2; *Gh*, growth hormone; *Hprt*, hypoxanthine-guanine phosphoribosyltransferase; *Prl*, prolactin; TA3, Triac; *Th*, tyrosine hydroxylase; *Tshb*, thyroid stimulating hormone subunit beta; WT, wildtype.

3.3.1. Does TA3 change body temperature and iBAT thermogenesis?

As a next step body temperature as well as heat production and heat loss were investigated by infrared thermography as THs have a crucial role in temperature homeostasis. No differences in the inner ear temperature as indicator of body temperature (**Figure 31A**), iBAT as heat production site (**Figure 31B**) and tail temperature as indicator of heat loss (**Figure 31C**) were detected.

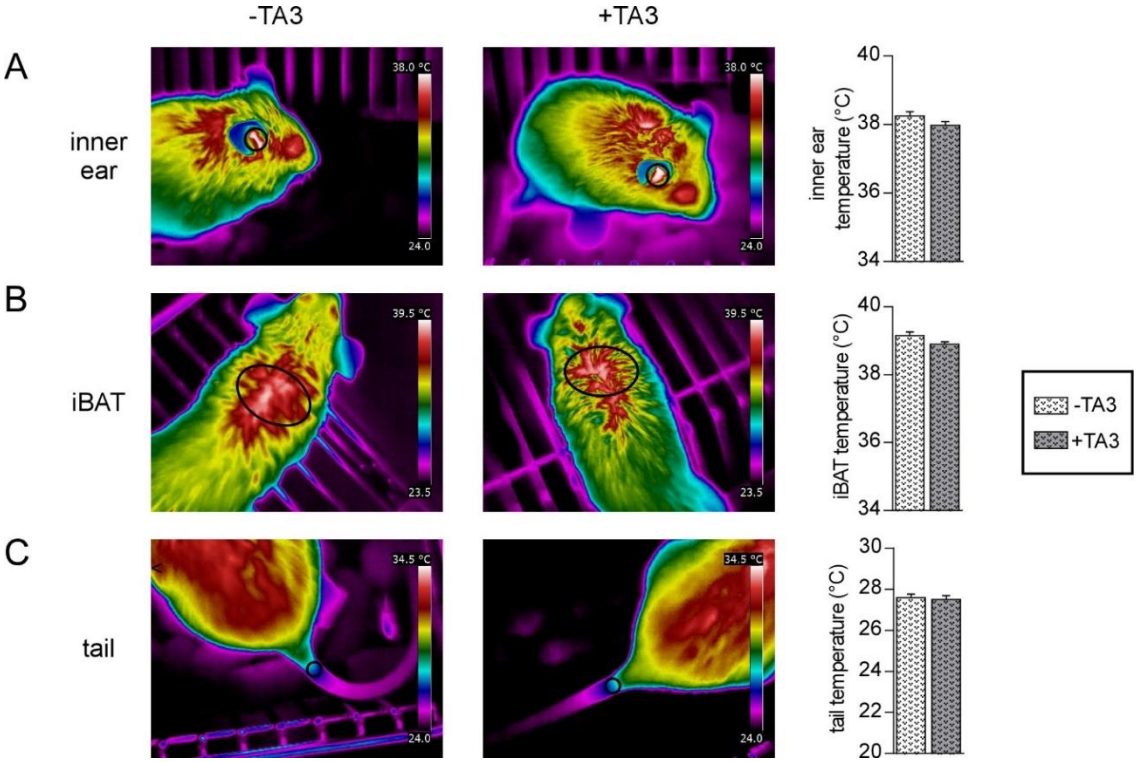

Figure 31: No change of heat production and loss is observed after TA3 treatment.
(A) Representative infrared images of the inner ear at 22°C without and with) TA3 treatment (left panels) and quantification of average maximum temperature (right panel; n=7/group).
(B) Representative infrared images of iBAT at 22°C without and with TA3 treatment (left panels) and quantification of average maximum temperature (right panel; n=7/group).
(C) Representative infrared images of the tail at 22°C without and with TA3 treatment (left panels) and quantification of average maximum temperature (right panel; n=7/group).
All values are shown as mean ± S.E.M and analyzed with unpaired Student's t-test. Black circles visualize area of measurement. iBAT, interscapular brown adipose tissue; TA3, Triac.

As the TA3-treated animals showed a significant increase in cumulative food intake but no change in body weight, the tissue weight of the distinct adipose depots were captured to identify possible body composition alterations. Nevertheless, there were no changes for iBAT, iWAT, and gWAT after TA3 treatment (**Figure 32A**).

To further investigate the thermoregulatory properties gene expression levels were measured. Similar to the *M/O* dko mice a significant reduction of *Dio2* was determined, indicating that iBAT is probably not in a hypothyroid state. In contrast to the *M/O* dko mice, neither *Ucp1* nor *Tfam*

were altered; however, *Adrb3* was significantly increased, suggesting a higher SNS input to the iBAT (**Figure 32B**).

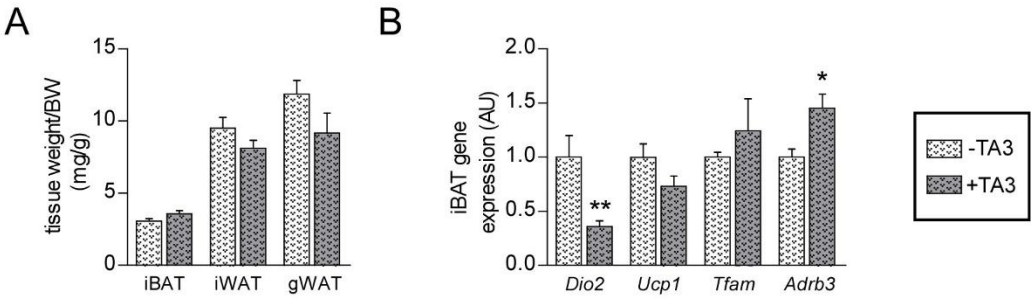

Figure 32: IBAT is not in a hypothyroid state after TA3 treatment.
(A) Tissue weight (mg) in relation to body weight (g) of adipose depots (n=7/group).
(B) Expression levels of genes in iBAT normalized against *Hprt* (n=7/group).
All values are shown as mean ± S.E.M and analyzed with unpaired Student's t-test *: p<0.05; **: p<0.01; vs. the untreated (-TA3) animals. *Adrb3*, adrenergic receptor beta 3; AU, arbitrary units; *Dio2*, iodothyronine deiodinase type II; gWAT, gonadal white adipose tissue; *Hprt*, hypoxanthine-guanine phosphoribosyltransferase; iBAT, interscapular brown adipose tissue; iWAT, inguinal white adipose tissue; TA3, Triac; *Tfam*, mitochondrial transcription factor A; *Ucp1*, uncoupling protein 1.

3.3.2. How is the liver affected by the TA3 treatment?

Hepatic gene expression analysis revealed strongly increased expression of *Dio1* and *Me1* as positively TH-regulated genes, indicating that treatment with TA3 induces hepatic hyperthyroidism (**Figure 33A**). Furthermore, *Pck1* was significantly increased, whereas the other tested genes (*Thrsp*, *Pklr*, *Ldha* and *Acaca*) were not influenced (**Figure 33A**). Hepatic glycogen content was also comparable between both groups (**Figure 33B**).

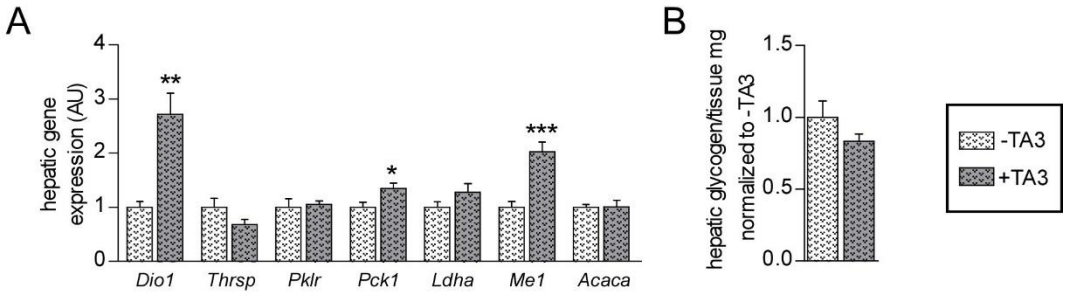

Figure 33: Induction of hepatic hyperthyroidism without changes in the glycogen content after TA3 treatment.
(A) Expression levels of genes in liver normalized against the mean of *Gapdh* and *Hprt* (n=7/group).
(B) Hepatic glycogen content normalized to animals without (-TA3) treatment (n=7/group).
All values are shown as mean ± S.E.M and analyzed with unpaired Student's t-test *: p<0.05; **: p<0.01; ***: p<0.001 vs. the untreated (-TA3) animals. Acaca, acetyl-CoA carboxylase 1; AU, arbitrary units; Dio1, iodothyronine deiodinase type I; Gapdh, glyceraldehyde-3-phosphate dehydrogenase; *Hprt*, hypoxanthine-guanine phosphoribosyltransferase; *Ldha*, lactate dehydrogenase; *Me1*, malic enzyme;

Pck1, phosphoenolpyruvate carboxykinase 1; *Pklr*, pyruvate kinase; TA3, Triac; *Thrsp*, thyroid hormone responsive gene spot 14.

3.3.3. Does TA3 administration influence the cardiovascular system?

As a next step, the cardiovascular system including blood pressure analysis, heart weight, and gene expression levels were analyzed. First, the blood pressure measured via the tail cuff system showed no differences between both groups (**Figure 34A**) and secondly, heart weight was also unchanged (**Figure 34B**). Lastly, gene expression analysis revealed distinct and somehow counterintuitive results, as *Hcn2*, a positively regulated TH response gene, was upregulated, as well as *Pln*, a negatively regulated TH response gene (**Figure 34C**). This could indicate that specific cell types respond differently to the TA3 treatment. The MHCs are major cardiac contractile proteins and a shift from α-*Mhc* to β-*Mhc* (a reduction in α-/β-*Mhc* ratio) was seen after TA3 treatment (**Figure 34C**). Other tested genes, including *Hcn4*, *Atp2a2*, *Nppb*, *Ryr2*, adrenergic receptors 1 and 2 (*Adrb1/2*) as well as muscarinic receptor 2 (*Chrm2*) were unchanged (**Figure 34C**).

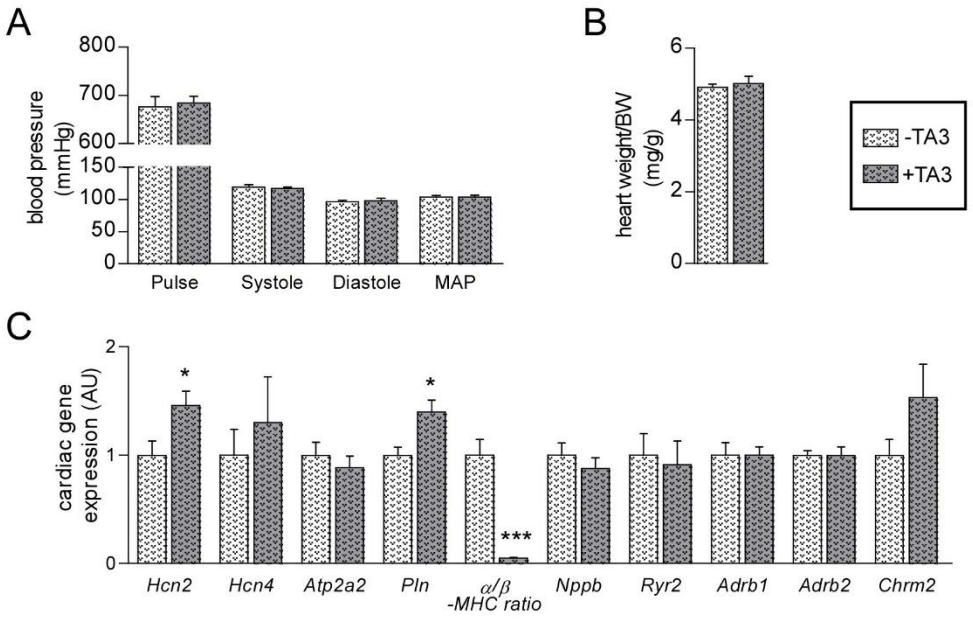

Figure 34: Distinct changes on molecular level in the heart after TA3 treatment.
(A) Pulse, systolic, diastolic and mean arterial pressure (MAP) (n=7/group).
(B) Heart weight (mg) in relation to body weight (g) (n=7/group).
(C) Cardiac gene expression levels normalized to the mean of *Cyclophilin* and *Rpl32* (n=7/group).
All values are shown as mean ± S.E.M and analyzed with unpaired Student's t-test *: $p<0.05$; **: $p<0.01$; ***: $p<0.001$ vs. the untreated (-TA3) animals. *Adrb1/2*, adrenergic receptor beta 1/2; *Atp2a2*, ATPase, calcium transporting, cardiac muscle, slow twitch; AU, arbitrary units; BW; body weight; *Chrm2*, muscarinic receptor 2; *Hcn2/4*, hyperpolarization-activated cyclic nucleotide-gated potassium channel 2/4; mmHg, millimeter of mercury; *Nppb*, brain natriuretic factor; *Pln*, phospholamban; *Ryr2*, ryanodine receptor 2; TA3, Triac; *α-MHC*, myosin heavy chain 6 cardiac muscle alpha; *β-MHC*, myosin heavy chain 7 cardiac muscle beta.

3.3.4. Has TA3 a similar effect on muscle metabolism as THs?

It has been shown, that systemic treatment with THs activates thermogenic pathways also in muscles leading to increased lipid uptake and muscle wasting (119). Therefore, a metabolic profile analysis of Musculus soleus (M. soleus) and Musculus gastrocnemius (M. gastr.) has been performed. The tissue weight of M. gastr. in relation to body weight was significantly reduced after TA3 treatment, whereas the tissue weight of M. soleus was not altered (**Figure 35A**). Further gene expression analysis of M. gastr. showed only a reduction of uncoupling protein 3 (*Ucp3*), which is involved in wasting cellular energy (201). However, further genes such as the mitochondrial shuttle glycerol-3-phosphate dehydrogenase 2 (*Gpd2*), the important regulator of muscle lipid metabolism peroxisome proliferator-activated receptor delta (*Pparδ*), as well as genes involved in Ca^{2+} cycling (sarcolipin (*Sln*) and ryanodine receptor 1 (*Ryr1*)) were not altered in M. gastr. (**Figure 35B**). Surprisingly, in M. soleus *Ucp3*, *Pparδ*, and *Gpd2* were significantly reduced and a trend for reduced *Sln* expression levels was measured after TA3 treatment (**Figure 35C**). However, investigation of protein levels of both SERCA2 (**Figure 35D**) and OXPHOS complexes (**Figure 35E**) were unchanged. Despite the unchanged protein levels, the exposed molecular alterations could point towards a hypothyroid state in the muscle.

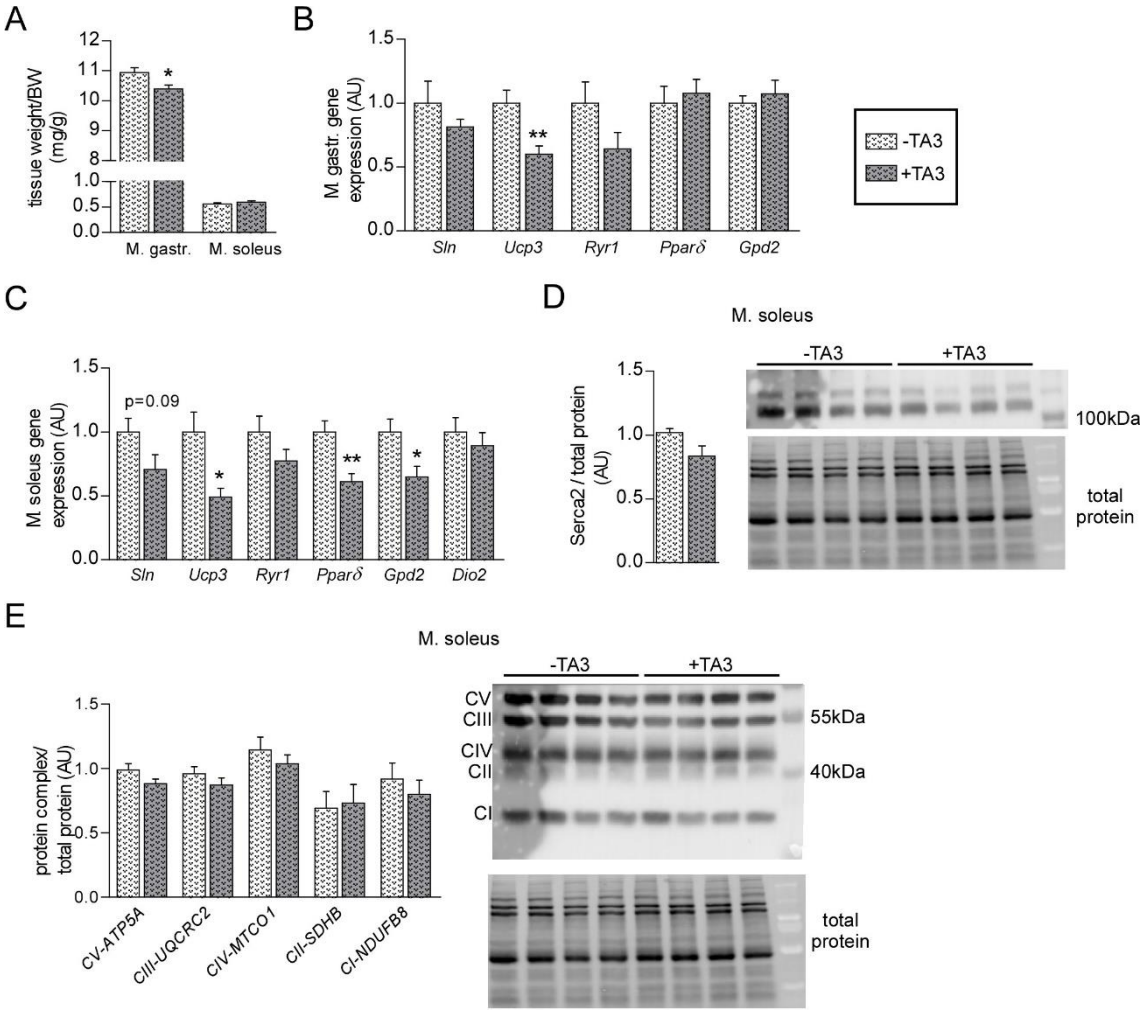

Figure 35: Genes responsible for muscle lipid oxidation, mitochondrial uncoupling, and metabolism are downregulated after TA3 treatment.

(A) Tissue weight (mg) in relation to body weight (g) of M. gastrocnemius and M. soleus (n=7/group).

(B) Expression levels of genes in M. gastrocnemius normalized to the mean of *Hprt* and *Gapdh* (n=7/group).

(C) Expression levels of genes in M. soleus normalized to the mean of *Cyclophilin* and *Hprt* (n=7/group).

(D) Quantification of SERCA2 protein levels normalized to total protein levels in M. soleus and a representative western blot image (n=7/group).

(E) Quantification of proteins representing the different OXPHOS complexes (CI – CV) normalized to total protein levels in M. soleus and a representative western blot image (n=7/group).

All values are shown as mean ± S.E.M and analyzed with unpaired Student's t-test *: $p<0.05$; **: $p<0.01$ vs. the untreated (-TA3) animals. AU, arbitrary units; BW, body weight; CIII-UQCRC2, Complex III ubiquinol-cytochrome c reductase core protein 2; CII-SDHB, Complex II succinate dehydrogenase subunit; CI-NDUFB8, NADH ubiquinone oxidoreductase subunit B8; CIV-MTCO1, Complex IV Cytochrome C Oxidase core subunit 1; CV-ATP5A, Complex V F1-F0 ATP synthase subunit; *Dio2*, iodothyronine deiodinase type II; *Gpd2*, glycerol-3-phosphate dehydrogenate 2; *Hprt*, hypoxanthine-guanine phosphoribosyltransferase; kDa, kilodaltons; M. gastr., Musculus gastrocnemius; M. soleus, Musculus soleus; OXPHOS, oxidative phosphorylation; *Pparδ*, peroxisome proliferator-activated receptor delta; *Ryr1*, ryanodine receptor 1; SERCA2, sarcoendoplasmic reticulum Ca^{2+}-ATPase; *Sln*, sarcolipin; TA3, Triac; *Ucp3*, uncoupling protein 3.

Taken together, the systemic TA3 treatment revealed no changes in heart pulse, blood pressure, and gene expression levels indicating that the heart is neither in a hypothyroid nor in a hyperthyroid state. Importantly, this is not the case for the liver, as TH responsive and metabolic genes were upregulated indicating that TA3 itself exerted strong thyromimetic effects in the liver. Furthermore, in the M. soleus the genes responsible for muscle lipid oxidation, mitochondrial uncoupling to dissipate energy in form of heat and metabolism are downregulated pointing towards hypothyroidism.

4. Discussion

This study demonstrates that distinct phenotypical traits of hyperthyroidism only develop if the central effects of THs are ensured and provided. This is of immediate relevance to the research field because during the last decades, research started to focus on the TH action in the brain instead of exclusively on the direct interaction of THs with the target tissue, which nevertheless remains an important research field. However, identifying the central contributions in the symptom development of TH diseases would pave the way for new treatment options and allow for a more custom-tailored treatment. Recent studies have shown that direct administration of T3 into the rodent brain mimics the effects of whole-body hyperthyroidism (95). These experiments are highly insightful as they identify the underlying mechanisms; however, they are somewhat unphysiological as they bypass several physiologically relevant control mechanisms such as the BBB. Even though intraventricular routes of drug administration in humans are used for chemotherapy, this approach is not an effective treatment for a bulky disease of brain tissue (202). In animal models, the separate modulation of the TH status in the brain versus the periphery has been tricky to achieve so far. Fortunately, the recent establishment of mouse models that are deficient in specific THTs, which leads to a unique tissue-specific TH state, have opened up new experimental approaches.

Here, I took advantage of mice lacking the THTs MCT8 and OATP1C1 (*M/O* dko mice), which present elevated serum T3 levels in the periphery while the brain is in a profoundly hypothyroid state. These mice were analyzed regarding their thermogenic and cardiovascular properties (Part A). In order to dissect the central contributions from the peripheral ones, WT animals were treated with a low T3 dose to achieve the same serum TH parameters as the *M/O* dko mice. This led to peripheral but more importantly to central hyperthyroidism in contrast to the *M/O* dko mice (Part B). The comparison of these two models allowed the differentiation between the central and peripheral site of TH action, which are summarized in **Table 18**. However, there are three potential explanations for the observed differences: (i) the absence of THTs in the peripheral tissues could negatively influence the TH import resulting in a hypothyroid state, (ii) the severe developmental defects in the brain of the *M/O* dko animals could alter the central control permanently and (iii) the hypothyroid brain could modulate the central control in the *M/O* dko mice. These scenarios will be further disentangled in the following discussion. As the *M/O* dko mice reflect the phenotype of AHDS patients, which carry inactivating mutations in MCT8, these findings might be clinically relevant. In the third part, the focus was shifted on possible side effects of pharmacological intervention with TA3 as a therapeutic drug, for which promising effects have been presented so far.

Table 18: Summary of the possible origins of the distinct phenotypic traits.

	Characteristics	*M/O* dko mice	T3-treated mice	Conclusion
Cardiovascular System	Heart weight	=	↑↑	Requires hyperthyroid CNS
	Heart rate	=	=	T3 dose is not sufficient
	Heart rate frequency distribution	Broader distribution with tachycardic bursts during locomotion	=	Hypothyroid CNS is responsible
	ANS	=	↑	Requires hyperthyroid CNS
	Intrinsic heart rate	=	↑↑	Requires hyperthyroid CNS
	Cardiac gene expression	=	Only *Pln* ↓↓, *Nppb* ↓↓	T3 dose is not sufficient
Thermoregulation	Body temperature	=	↑↑	Requires hyperthyroid CNS
	Activity	=	=	No effect
	IBAT temperature	=	=	No effect
	Thermogenic markers	↓↓	=/↓	Hypothyroid CNS is responsible/long term adaptation to elevated T3 levels
	Tail temperature	=	=	No effect

ANS, automatic nervous system; CNS, central nervous system; iBAT, interscapular brown adipose tissue; *Nppb*, brain natriuretic factor; *Pln*, phospholamban; =, unchanged; ↑ tendency for increase; ↑↑ significantly increased; ↓ tendency for reduction; ↓↓ significantly reduced.

4.1. Are MCT8 and OATP1C1 critical for TH uptake in the periphery?

In order to interpret the presented results, it is essential to first evaluate the tissue-specific TH status in the absence of MCT8 and/or OATP1C1 as this could also lead to a hypothyroid state in selected organs other than the brain. The OATP1C1 transporter shows a very restricted expression pattern in the brain, particularly in the paraventricular region. Also in line, the single *Oatp1c1* ko mice presented an unremarkable phenotype with normal gene expression levels, despite a decrease in brain T4 content (176). Furthermore, the only striking effect seen in the *Oatp1c1* ko mice was after cold exposure, as the animals had problems defending their body temperature. This is similar to what has been described for the first patient with a loss of OATP1C1, who has been identified very recently. In particular, the patient suffered from cold intolerance with low body temperature (<37°C) and cold hands and feet (203).

Mct8 is more broadly expressed than *Oatp1c1* but the absence of MCT8 did also not lead to a hypothyroid state in the investigated tissues. This was examined by expression levels of *Dio1* and *Dio2* as they are positively and negatively regulated by THs, respectively (17). The hepatic *Dio1* mRNA levels were elevated indicating that THs are still transported into the liver. Furthermore, *Dio2* expression levels were reduced in iBAT demonstrating that THs are sufficiently present in iBAT. Even more important, it has been shown by others that the liver, skeletal muscle, iBAT, and kidney has either increased or normal T3 content in the absence of MCT8 (154, 167, 169, 170). Regarding the heart, the T3 sensitive pacemaker channels *Hcn2* and *Hcn4* were not reduced, instead they were even mildly elevated, indicating that the heart is probably not in a hypothyroid state. This lack of effect can be explained by the presence of additional THTs, such as MCT10, which was detected in the liver, heart, and iBAT. Taken together, this suggests that the described effects in the *M/O* dko mice are probably not caused by an impaired TH transport into the liver, iBAT, and heart.

4.2. Could the effects be the result from a developmental brain defect?

Another point to be considered for interpreting the results is the comparison between acute and developmental effects. THs are essential during nervous system development as they regulate various processes, including neuronal proliferation, migration, growth of axons and dendrites, synapse formation, and myelination (reviewed in (204)). Additionally, insufficient TH supply early postnatally results in growth retardation, delayed motor development and severe mental impairments. A recent study from our group presented detailed information on the correlation between TH absence (prenatal or postnatal) and development of specific neuron populations in the brain (112). More in detail, in the *M/O* dko mice the neuronal populations in the motor cortex were significantly reduced, which shows that the *M/O* dko mice have indeed developmental impairments (112). These developmental impairments could result in a phenotype that is observed

in the *M/O* dko mice but not in the T3-treated animals. As populations of parvalbuminergic neurons are directly linked to blood pressure and the cardiovascular system, the altered heart rate frequency distribution with tachycardic bursts and bradycardic episodes in the *M/O* dko mice could be a developmental brain problem (96). Despite this question of origin, the *M/O* dko model reflects the combination of acute and developmental brain hypothyroidism also seen in the AHDS patients and is therefore of clinical interest. Furthermore, these developmental defects are downstream of the defective TH transport into the brain. Therefore, it is irrelevant for the presented results whether the neuroanatomical structures responsible for processing the T3 effects are properly developed because T3 does not get transported into the brain in the first place. Taken together, the differences observed between the *M/O* dko model and T3-treated animals are caused primarily by a general lack of central T3 action, independent of additional developmental defects.

4.3. What are the central contributions to metabolism and thermoregulation?

Adaptation of whole-body energy homeostasis in M/O dko mice.

The aspect of energy homeostasis is of great interest, as all AHDS patients suffer from weight loss (188). It has been published, that the *Mct8* ko mice are hyperphagic, with the tendency to use more carbohydrate as fuel during the dark phase (141, 170). Furthermore, it was reported that the *Mct8* ko mice were leaner with a reduction in fat mass as compared to the controls and that they also had a greater total energy expenditure independent of motor activity (170). In this study, the *M/O* dko mice also had a tendency for reduced body weight compared to the WT animals, and they had significantly increased food intake with comparable motor activity. In contrast, the *Mct8* ko mice presented normal body weight and food intake compared to the WT animals. This is contrary to the published data, but the age of the animals during experiments differs: The animals in this study were analyzed at the age of four to five months in contrast to the rather young ten to twelve weeks old animals in the published study (170). Therefore, the observed differences could be due to two reasons: First, mice continue to grow throughout their entire life, which could result in additional weight gain. Second, THs positively influence growth hormone synthesis, which could lead to an increased growth rate during thyrotoxicosis (reviewed in (205)). Nevertheless, the reduction in body weight and presence of hyperphagia in *M/O* dko mice demonstrates difficulties in maintaining body weight, which might be partially due to increased energy expenditure in response to the high serum T3 levels as published for the *Mct8* ko mice (170).

Hepatic switch from glycolysis to gluconeogenesis in response to hyperthyroidism requires central TH action.

The investigation of metabolic changes in the liver revealed strongly elevated *Dio1* and *Spot14* gene expression levels after T3 treatment, clearly demonstrating the hyperthyroid state of the liver. The *M/O* dko mice had similar changes, which highlights the fact that the liver does not rely

solely on MCT8 as THT and that the elevated TH levels affect the liver directly. After T3 treatment, enhanced level of *Pck1* and reduced *Pklr* transcript levels were detected in the WT mice, which points to a switch from glycolysis to gluconeogenesis. This switch was accompanied by a reduction in hepatic glycogen stores, both indicating increased glucose demand in the body. Furthermore, this clear pattern was not observed in the *M/O* dko mice and suggests that the central TH action is required for the induction of hepatic glucose production. The described phenomenon has already been previously observed in a study in which rats underwent hepatic sympathetic denervation and precise administration of T3 within the hypothalamus was performed afterwards. The denervation completely prevented the hypothalamic T3-induced endogenous glucose production (191). Furthermore, a recent study demonstrated that central T3 increases lipid oxidation through the vagus nerve and downstream effects of c-Jun N-terminal kinase 1 (206). This kinase plays an essential role in hypothalamic regulation of feeding and glucose and metabolism (207). Despite the growing understanding of the molecular mechanisms, the exact physiological role of central T3 in regard to the liver is still unknown.

Daytime elevation of body temperature in the T3-treated mice.

Hyperthyroidism also influences energy homeostasis and results in heat intolerance in patients. Already after nine to twelve days of T3 treatment, the animals had an increase in body temperature of about 0.6°C during the light phase. This increase is comparable to studies which used even higher T3 concentrations and/or T4 treatment (119, 208). Investigation of the tail and iBAT temperature revealed no differences in the T3-treated animals. Therefore, the observed increase in body temperature indicates that all heating defense mechanisms have been overturned. As this elevation occurs only during daytime, which is the resting phase for mice, the mice are curled up in their nest and the heat dissipation over the tail surface is less efficient. Interestingly, this body temperature increase was absent in both, the *Mct8* ko and the *M/O* dko mice despite their similarly elevated T3 serum levels. However, both mouse models showed a small albeit not significant difference in iBAT temperature, which was accompanied by significant reductions in the thermoregulatory gene expression levels, in contrast to the T3-treated mice. The increase in body temperature and the unchanged iBAT temperature as well as gene expression levels after T3 treatment seem contrary, because it has been shown that central T3 leads to iBAT activation in rats (95, 118). However, recently our group could demonstrate that T3 modulates the central body temperature setpoint influencing body temperature and depending on the ambient temperature resulting in hyperthermia and/or pyrexia (119). From these data, it can be concluded that in the present study the T3 shifts the central setpoint in WT animals, leading to the increase in body temperature. This central resetting does not occur in the *M/O* dko mice, as these mice have strongly reduced TH levels in the brain. Therefore, these mice defend a lower body temperature. Furthermore, the reduction of the thermoregulatory markers could be a long-term adaptation to

the high serum TH levels. Taken together, these data show an elevation of daytime body temperature due to the hyperthyroid status of the brain.

4.4. What are the central contributions regarding the cardiovascular system?

Cardiac hypertrophy in the T3-treated mice.

Hyperthyroidism has many effects on the cardiovascular system and one key hallmark is the cardiac hypertrophy. This was also present in the T3-treated animals, which showed a 15% increase in heart weight. Taking the subtle changes of cardiac gene expression levels and the limited duration of hyperthyroidism into account, it is to an extent comparable to a physiological hypertrophic phenotype (reviewed in (105)). Surprisingly, the *M/O* dko mice did not show any signs of cardiac hypertrophy, despite their similarly elevated serum T3 levels. One could speculate that the absence of MCT8 in the heart prevents the exposure to the elevated serum T3 levels. However, the hearts of the *Mct8* ko and *M/O* dko mice did not show any molecular signs pointing towards hypothyroidism as evidenced by unchanged gene expression levels, the even mildly elevated T3 responsive genes *Hcn2* and *Hcn4*, and the comparable intrinsic properties in the pharmacologically denervated heart. Therefore, the absence of hypothyroidism probably indicates compensation by another THT, most likely MCT10. It can be concluded that the central contribution is obligatory for the T3-induced cardiac hypertrophy. This is supported by a previous study, which used heart transplantation to differentiate between indirect and direct effects of THs. It revealed that hyperthyroidism resulted in cardiac hypertrophy only in the thoracic working heart but not in the heterotopic transplanted heart (209, 210). In line with this are more recent studies demonstrating that the SNS plays a crucial role in developing hypertrophy by using either β-blocker (propranolol, (211)) or β-less mice (lacking the three known β-ARs, (212)), which still showed an increase in heart weight in response to hyperthyroidism. Furthermore, overexpression of human DIO2 selectively in the myocardium resulted in an increase in the myocardial thyroid status in the presence of systemic euthyroidism. The local T3 increase led to tachycardia but not to hypertrophy, showing that T3 alone is not sufficient to induce hypertrophy (213). Taken together, these data indicate that the hyperthyroid brain is required for developing cardiac hypertrophy.

No signs of tachycardia.

Unexpectedly, neither the *Mct8* ko nor the *M/O* dko mice showed any signs of chronic tachycardia, even though it is another key characteristic of hyperthyroidism (214). Surprisingly, also the T3-treated animals presented normal heart rates and no tachycardia, suggesting that the increase in serum T3 is not sufficient to induce tachycardia. This hypothesis is supported by the literature, as the classical landmark study used fourfold higher T3 doses, which resulted in a 25% increase in heart rate (215). Another study in which the overexpression of human DIO2 in the

myocardium resulted in tachycardia along with increased levels of *Hcn2* supports this further (213). The gene expression data from the *M/O* dko and T3-treated mice revealed no differences, which would have been expected in case of cardiac thyrotoxicosis. Furthermore, according to the gene expression data the hearts were also not in a hypothyroid state, which further highlights the role of the low T3 dose with approximately 800 ng/day. Nevertheless, a long-term adaptation of the *M/O* dko heart could additionally contribute to the lack of T3 response. The absence of tachycardia is contrary to the AHDS patients, who present a high resting heart rate (188). However, the heart rate recording has been performed by an external device that was attached to the bodies for a prolonged time period. This change in general routine is likely an enormous stress factor for mentally retarded children and could therefore potentially result in an increase in heart rate. Furthermore, there could be other possible explanations as human and mice differ among others in the autonomic control as well as in the environmental temperature. Regarding the former, in humans the parasympathetic tone is predominant, whereas in mice it is mainly the sympathetic tone leading to a higher resting heart rate (64). The latter aims for the fact that humans create mostly a thermoneutral zone for themselves, while laboratory mice are constantly cold challenged (216). Under these conditions, the mice are stressed, leading to a higher energy expenditure and increased sympathetic tone. Therefore, either the elevated serum T3 levels, the exposure to stress, or species-specific differences could be the origin of tachycardia but it cannot definitely be identified. Despite the lack of tachycardia, the T3-treated animals showed a significant but mild increase in the intrinsic heart rate, which displays the heart rate in a full denervated state. Furthermore, pharmacological intervention revealed a tendency for increased SNS tone in the T3-treated animals, in contrast to the *M/O* dko mice which presented unaffected SNS and PSNS tone. This suggests that the ANS is in general capable of compensating minor T3 effects in the heart. As the administration of pharmacological blockers aimed to identify long-term changes in the ANS, it can be summarized that the *M/O* dko mice have no chronic alterations in the autonomic control of the heart.

Significant altered heart rate frequency distribution in the M/O dko mice.

Using the heart rate telemetry data over 72 hours with data collection every minute, the frequency distribution was calculated, which describes acute changes in the autonomic system. Most remarkably, significant changes in frequency percentages exclusively in the *M/O* dko mice were detected but were neither present in the *Mct8* ko nor in the T3-treated animals. These changes consisted of especially increased lower (180 and 200 bpm) and higher (400 and 420 bpm) heart rates with reduced medium heart rates. A shift in heart rate frequency distribution has been also observed in animals of the TRα1 mutant mice (217). These mice displayed a general reduction in medium frequencies compared to control animals, which is probably due to the hypothyroid state of the heart in these animals. Another main finding of this work was the correlation between the heart rate values of every minute with the locomotor activity in the *M/O* dko mice. More in detail,

tachycardic bursts occurred during short periods of locomotor activity, while bradycardic episodes occurred at rest. In general, cardiovascular adjustments have to occur during exercise to meet the demands of working muscles and skin blood. Therefore, after initiation of physical activity several signals from higher brain centers are sent into the medullary cardiovascular center, which then triggers a rapid increase in heart rate and a shift from a parasympathetic to a mainly sympathetic control (218). This shift in parasympathetic and sympathetic contribution can be deducted from the heart rate variability, which is the quantification of the distribution of time intervals between successive heartbeats. Interestingly, prolonged exercise duration can be linked to parasympathetic withdrawal (lower heart rate variability) and increase in heart rate, which might contribute to a cardiovascular drift (219). In the *M/O* dko animals the tachycardic bursts occurred mostly for only a three minute duration suggesting that the impaired central autonomic control is triggered by short-term physical activity. Furthermore, such tachycardic bursts have also recently been found in AHDS patients, which seems to be a frequent cause for the sudden death of these patients (188).

4.5. Which effects have been observed after TA3 treatment and what is the translational value?

In this part, possible side effects of TA3 treatment in WT animals were evaluated. This is of special interest for the AHDS patients as TA3 has the greatest beneficial effects among all tested treatment options so far. First of all, TA3 has been successfully used before in clinical trials in patients with thyroid cancer (220) and also with resistance to THs due to mutations in THRB (221). Furthermore, several *in vitro* studies showed that TA3 promotes cerebellar Purkinje cell differentiation and that the cellular uptake is independent of MCT8 (179, 222). More importantly, daily treatment with TA3 in *M/O* dko mice between postnatal days one to twelve largely prevented the abnormal brain development indicating that TA3 can replace T3 during brain development (179). Therefore, the first clinical trial administering TA3 was launched in 2014 and revealed beneficial effects on the peripheral phenotype in patients with AHDS (188). This trial only focused on the peripheral phenotype and therefore, a second clinical trial is on its way to evaluate the effects of TA3 administration to younger patients with the focus on the neurological phenotype (https://clinicaltrials.gov/ct2/show/NCT02396459). Consequently, it is essential to further investigate TA3 as a potential treatment option and to identify any pitfalls.

Impact on the metabolic and thermoregulatory properties.

After 14 days of TA3 treatment the serum TH parameters showed unchanged total T3 serum levels with significantly reduced total T4 serum levels. This reduction in total T4 levels has been reported previously (200) and is due to the TSH-suppressive effects of TA3, also seen in the reduction of pituitary *Tshb* gene expression levels (223, 224). This consequently leads to a

decrease in plasma T4 levels (225). Furthermore, starting at day seven of TA3 treatment the mice consumed more food until the end of the treatment, which is comparable to the increased food intake during T3 treatment. Differently, the food intake did not result in an increase in body weight or in adipose tissue depots weight. Regarding the AHDS patients, an increase in body weight after twelve months of treatment has been documented, which might be due to the divergent starting conditions (188). The AHDS patients present peripheral thyrotoxicosis with remarkable body weight loss and the TA3-treated WT animals were euthyroid before treatment. The further investigation of the thermoregulatory capacities including inner ear, iBAT, and tail temperature revealed no differences at the time of measurement; however, iBAT seems not to be in a hypothyroid state as indicated by reduced *Dio2* gene expression levels. Nevertheless, it is still possible that thermoregulatory effects directly following Triac administration could have been missed as the experiments were performed approximately 24 hours after the administration and TA3 has a half-life of six hours in humans (226). Another aspect that was studied was the effect of TA3 on the liver and most importantly, an increase of hepatic T3-responsive genes was found after TA3 treatment. This indicates that TA3 itself has strong thyromimetic effects in the liver. However, it has been described that in most patients the hypermetabolic state of the liver was reversed. Nevertheless, hepatic failure has also been observed in one patient (188). Therefore, it is of immediate clinical relevance because the hyperthyroid state of the liver could be even more induced, which needs to be further evaluated.

Impact on the cardiovascular system.

Recently, high systolic blood pressure was uncovered in AHDS patients, which was reversed during the TA3 trial (188). Regarding the blood pressure in the *M/O* dko mice, the systolic pressure was not changed compared to the control animals. However, in the two-way ANOVA a significant value for the genotype interaction was observed. This indicates that the combined absence of both transporters, MCT8 and OATP1C1, could affect blood pressure regulation in contrast to absence of MCT8 or OATP1C1 alone. Furthermore, the TA3 treatment had no effects on the blood pressure after 12-14 days of treatment. The heart weight after TA3 treatment was unaltered, however, *Hcn2* gene expression levels were increased with simultaneously reduced *Pln* levels. One explanation could be that specific cell types respond differently to the TA3 treatment. More strikingly, a shift from α-*Mhc* to β-*Mhc* (a reduction in α-/β-*Mhc* ratio) was seen after TA3 treatment. Such a shift from α-MHC to β-MHC had been shown to be associated with the development of cardiac hypertrophy (227). One could speculate that these molecular changes could hint to a development of cardiac hypertrophy in the long run as seen in the T3-treated animals. The same clinical study exposed the presence of high frequencies of premature atrial complexes in AHDS patients (188). This presence predisposes the patients to arrhythmias and cardiac death, which has been identified as a frequent cause of death in these patients. The arrhythmias could develop due to changes in heart rate frequency distribution as observed in the

M/O dko mice and could be triggered by physical activity. As mice can also develop spontaneous arrhythmias, the translation to the human situation is possible. Therefore, these arrhythmic events constitute a major risk factor in the AHDS patients. So, these data advocate strategies using TH analogues such as TA3, to restore central TH action and reduce the risk of arrhythmias (188). Another approach could be an autonomic regulation therapy via chronic vagus nerve stimulation to control the sympatho-vagal balance. This stimulation has been shown to modulate autonomic mechanisms that reduced heart failure symptom expression, and favorably alter markers of risk for fatal arrhythmias, including heart rate turbulences (228-231). In the future the disruption of the BBB using focused ultrasound could be an alternative therapeutic approach, which is a novel non-invasive technology that could circumvent some of the anatomical limitations of the BBB. This technology is studied in several animal models with regard to treating tumors and allowing thereby the local delivery of drugs into the brain (232-234). Furthermore, a recent study showed that the disruption of the brainstem BBB in rats was feasible and led to enhanced drug delivery (235). Remarkably, this technique has been translated clinically and a helmet was designed that enables ultrasound waves to penetrate the human skull (ExAblate low frequency system, InSightec) (236). One could speculate that this technique in an advanced form might support the drug and/or TH delivery into the brain of AHDS patients.

Impact on muscular properties.

In AHDS patients the remarkable weight loss is accompanied by muscle wasting und uncontrolled motor movements (125, 126). It has been shown that the skeletal muscle is also a main target tissue of THs signaling (reviewed in (237, 238)). Furthermore, systemic hyperthyroidism activates thermogenic pathways also in muscles resulting in increased lipid uptake und muscle wasting (119). Recently, Mayerl et al. showed for the first time that skeletal regulation is delayed in the *M/O* dko mice (154). Furthermore, the analyzed tibialis anterior muscle, which is located on the lateral side of the tibia, was in a hyperthyroid state as evidence by increased T3 content. However, the TH status differed between cells leading to a hyperthyroid state in some cells, while others were hypothyroid. This points to muscle-intrinsic and cell-specific alterations in the investigated *M/O* dko muscles (154). Therefore, it is of great interest to elucidate the effects of TA3 treatment on skeletal muscles with varying proportions of the fiber types. Consequently, the muscles M. gastr., which consists of >50% fast-twitch muscle fibers, and M. soleus, with a predominance of slow-twitch muscle fibers, were chosen for further analysis. This analysis consisted of a selection of several genes that had been shown to be mainly upregulated in systemic hyperthyroidism (119). Among the tested genes in the M. gastr., the expression levels of *Ucp3* were reduced. Surprisingly, after TA3 treatment a downregulation of all investigated genes was observed in M. soleus. These findings are contrary to what was expected as the data point towards a hypothyroid state in the muscle. However, this hypothesis is supported by the similar expression pattern of MCT8 and MCT10 in skeletal muscle with the highest expression in satellite cells

(154). Importantly, it has been shown that neither MCT8 nor MCT10 transports TA3 *in vitro* (179). Therefore, one explanation for the hypothyroid state of the muscle could be that TA3 might not be transported into the muscle. This would then lead to an improvement of the hypermetabolic state of the muscle in the AHDS patients as they present symptoms of congenital hypotonia. Such an improvement has been in fact observed during the first TA3 trial (188). Nevertheless, the TA3 transporter is still unknown to date and therefore, more information about TA3 transport into the different muscle cells is essential to optimize treatment options (226).

4.6. Summary and outlook

Taken together, this study was the first to dissect the central versus peripheral actions of THs *in vivo* on thermoregulation and cardiac properties using a mouse model of the AHDS. The main findings of this study are that central actions are required for TH-induced cardiac hypertrophy and elevation in body temperature. Furthermore, the TH status of the brain is crucial for the heart rate frequency distribution and a stable autonomic control. These findings are of great interest as they are puzzle pieces to the growing picture of understanding the individual contributions in the multi-layered and tightly controlled action of THs.

Nevertheless, further experiments have to be conducted to understand the underlying mechanisms. Therefore, it would be essential to render the *M/O* dko mice even more hyperthyroid in comparison with WT T3-treated animals, as the administered T3 dose was relatively low. On the other hand, administration of thyreostatic drugs to *M/O* dko mice would result in peripheral hypothyroidism. By comparing these two approaches, this would accentuate the central and peripheral actions of THs further.

5. References

1. Singer C (1962) A short history of medicine. *Oxford University Press* 2nd. ed. Oxford:519-534.
2. Khattak RM, Ittermann T, Nauck M, Below H, & Völzke H (2016) Monitoring the prevalence of thyroid disorders in the adult population of Northeast Germany. *Population health metrics* 14:39.
3. Taylor PN, *et al.* (2018) Global epidemiology of hyperthyroidism and hypothyroidism. *Nat Rev Endocrinol* 14(5):301-316.
4. Morley JE (1981) Neuroendocrine Control of Thyrotropin Secretion. *Endocrine Reviews* 2(4):396-436.
5. Yen PM (2001) Physiological and molecular basis of thyroid hormone action. *Physiol Rev* 81(3):1097-1142.
6. Nishimura M & Naito S (2008) Tissue-specific mRNA expression profiles of human solute carrier transporter superfamilies. *Drug metabolism and pharmacokinetics* 23(1):22-44.
7. Nicoloff JT, Low JC, Dussault JH, & Fisher DA (1972) Simultaneous measurement of thyroxine and triiodothyronine peripheral turnover kinetics in man. *J Clin Invest* 51(3):473-483.
8. Bianco AC, *et al.* (2014) American Thyroid Association Guide to investigating thyroid hormone economy and action in rodent and cell models. *Thyroid* 24(1):88-168.
9. Gereben B, *et al.* (2008) Cellular and molecular basis of deiodinase-regulated thyroid hormone signaling. *Endocr Rev* 29(7):898-938.
10. Pilo A, *et al.* (1990) Thyroidal and peripheral production of 3,5,3'-triiodothyronine in humans by multicompartmental analysis. *The American journal of physiology* 258(4 Pt 1):E715-726.
11. St Germain DL, Galton VA, & Hernandez A (2009) Minireview: Defining the roles of the iodothyronine deiodinases: current concepts and challenges. *Endocrinology* 150(3):1097-1107.
12. Leonard JL & Rosenberg IN (1981) Solubilization of a phospholipid-requiring enzyme, iodothyronine 5'-deiodinase, from rat kidney membranes. *Biochim Biophys Acta* 659(1):205-218.
13. Köhrle J (2000) The selenoenzyme family of deiodinase isozymes controls local thyroid hormone availability. *Reviews in endocrine & metabolic disorders* 1(1-2):49-58.
14. Gereben B, McAninch EA, Ribeiro MO, & Bianco AC (2015) Scope and limitations of iodothyronine deiodinases in hypothyroidism. *Nat Rev Endocrinol* 11(11):642-652.
15. Accorroni A, Saponaro F, & Zucchi R (2016) Tissue thyroid hormones and thyronamines. *Heart Fail Rev* 21(4):373-390.
16. Berry MJ, Banu L, & Larsen PR (1991) Type I iodothyronine deiodinase is a selenocysteine-containing enzyme. *Nature* 349(6308):438-440.
17. Bianco AC, Salvatore D, Gereben B, Berry MJ, & Larsen PR (2002) Biochemistry, cellular and molecular biology, and physiological roles of the iodothyronine selenodeiodinases. *Endocr Rev* 23(1):38-89.
18. Huang SA, Dorfman DM, Genest DR, Salvatore D, & Larsen PR (2003) Type 3 iodothyronine deiodinase is highly expressed in the human uteroplacental unit and in fetal epithelium. *J Clin Endocrinol Metab* 88(3):1384-1388.
19. Wu SY, Green WL, Huang WS, Hays MT, & Chopra IJ (2005) Alternate pathways of thyroid hormone metabolism. *Thyroid* 15(8):943-958.

20. Wood WJ, Geraci T, Nilsen A, DeBarber AE, & Scanlan TS (2009) Iodothyronamines are oxidatively deaminated to iodothyroacetic acids in vivo. *Chembiochem* 10(2):361-365.
21. Szpirer C, *et al.* (1991) Chromosomal assignment of five cancer-associated rat genes: two thyroid hormone receptor (ERBA) genes, two ERBB genes and the retinoblastoma gene. *Oncogene* 6(8):1319-1324.
22. Spurr NK, *et al.* (1984) Chromosomal localisation of the human homologues to the oncogenes erbA and B. *Embo j* 3(1):159-163.
23. Lazar MA (1993) Thyroid hormone receptors: multiple forms, multiple possibilities. *Endocr Rev* 14(2):184-193.
24. Cheng SY, Leonard JL, & Davis PJ (2010) Molecular aspects of thyroid hormone actions. *Endocr Rev* 31(2):139-170.
25. Bassett JH & Williams GR (2009) The skeletal phenotypes of TRalpha and TRbeta mutant mice. *Journal of molecular endocrinology* 42(4):269-282.
26. Bianco AC & McAninch EA (2013) The role of thyroid hormone and brown adipose tissue in energy homoeostasis. *The Lancet Diabetes & Endocrinology* 1(3):250-258.
27. Chen JD & Evans RM (1995) A transcriptional co-repressor that interacts with nuclear hormone receptors. *Nature* 377(6548):454-457.
28. Hörlein AJ, *et al.* (1995) Ligand-independent repression by the thyroid hormone receptor mediated by a nuclear receptor co-repressor. *Nature* 377(6548):397-404.
29. Lin BC, Hong SH, Krig S, Yoh SM, & Privalsky ML (1997) A conformational switch in nuclear hormone receptors is involved in coupling hormone binding to corepressor release. *Mol Cell Biol* 17(10):6131-6138.
30. Fondell JD, Ge H, & Roeder RG (1996) Ligand induction of a transcriptionally active thyroid hormone receptor coactivator complex. *Proc Natl Acad Sci U S A* 93(16):8329-8333.
31. Flamant F, *et al.* (2017) Thyroid Hormone Signaling Pathways: Time for a More Precise Nomenclature. *Endocrinology* 158(7):2052-2057.
32. Sinha RA, Singh BK, & Yen PM (2014) Thyroid hormone regulation of hepatic lipid and carbohydrate metabolism. *Trends Endocrinol Metab* 25(10):538-545.
33. Mendoza A & Hollenberg AN (2017) New insights into thyroid hormone action. *Pharmacology & therapeutics* 173:135-145.
34. Curling TB (1850) Two Cases of absence of the Thyroid body, and symmetrical swellings of fat tissue at the sides of the neck, connected with defective cerebral development. *Medico-chirurgical transactions* 33:303-306.
35. Pyzik A, Grywalska E, Matyjaszek-Matuszek B, & Roliński J (2015) Immune disorders in Hashimoto's thyroiditis: what do we know so far? *Journal of immunology research* 2015:979167.
36. Cooper DS (2001) Clinical practice. Subclinical hypothyroidism. *The New England journal of medicine* 345(4):260-265.
37. Evered DC, Ormston BJ, Smith PA, Hall R, & Bird T (1973) Grades of hypothyroidism. *British medical journal* 1(5854):657-662.
38. Kahaly GJ & Dillmann WH (2005) Thyroid hormone action in the heart. *Endocr Rev* 26(5):704-728.
39. Pearce EN (2012) Thyroid hormone and obesity. *Curr Opin Endocrinol Diabetes Obes* 19(5):408-413.
40. Longhi S & Radetti G (2013) Thyroid function and obesity. *Journal of clinical research in pediatric endocrinology* 5 Suppl 1(Suppl 1):40-44.
41. Silva JE (2003) The thermogenic effect of thyroid hormone and its clinical implications. *Annals of internal medicine* 139(3):205-213.

42. Bahn Chair RS, *et al.* (2011) Hyperthyroidism and other causes of thyrotoxicosis: management guidelines of the American Thyroid Association and American Association of Clinical Endocrinologists. *Thyroid* 21(6):593-646.
43. Topliss DJ & Eastman CJ (2004) 5: Diagnosis and management of hyperthyroidism and hypothyroidism. *The Medical journal of Australia* 180(4):186-193.
44. Rapoport B, Chazenbalk GD, Jaume JC, & McLachlan SM (1998) The thyrotropin (TSH) receptor: interaction with TSH and autoantibodies. *Endocr Rev* 19(6):673-716.
45. Laurberg P, *et al.* (2012) Thyroid function and obesity. *Eur Thyroid J* 1(3):159-167.
46. Silverman ME & Hollman A (2007) Discovery of the sinus node by Keith and Flack: on the centennial of their 1907 publication. *Heart* 93(10):1184-1187.
47. Lehrer SS (1994) The regulatory switch of the muscle thin filament: Ca2+ or myosin heads? *Journal of muscle research and cell motility* 15(3):232-236.
48. Lyons GE, Schiaffino S, Sassoon D, Barton P, & Buckingham M (1990) Developmental regulation of myosin gene expression in mouse cardiac muscle. *The Journal of cell biology* 111(6 Pt 1):2427-2436.
49. Lakatta EG & DiFrancesco D (2009) What keeps us ticking: a funny current, a calcium clock, or both? *J Mol Cell Cardiol* 47(2):157-170.
50. Brown HF, DiFrancesco D, & Noble SJ (1979) How does adrenaline accelerate the heart? *Nature* 280(5719):235-236.
51. Santoro B, Grant SG, Bartsch D, & Kandel ER (1997) Interactive cloning with the SH3 domain of N-src identifies a new brain specific ion channel protein, with homology to eag and cyclic nucleotide-gated channels. *Proc Natl Acad Sci U S A* 94(26):14815-14820.
52. Ludwig A, Zong X, Jeglitsch M, Hofmann F, & Biel M (1998) A family of hyperpolarization-activated mammalian cation channels. *Nature* 393(6685):587-591.
53. DiFrancesco D (1985) The cardiac hyperpolarizing-activated current, if. Origins and developments. *Progress in biophysics and molecular biology* 46(3):163-183.
54. Lakatta EG, Maltsev VA, & Vinogradova TM (2010) A coupled SYSTEM of intracellular Ca2+ clocks and surface membrane voltage clocks controls the timekeeping mechanism of the heart's pacemaker. *Circ Res* 106(4):659-673.
55. Cheng H, Lederer WJ, & Cannell MB (1993) Calcium sparks: elementary events underlying excitation-contraction coupling in heart muscle. *Science (New York, N.Y.)* 262(5134):740-744.
56. Bassani JW, Bassani RA, & Bers DM (1994) Relaxation in rabbit and rat cardiac cells: species-dependent differences in cellular mechanisms. *The Journal of physiology* 476(2):279-293.
57. Tada M, Kirchberger MA, & Katz AM (1975) Phosphorylation of a 22,000-dalton component of the cardiac sarcoplasmic reticulum by adenosine 3':5'-monophosphate-dependent protein kinase. *J Biol Chem* 250(7):2640-2647.
58. LaRaia PJ & Morkin E (1974) Adenosine 3', 5'-Monophosphate-Dependent Membrane Phosphorylation. *Circulation Research* 35(2):298-306.
59. Ruknudin A, He S, Lederer WJ, & Schulze DH (2000) Functional differences between cardiac and renal isoforms of the rat Na+-Ca2+ exchanger NCX1 expressed in Xenopus oocytes. *The Journal of physiology* 529 Pt 3(Pt 3):599-610.
60. Berridge MJ, Bootman MD, & Roderick HL (2003) Calcium signalling: dynamics, homeostasis and remodelling. *Nature reviews. Molecular cell biology* 4(7):517-529.
61. Rohrer DK, Chruscinski A, Schauble EH, Bernstein D, & Kobilka BK (1999) Cardiovascular and metabolic alterations in mice lacking both beta1- and beta2-adrenergic receptors. *J Biol Chem* 274(24):16701-16708.
62. Rockman HA, Koch WJ, & Lefkowitz RJ (2002) Seven-transmembrane-spanning receptors and heart function. *Nature* 415(6868):206-212.

63. Xiang Y & Kobilka BK (2003) Myocyte adrenoceptor signaling pathways. *Science (New York, N.Y.)* 300(5625):1530-1532.
64. Janssen BJ & Smits JF (2002) Autonomic control of blood pressure in mice: basic physiology and effects of genetic modification. *American journal of physiology. Regulatory, integrative and comparative physiology* 282(6):R1545-1564.
65. Swoap SJ, *et al.* (2008) Vagal tone dominates autonomic control of mouse heart rate at thermoneutrality. *Am J Physiol Heart Circ Physiol* 294(4):H1581-1588.
66. Hayes JP & Garland T, Jr. (1995) The Evolution of Endothermy: Testing the aerobic capacity model. *Evolution; international journal of organic evolution* 49(5):836-847.
67. Silva JE (2006) Thermogenic mechanisms and their hormonal regulation. *Physiol Rev* 86(2):435-464.
68. Gordon CJ (1993) Temperature regulation in laboratory rodents. *Cambridge England; New York, NY, USA, Cambridge University Press*.
69. Nakamura K & Morrison SF (2008) A thermosensory pathway that controls body temperature. *Nat Neurosci* 11(1):62-71.
70. Cannon B & Nedergaard J (2004) Brown adipose tissue: function and physiological significance. *Physiol Rev* 84(1):277-359.
71. Nicholls DG & Locke RM (1984) Thermogenic mechanisms in brown fat. *Physiol Rev* 64(1):1-64.
72. Bal NC, *et al.* (2012) Sarcolipin is a newly identified regulator of muscle-based thermogenesis in mammals. *Nat Med* 18(10):1575-1579.
73. Wu J, *et al.* (2012) Beige adipocytes are a distinct type of thermogenic fat cell in mouse and human. *Cell* 150(2):366-376.
74. Harms M & Seale P (2013) Brown and beige fat: development, function and therapeutic potential. *Nat Med* 19(10):1252-1263.
75. Bartelt A & Heeren J (2014) Adipose tissue browning and metabolic health. *Nat Rev Endocrinol* 10(1):24-36.
76. Gesner C (1551) Medici Tigurini Historiae Animalium Liber I de Quadrupedibusuiuiparis. *Froschauer*:840-844.
77. Nedergaard J, Bengtsson T, & Cannon B (2007) Unexpected evidence for active brown adipose tissue in adult humans. *Am J Physiol Endocrinol Metab* 293(2):E444-452.
78. Cypess AM, *et al.* (2009) Identification and importance of brown adipose tissue in adult humans. *The New England journal of medicine* 360(15):1509-1517.
79. Virtanen KA, *et al.* (2009) Functional brown adipose tissue in healthy adults. *The New England journal of medicine* 360(15):1518-1525.
80. van Marken Lichtenbelt WD, *et al.* (2009) Cold-activated brown adipose tissue in healthy men. *The New England journal of medicine* 360(15):1500-1508.
81. Nedergaard J & Cannon B (2013) How brown is brown fat? It depends where you look. *Nat Med* 19(5):540-541.
82. Napolitano L (1963) The Differentiation of White Adipose Cells. An Electron Microscope Study. *The Journal of cell biology* 18(3):663-679.
83. Napolitano L & Fawcett D (1958) The fine structure of brown adipose tissue in the newborn mouse and rat. *The Journal of biophysical and biochemical cytology* 4(6):685-692.
84. Shabalina IG, *et al.* (2013) UCP1 in brite/beige adipose tissue mitochondria is functionally thermogenic. *Cell reports* 5(5):1196-1203.
85. Warner A & Mittag J (2012) Thyroid hormone and the central control of homeostasis. *Journal of molecular endocrinology* 49(1):R29-35.
86. Derry DM, Schönbaum E, & Steiner G (1969) Two sympathetic nerve supplies to brown adipose tissue of the rat. *Can J Physiol Pharmacol* 47(1):57-63.

87. Lin CS & Klingenberg M (1980) Isolation of the uncoupling protein from brown adipose tissue mitochondria. *FEBS letters* 113(2):299-303.
88. Smith RE & Roberts JC (1964) Thermogenesis of Brown Adipose Tissue in Cold-Acclimated Rats. *The American journal of physiology* 206:143-148.
89. Nedergaard J & Cannon B (2018) Brown adipose tissue as a heat-producing thermoeffector. *Handbook of clinical neurology* 156:137-152.
90. Fedorenko A, Lishko PV, & Kirichok Y (2012) Mechanism of fatty-acid-dependent UCP1 uncoupling in brown fat mitochondria. *Cell* 151(2):400-413.
91. Silva JE & Larsen PR (1983) Adrenergic activation of triiodothyronine production in brown adipose tissue. *Nature* 305(5936):712-713.
92. López M, Alvarez CV, Nogueiras R, & Diéguez C (2013) Energy balance regulation by thyroid hormones at central level. *Trends in molecular medicine* 19(7):418-427.
93. Lowell BB & Spiegelman BM (2000) Towards a molecular understanding of adaptive thermogenesis. *Nature* 404(6778):652-660.
94. Klein I & Ojamaa K (2001) Thyroid hormone and the cardiovascular system. *The New England journal of medicine* 344(7):501-509.
95. López M, *et al.* (2010) Hypothalamic AMPK and fatty acid metabolism mediate thyroid regulation of energy balance. *Nat Med* 16(9):1001-1008.
96. Mittag J, *et al.* (2013) Thyroid hormone is required for hypothalamic neurons regulating cardiovascular functions. *J Clin Invest* 123(1):509-516.
97. Everts ME, *et al.* (1996) Uptake of thyroid hormones in neonatal rat cardiac myocytes. *Endocrinology* 137(10):4235-4242.
98. Croteau W, Davey JC, Galton VA, & St Germain DL (1996) Cloning of the mammalian type II iodothyronine deiodinase. A selenoprotein differentially expressed and regulated in human and rat brain and other tissues. *J Clin Invest* 98(2):405-417.
99. Gloss B, *et al.* (2001) Cardiac ion channel expression and contractile function in mice with deletion of thyroid hormone receptor alpha or beta. *Endocrinology* 142(2):544-550.
100. Pantos C, *et al.* (2007) Time-dependent changes in the expression of thyroid hormone receptor alpha 1 in the myocardium after acute myocardial infarction: possible implications in cardiac remodelling. *Eur J Endocrinol* 156(4):415-424.
101. Wikström L, *et al.* (1998) Abnormal heart rate and body temperature in mice lacking thyroid hormone receptor alpha 1. *Embo j* 17(2):455-461.
102. Gustafson TA, Markham BE, & Morkin E (1986) Effects of thyroid hormone on alpha-actin and myosin heavy chain gene expression in cardiac and skeletal muscles of the rat: measurement of mRNA content using synthetic oligonucleotide probes. *Circ Res* 59(2):194-201.
103. Gustafson TA, Markham BE, Bahl JJ, & Morkin E (1987) Thyroid hormone regulates expression of a transfected alpha-myosin heavy-chain fusion gene in fetal heart cells. *Proc Natl Acad Sci U S A* 84(10):3122-3126.
104. Kiss E, *et al.* (1998) Thyroid hormone-induced alterations in phospholamban-deficient mouse hearts. *Circ Res* 83(6):608-613.
105. Dillmann W (2010) Cardiac hypertrophy and thyroid hormone signaling. *Heart Fail Rev* 15(2):125-132.
106. Pachucki J, Burmeister LA, & Larsen PR (1999) Thyroid hormone regulates hyperpolarization-activated cyclic nucleotide-gated channel (HCN2) mRNA in the rat heart. *Circ Res* 85(6):498-503.
107. Danzi S & Klein I (2014) Thyroid disease and the cardiovascular system. *Endocrinol Metab Clin North Am* 43(2):517-528.
108. Ojamaa K, Klemperer JD, & Klein I (1996) Acute effects of thyroid hormone on vascular smooth muscle. *Thyroid* 6(5):505-512.

109. Ojamaa K, Sabet A, Kenessey A, Shenoy R, & Klein I (1999) Regulation of rat cardiac Kv1.5 gene expression by thyroid hormone is rapid and chamber specific. *Endocrinology* 140(7):3170-3176.
110. Walker JD, Crawford FA, Kato S, & Spinale FG (1994) The novel effects of 3,5,3'-triiodo-L-thyronine on myocyte contractile function and beta-adrenergic responsiveness in dilated cardiomyopathy. *The Journal of thoracic and cardiovascular surgery* 108(4):672-679.
111. Kenessey A & Ojamaa K (2006) Thyroid hormone stimulates protein synthesis in the cardiomyocyte by activating the Akt-mTOR and p70S6K pathways. *J Biol Chem* 281(30):20666-20672.
112. Harder L, *et al.* (2018) Maternal thyroid hormone is required for parvalbumin neurone development in the anterior hypothalamic area. *Journal of neuroendocrinology* 30(3):e12573.
113. Jabbar A, *et al.* (2017) Thyroid hormones and cardiovascular disease. *Nature reviews. Cardiology* 14(1):39-55.
114. Bianco AC & Silva JE (1987) Nuclear 3,5,3′-Triiodothyronine (T3) in Brown Adipose Tissue: Receptor Occupancy and Sources of T3 as Determined by in Vivo Techniques*. *Endocrinology* 120(1):55-62.
115. Ribeiro MO, *et al.* (2001) Thyroid hormone-sympathetic interaction and adaptive thermogenesis are thyroid hormone receptor isoform-specific. *J Clin Invest* 108(1):97-105.
116. Sjogren M, *et al.* (2007) Hypermetabolism in mice caused by the central action of an unliganded thyroid hormone receptor alpha1. *EMBO J* 26(21):4535-4545.
117. López M, *et al.* (2008) Hypothalamic fatty acid metabolism mediates the orexigenic action of ghrelin. *Cell Metab* 7(5):389-399.
118. Alvarez-Crespo M, *et al.* (2016) Essential role of UCP1 modulating the central effects of thyroid hormones on energy balance. *Molecular metabolism* 5(4):271-282.
119. Johann K, *et al.* (2019) Thyroid-Hormone-Induced Browning of White Adipose Tissue Does Not Contribute to Thermogenesis and Glucose Consumption. *Cell reports* 27(11):3385-3400.e3383.
120. Hennemann G, *et al.* (2001) Plasma membrane transport of thyroid hormones and its role in thyroid hormone metabolism and bioavailability. *Endocr Rev* 22(4):451-476.
121. Ben-Zvi A, *et al.* (2014) Mfsd2a is critical for the formation and function of the blood-brain barrier. *Nature* 509(7501):507-511.
122. Dratman MB, Crutchfield FL, & Schoenhoff MB (1991) Transport of iodothyronines from bloodstream to brain: contributions by blood:brain and choroid plexus:cerebrospinal fluid barriers. *Brain research* 554(1-2):229-236.
123. Dziegielewska KM, Ek J, Habgood MD, & Saunders NR (2001) Development of the choroid plexus. *Microscopy research and technique* 52(1):5-20.
124. Friesema ECH, *et al.* (2004) Association between mutations in a thyroid hormone transporter and severe X-linked psychomotor retardation. *The Lancet* 364(9443):1435-1437.
125. Dumitrescu AM, Liao XH, Best TB, Brockmann K, & Refetoff S (2004) A novel syndrome combining thyroid and neurological abnormalities is associated with mutations in a monocarboxylate transporter gene. *American journal of human genetics* 74(1):168-175.
126. Schwartz CE, *et al.* (2005) Allan-Herndon-Dudley syndrome and the monocarboxylate transporter 8 (MCT8) gene. *American journal of human genetics* 77(1):41-53.
127. Visser WE, Friesema ECH, Jansen J, & Visser TJ (2007) Thyroid hormone transport by monocarboxylate transporters. *Best Pract Res Clin Endocrinol Metab* 21(2):223-236.

128. Hagenbuch B (2007) Cellular entry of thyroid hormones by organic anion transporting polypeptides. *Best Pract Res Clin Endocrinol Metab* 21(2):209-221.
129. Kanai Y & Endou H (2001) Heterodimeric amino acid transporters: molecular biology and pathological and pharmacological relevance. *Current drug metabolism* 2(4):339-354.
130. Schweizer U, Johannes J, Bayer D, & Braun D (2014) Structure and function of thyroid hormone plasma membrane transporters. *Eur Thyroid J* 3(3):143-153.
131. Halestrap AP & Meredith D (2004) The SLC16 gene family-from monocarboxylate transporters (MCTs) to aromatic amino acid transporters and beyond. *Pflugers Arch* 447(5):619-628.
132. Friesema ECH, *et al.* (2003) Identification of monocarboxylate transporter 8 as a specific thyroid hormone transporter. *J Biol Chem* 278(41):40128-40135.
133. Friesema ECH, *et al.* (2008) Effective cellular uptake and efflux of thyroid hormone by human monocarboxylate transporter 10. *Mol Endocrinol* 22(6):1357-1369.
134. Lafrenière RG, Carrel L, & Willard HF (1994) A novel transmembrane transporter encoded by the XPCT gene in Xq13.2. *Human Molecular Genetics* 3(7):1133-1139.
135. Schwartz CE & Stevenson RE (2007) The MCT8 thyroid hormone transporter and Allan-Herndon-Dudley syndrome. *Best Pract Res Clin Endocrinol Metab* 21(2):307-321.
136. Kim DK, *et al.* (2001) Expression cloning of a Na+-independent aromatic amino acid transporter with structural similarity to H+/monocarboxylate transporters. *J Biol Chem* 276(20):17221-17228.
137. Kim DK, *et al.* (2002) The human T-type amino acid transporter-1: characterization, gene organization, and chromosomal location. *Genomics* 79(1):95-103.
138. Braun D, *et al.* (2011) Developmental and cell type-specific expression of thyroid hormone transporters in the mouse brain and in primary brain cells. *Glia* 59(3):463-471.
139. Müller J & Heuer H (2014) Expression pattern of thyroid hormone transporters in the postnatal mouse brain. *Front Endocrinol (Lausanne)* 5:92.
140. Roberts LM, *et al.* (2008) Expression of the thyroid hormone transporters monocarboxylate transporter-8 (SLC16A2) and organic ion transporter-14 (SLCO1C1) at the blood-brain barrier. *Endocrinology* 149(12):6251-6261.
141. Heuer H, *et al.* (2005) The monocarboxylate transporter 8 linked to human psychomotor retardation is highly expressed in thyroid hormone-sensitive neuron populations. *Endocrinology* 146(4):1701-1706.
142. Wirth EK, *et al.* (2009) Neuronal 3',3,5-triiodothyronine (T3) uptake and behavioral phenotype of mice deficient in Mct8, the neuronal T3 transporter mutated in Allan-Herndon-Dudley syndrome. *J Neurosci* 29(30):9439-9449.
143. Wilpert NM, *et al.* (2020) Spatiotemporal Changes of Cerebral Monocarboxylate Transporter 8 Expression. *Thyroid*.
144. López-Espíndola D, *et al.* (2019) Thyroid hormone availability in the human fetal brain: novel entry pathways and role of radial glia. *Brain structure & function* 224(6):2103-2119.
145. Abe T, *et al.* (1999) Identification of a novel gene family encoding human liver-specific organic anion transporter LST-1. *J Biol Chem* 274(24):17159-17163.
146. Cattori V, *et al.* (2000) Identification of organic anion transporting polypeptide 4 (Oatp4) as a major full-length isoform of the liver-specific transporter-1 (rlst-1) in rat liver. *FEBS letters* 474(2-3):242-245.
147. Westholm DE, *et al.* (2010) Evidence of evolutionary conservation of function between the thyroxine transporter Oatp1c1 and major facilitator superfamily members. *Endocrinology* 151(12):5941-5951.
148. Pizzagalli F, *et al.* (2002) Identification of a novel human organic anion transporting polypeptide as a high affinity thyroxine transporter. *Mol Endocrinol* 16(10):2283-2296.

149. Sugiyama D, *et al.* (2003) Functional characterization of rat brain-specific organic anion transporter (Oatp14) at the blood-brain barrier: high affinity transporter for thyroxine. *J Biol Chem* 278(44):43489-43495.
150. Vatine GD, *et al.* (2013) Zebrafish as a model for monocarboxyl transporter 8-deficiency. *J Biol Chem* 288(1):169-180.
151. Ito K, *et al.* (2011) Quantitative membrane protein expression at the blood-brain barrier of adult and younger cynomolgus monkeys. *J Pharm Sci* 100(9):3939-3950.
152. Sun YN, *et al.* (2014) Expression of organic anion transporting polypeptide 1c1 and monocarboxylate transporter 8 in the rat placental barrier and the compensatory response to thyroid dysfunction. *PloS one* 9(4):e96047.
153. Gao B, *et al.* (2005) Localization of organic anion transporting polypeptides in the rat and human ciliary body epithelium. *Exp Eye Res* 80(1):61-72.
154. Mayerl S, *et al.* (2018) Thyroid Hormone Transporters MCT8 and OATP1C1 Control Skeletal Muscle Regeneration. *Stem cell reports* 10(6):1959-1974.
155. Segawa H, *et al.* (1999) Identification and functional characterization of a Na+-independent neutral amino acid transporter with broad substrate selectivity. *J Biol Chem* 274(28):19745-19751.
156. Fort J, *et al.* (2007) The structure of human 4F2hc ectodomain provides a model for homodimerization and electrostatic interaction with plasma membrane. *J Biol Chem* 282(43):31444-31452.
157. Rosell A, *et al.* (2014) Structural bases for the interaction and stabilization of the human amino acid transporter LAT2 with its ancillary protein 4F2hc. *Proc Natl Acad Sci U S A* 111(8):2966-2971.
158. Ritchie JW, Peter GJ, Shi YB, & Taylor PM (1999) Thyroid hormone transport by 4F2hc-IU12 heterodimers expressed in Xenopus oocytes. *The Journal of endocrinology* 163(2):R5-9.
159. Friesema ECH, *et al.* (2001) Thyroid hormone transport by the heterodimeric human system L amino acid transporter. *Endocrinology* 142(10):4339-4348.
160. Rossier G, *et al.* (1999) LAT2, a new basolateral 4F2hc/CD98-associated amino acid transporter of kidney and intestine. *J Biol Chem* 274(49):34948-34954.
161. Nakada N, *et al.* (2014) Unique and selective expression of L-amino acid transporter 1 in human tissue as well as being an aspect of oncofetal protein. *Histol Histopathol* 29(2):217-227.
162. Allan W, Herndon CN, & Dudley FC (1944) Some examples of the inheritance of mental deficiency: apparently sex-linked idiocy and microcephaly. *American Journal of Mental Deficiency* 48:325-334.
163. Friesema ECH, Visser WE, & Visser TJ (2010) Genetics and phenomics of thyroid hormone transport by MCT8. *Molecular and cellular endocrinology* 322(1-2):107-113.
164. Groeneweg S, van Geest FS, Peeters RP, Heuer H, & Visser WE (2019) Thyroid Hormone Transporters. *Endocrine Reviews* 41(2):146-201.
165. Stevenson RE, *et al.* (1990) Allan-Herndon syndrome. I. Clinical studies. *American journal of human genetics* 47(3):446-453.
166. Matheus MG, Lehman RK, Bonilha L, & Holden KR (2015) Redefining the Pediatric Phenotype of X-Linked Monocarboxylate Transporter 8 (MCT8) Deficiency: Implications for Diagnosis and Therapies. *Journal of child neurology* 30(12):1664-1668.
167. Dumitrescu AM, Liao XH, Weiss RE, Millen K, & Refetoff S (2006) Tissue-specific thyroid hormone deprivation and excess in monocarboxylate transporter (mct) 8-deficient mice. *Endocrinology* 147(9):4036-4043.
168. Mayerl S, *et al.* (2014) Transporters MCT8 and OATP1C1 maintain murine brain thyroid hormone homeostasis. *J Clin Invest* 124(5):1987-1999.

169. Trajkovic-Arsic M, *et al.* (2010) Consequences of monocarboxylate transporter 8 deficiency for renal transport and metabolism of thyroid hormones in mice. *Endocrinology* 151(2):802-809.
170. Di Cosmo C, *et al.* (2013) Mct8-deficient mice have increased energy expenditure and reduced fat mass that is abrogated by normalization of serum T3 levels. *Endocrinology* 154(12):4885-4895.
171. Trajkovic M, *et al.* (2007) Abnormal thyroid hormone metabolism in mice lacking the monocarboxylate transporter 8. *J Clin Invest* 117(3):627-635.
172. Wirth EK, *et al.* (2011) Monocarboxylate transporter 8 deficiency: altered thyroid morphology and persistent high triiodothyronine/thyroxine ratio after thyroidectomy. *Eur J Endocrinol* 165(4):555-561.
173. Di Cosmo C, *et al.* (2010) Mice deficient in MCT8 reveal a mechanism regulating thyroid hormone secretion. *J Clin Invest* 120(9):3377-3388.
174. Trajkovic-Arsic M, *et al.* (2010) Impact of monocarboxylate transporter-8 deficiency on the hypothalamus-pituitary-thyroid axis in mice. *Endocrinology* 151(10):5053-5062.
175. Wirth EK, Rijntjes E, Meyer F, Köhrle J, & Schweizer U (2015) High T3, Low T4 Serum Levels in Mct8 Deficiency Are Not Caused by Increased Hepatic Conversion through Type I Deiodinase. *Eur Thyroid J* 4(Suppl 1):87-91.
176. Mayerl S, Visser TJ, Darras VM, Horn S, & Heuer H (2012) Impact of Oatp1c1 deficiency on thyroid hormone metabolism and action in the mouse brain. *Endocrinology* 153(3):1528-1537.
177. Wemeau JL, *et al.* (2008) Beneficial effects of propylthiouracil plus L-thyroxine treatment in a patient with a mutation in MCT8. *J Clin Endocrinol Metab* 93(6):2084-2088.
178. Visser WE, *et al.* (2013) Identification, functional analysis, prevalence and treatment of monocarboxylate transporter 8 (MCT8) mutations in a cohort of adult patients with mental retardation. *Clinical endocrinology* 78(2):310-315.
179. Kersseboom S, *et al.* (2014) In vitro and mouse studies supporting therapeutic utility of triiodothyroacetic acid in MCT8 deficiency. *Mol Endocrinol* 28(12):1961-1970.
180. Takeda T, Suzuki S, Liu RT, & DeGroot LJ (1995) Triiodothyroacetic acid has unique potential for therapy of resistance to thyroid hormone. *The Journal of Clinical Endocrinology & Metabolism* 80(7):2033-2040.
181. Messier N & Langlois MF (2000) Triac regulation of transcription is T(3) receptor isoform- and response element-specific. *Molecular and cellular endocrinology* 165(1-2):57-66.
182. Martínez L, *et al.* (2009) Gaining ligand selectivity in thyroid hormone receptors via entropy. *Proc Natl Acad Sci U S A* 106(49):20717-20722.
183. Mittag J, Davis B, Vujovic M, Arner A, & Vennstrom B (2010) Adaptations of the autonomous nervous system controlling heart rate are impaired by a mutant thyroid hormone receptor-alpha1. *Endocrinology* 151(5):2388-2395.
184. Andersen CL, Jensen JL, & Ørntoft TF (2004) Normalization of real-time quantitative reverse transcription-PCR data: a model-based variance estimation approach to identify genes suited for normalization, applied to bladder and colon cancer data sets. *Cancer research* 64(15):5245-5250.
185. Short RP, A. (2011) Stain-free Approach for Western Blotting. *Genetic Engineering & Biotechnology News* 31(20):22-23.
186. Jastroch M, Hirschberg V, & Klingenspor M (2012) Functional characterization of UCP1 in mammalian HEK293 cells excludes mitochondrial uncoupling artefacts and reveals no contribution to basal proton leak. *Biochim Biophys Acta* 1817(9):1660-1670.

187. Vujovic M, *et al.* (2009) Interference of a mutant thyroid hormone receptor alpha1 with hepatic glucose metabolism. *Endocrinology* 150(6):2940-2947.
188. Groeneweg S, *et al.* (2019) Effectiveness and safety of the tri-iodothyronine analogue Triac in children and adults with MCT8 deficiency: an international, single-arm, open-label, phase 2 trial. *The lancet. Diabetes & endocrinology* 7(9):695-706.
189. Herrmann B, *et al.* (2020) Central Hypothyroidism Impairs Heart Rate Stability and Prevents Thyroid Hormone-Induced Cardiac Hypertrophy and Pyrexia. *Thyroid*.
190. Flores-Morales A, *et al.* (2002) Patterns of liver gene expression governed by TRbeta. *Mol Endocrinol* 16(6):1257-1268.
191. Klieverik LP, *et al.* (2009) Thyroid hormone modulates glucose production via a sympathetic pathway from the hypothalamic paraventricular nucleus to the liver. *Proc Natl Acad Sci U S A* 106(14):5966-5971.
192. Song MK, Dozin B, Grieco D, Rall JE, & Nikodem VM (1988) Transcriptional activation and stabilization of malic enzyme mRNA precursor by thyroid hormone. *J Biol Chem* 263(34):17970-17974.
193. Takeuchi Y, *et al.* (2002) Steroid receptor coactivator-1 deficiency causes variable alterations in the modulation of T(3)-regulated transcription of genes in vivo. *Endocrinology* 143(4):1346-1352.
194. Lompré AM, Nadal-Ginard B, & Mahdavi V (1984) Expression of the cardiac ventricular alpha- and beta-myosin heavy chain genes is developmentally and hormonally regulated. *J Biol Chem* 259(10):6437-6446.
195. Mai W, *et al.* (2004) Thyroid hormone receptor alpha is a molecular switch of cardiac function between fetal and postnatal life. *Proc Natl Acad Sci U S A* 101(28):10332-10337.
196. Klein I (1988) Thyroxine-induced cardiac hypertrophy: time course of development and inhibition by propranolol. *Endocrinology* 123(1):203-210.
197. Lin JZ, *et al.* (2015) Pharmacological Activation of Thyroid Hormone Receptors Elicits a Functional Conversion of White to Brown Fat. *Cell reports* 13(8):1528-1537.
198. Kohno M, *et al.* (1993) Stimulation of brain natriuretic peptide release from the heart by thyroid hormone. *Metabolism: clinical and experimental* 42(8):1059-1064.
199. Liang F, Webb P, Marimuthu A, Zhang S, & Gardner DG (2003) Triiodothyronine increases brain natriuretic peptide (BNP) gene transcription and amplifies endothelin-dependent BNP gene transcription and hypertrophy in neonatal rat ventricular myocytes. *J Biol Chem* 278(17):15073-15083.
200. Bárez-López S, *et al.* (2016) Effect of Triiodothyroacetic Acid Treatment in Mct8 Deficiency: A Word of Caution. *Thyroid : official journal of the American Thyroid Association* 26(5):618-626.
201. Cannon B & Nedergaard J (2010) Thyroid hormones: igniting brown fat via the brain. *Nat Med* 16(9):965-967.
202. Fleischhack G, Jaehde U, & Bode U (2005) Pharmacokinetics following intraventricular administration of chemotherapy in patients with neoplastic meningitis. *Clinical pharmacokinetics* 44(1):1-31.
203. Strømme P, *et al.* (2018) Mutated Thyroid Hormone Transporter OATP1C1 Associates with Severe Brain Hypometabolism and Juvenile Neurodegeneration. *Thyroid* 28(11):1406-1415.
204. Bernal J (2000) Thyroid Hormones in Brain Development and Function. *Endotext*, eds Feingold KR, Anawalt B, Boyce A, Chrousos G, Dungan K, Grossman A, Hershman JM, Kaltsas G, Koch C, Kopp P, *et al.* (MDText.com, Inc. Copyright © 2000-2020, MDText.com, Inc., South Dartmouth (MA)).
205. Cabello G & Wrutniak C (1989) Thyroid hormone and growth: relationships with growth hormone effects and regulation. *Reproduction, nutrition, development* 29(4):387-402.

206. Martínez-Sánchez N, *et al.* (2017) Hypothalamic AMPK-ER Stress-JNK1 Axis Mediates the Central Actions of Thyroid Hormones on Energy Balance. *Cell Metab* 26(1):212-229.e212.
207. Sabio G, *et al.* (2010) Role of muscle c-Jun NH2-terminal kinase 1 in obesity-induced insulin resistance. *Mol Cell Biol* 30(1):106-115.
208. Hoefig CS, *et al.* (2016) Thermoregulatory and Cardiovascular Consequences of a Transient Thyrotoxicosis and Recovery in Male Mice. *Endocrinology* 157(7):2957-2967.
209. Klein I & Hong C (1986) Effects of thyroid hormone on cardiac size and myosin content of the heterotopically transplanted rat heart. *J Clin Invest* 77(5):1694-1698.
210. Ojamaa K, Samarel AM, Kupfer JM, Hong C, & Klein I (1992) Thyroid hormone effects on cardiac gene expression independent of cardiac growth and protein synthesis. *The American journal of physiology* 263(3 Pt 1):E534-540.
211. Hu LW, Benvenuti LA, Liberti EA, Carneiro-Ramos MS, & Barreto-Chaves ML (2003) Thyroxine-induced cardiac hypertrophy: influence of adrenergic nervous system versus renin-angiotensin system on myocyte remodeling. *American journal of physiology. Regulatory, integrative and comparative physiology* 285(6):R1473-1480.
212. Bachman ES, *et al.* (2004) The metabolic and cardiovascular effects of hyperthyroidism are largely independent of beta-adrenergic stimulation. *Endocrinology* 145(6):2767-2774.
213. Pachucki J, *et al.* (2001) Type 2 iodothyronin deiodinase transgene expression in the mouse heart causes cardiac-specific thyrotoxicosis. *Endocrinology* 142(1):13-20.
214. Klein I & Danzi S (2007) Thyroid disease and the heart. *Circulation* 116(15):1725-1735.
215. Zierhut W & Zimmer HG (1989) Differential effects of triiodothyronine on rat left and right ventricular function and the influence of metoprolol. *J Mol Cell Cardiol* 21(6):617-624.
216. Fischer AW, Cannon B, & Nedergaard J (2018) Optimal housing temperatures for mice to mimic the thermal environment of humans: An experimental study. *Molecular metabolism* 7:161-170.
217. Tinnikov A, *et al.* (2002) Retardation of post-natal development caused by a negatively acting thyroid hormone receptor alpha1. *Embo j* 21(19):5079-5087.
218. White DW & Raven PB (2014) Autonomic neural control of heart rate during dynamic exercise: revisited. *The Journal of physiology* 592(12):2491-2500.
219. Kukielka M, Seals DR, & Billman GE (2006) Cardiac vagal modulation of heart rate during prolonged submaximal exercise in animals with healed myocardial infarctions: effects of training. *Am J Physiol Heart Circ Physiol* 290(4):H1680-1685.
220. Mueller-Gaertner HW & Schneider C (1988) 3,5,3'-Triiodothyroacetic acid minimizes the pituitary thyrotrophin secretion in patients on levo-thyroxine therapy after ablative therapy for differentiated thyroid carcinoma. *Clinical endocrinology* 28(4):345-351.
221. Groeneweg S, Peeters RP, Visser TJ, & Visser WE (2017) Therapeutic applications of thyroid hormone analogues in resistance to thyroid hormone (RTH) syndromes. *Molecular and cellular endocrinology* 458:82-90.
222. Horn S, *et al.* (2013) Tetrac can replace thyroid hormone during brain development in mouse mutants deficient in the thyroid hormone transporter mct8. *Endocrinology* 154(2):968-979.
223. Bracco D, *et al.* (1993) Comparison of the metabolic and endocrine effects of 3,5,3'-triiodothyroacetic acid and thyroxine. *The Journal of Clinical Endocrinology & Metabolism* 77(1):221-228.
224. Everts ME, *et al.* (1994) Uptake of triiodothyroacetic acid and its effect on thyrotropin secretion in cultured anterior pituitary cells. *Endocrinology* 135(6):2700-2707.

225. Medina-Gomez G, Calvo RM, & Obregon MJ (2008) Thermogenic effect of triiodothyroacetic acid at low doses in rat adipose tissue without adverse side effects in the thyroid axis. *Am J Physiol Endocrinol Metab* 294(4):E688-697.
226. Groeneweg S, Peeters RP, Visser TJ, & Visser WE (2017) Triiodothyroacetic acid in health and disease. *The Journal of endocrinology* 234(2):R99-r121.
227. Krenz M & Robbins J (2004) Impact of beta-myosin heavy chain expression on cardiac function during stress. *J Am Coll Cardiol* 44(12):2390-2397.
228. De Ferrari GM, *et al.* (2011) Chronic vagus nerve stimulation: a new and promising therapeutic approach for chronic heart failure. *Eur Heart J* 32(7):847-855.
229. Premchand RK, *et al.* (2014) Autonomic regulation therapy via left or right cervical vagus nerve stimulation in patients with chronic heart failure: results of the ANTHEM-HF trial. *J Card Fail* 20(11):808-816.
230. Verrier RL, *et al.* (2011) Microvolt T-wave alternans physiological basis, methods of measurement, and clinical utility-consensus guideline by International Society for Holter and Noninvasive Electrocardiology. *J Am Coll Cardiol* 58(13):1309-1324.
231. Bauer A, *et al.* (2008) Heart rate turbulence: standards of measurement, physiological interpretation, and clinical use: International Society for Holter and Noninvasive Electrophysiology Consensus. *J Am Coll Cardiol* 52(17):1353-1365.
232. Hynynen K, McDannold N, Vykhodtseva N, & Jolesz FA (2001) Noninvasive MR imaging-guided focal opening of the blood-brain barrier in rabbits. *Radiology* 220(3):640-646.
233. Hynynen K, McDannold N, Sheikov NA, Jolesz FA, & Vykhodtseva N (2005) Local and reversible blood-brain barrier disruption by noninvasive focused ultrasound at frequencies suitable for trans-skull sonications. *Neuroimage* 24(1):12-20.
234. Kinoshita M, McDannold N, Jolesz FA, & Hynynen K (2006) Targeted delivery of antibodies through the blood-brain barrier by MRI-guided focused ultrasound. *Biochem Biophys Res Commun* 340(4):1085-1090.
235. Alli S, *et al.* (2018) Brainstem blood brain barrier disruption using focused ultrasound: A demonstration of feasibility and enhanced doxorubicin delivery. *Journal of controlled release : official journal of the Controlled Release Society* 281:29-41.
236. Clement GT & Hynynen K (2002) A non-invasive method for focusing ultrasound through the human skull. *Physics in medicine and biology* 47(8):1219-1236.
237. Lee JW, Kim NH, & Milanesi A (2014) Thyroid Hormone Signaling in Muscle Development, Repair and Metabolism. *Journal of endocrinology, diabetes & obesity* 2(3):1046.
238. Salvatore D, Simonides WS, Dentice M, Zavacki AM, & Larsen PR (2014) Thyroid hormones and skeletal muscle-new insights and potential implications. *Nat Rev Endocrinol* 10(4):206-214.

6. Appendix

6.1. Statistical analysis of Part A

In vivo and gene expression data were analyzed using two-way ANOVA with the genotypes *Mct8* and *Oatp1c1* as independent factors for the respective figures. Furthermore, a Bonferroni post-hoc test was applied (Supplementary Table 1). Heart rate frequency distribution was analyzed using two-way ANOVA multiple comparisons test with a Holm-Sidak's correction (Supplementary Table 2).

Supplementary Table 1: Statistical analysis of Part A – two-way ANOVA with Bonferroni post-hoc Test.

		two-way ANOVA			**Bonferroni post-hoc Test**				
		Inter-action	*Oatp1c1*	*Mct8*	WT vs. *Mct8* ko	WT vs. *Oatp1c1* ko	WT vs. *M/O* dko	*Mct8* ko vs. *M/O* dko	*Oatp1c1* ko vs. *M/O* dko
Figure 9									
B	Body weight	0.0425 *	0.0062 **	0.2424 ns	ns	ns	0.0698 ns	**	ns
C	Food (kcal)	0.0176 *	0.3230 ns	0.0043 **	ns	ns	*	ns	**
D	Water (mL)	0.0158 *	0.7114 ns	0.0607 ns	ns	ns	ns	ns	*
F	Activity Light	0.3707 ns	0.3948 ns	0.7561 ns	x	x	x	x	x
	Activity Dark	0.9866 ns	0.1280 ns	0.3692 ns	x	x	x	x	x
Figure 10									
B	Body temp Light	0.4606 ns	0.9184 ns	0.6426 ns	x	x	x	x	x
	Body temp Dark	0.6065 ns	0.9322 ns	0.3461 ns	x	x	x	x	x
Figure 11									
C	iBAT (°C)	0.5897 ns	0.3252 ns	0.1313 ns	x	x	x	x	x
D	Tail (°C)	0.9263 ns	0.1776 ns	0.1776 ns	x	x	x	x	x
Figure 12									
C	Inner ear (°C) 10°C	0.5276 ns	0.0477 *	0.8588 ns	ns	ns	ns	ns	ns
D	iBAT (°C) 10°C	0.5838 ns	0.5382 ns	0.2612 ns	x	x	x	x	x
E	Tail (°C) 38°C	0.1945 ns	0.1809 ns	0.4909 ns	x	x	x	x	x
	Tail (°C) 32°C	0.1050 ns	0.3033 ns	0.0012 **	**	ns	ns	ns	ns
	Tail (°C) 10°C	0.4133 ns	0.2427 ns	0.1597 ns	x	x	x	x	x

Figure 13									
A	iBAT	0.1506 ns	0.8932 ns	0.9451 ns	x	x	x	x	x
	iWAT	0.0750 ns	0.5104 ns	0.0824 ns	x	x	x	x	x
	gWAT	0.0347 *	0.4957 ns	0.0682 ns	ns	ns	ns	ns	*
B	*Dio2*	0.0900 ns	0.0450 *	0.0008 ***	**	ns	**	ns	ns
	Ucp1	0.2339 ns	0.6110 ns	0.0002 ***	ns	ns	*	ns	**
	Tfam	0.0391 *	0.2627 ns	0.0010 **	ns	ns	*	ns	**
	Adrb3	0.7961 ns	0.0398 *	<0.0001 ****	**	ns	***	ns	*
C	cAMP	0.5791 ns	0.1789 ns	0.6600 ns	x	x	x	x	x
D	UCP1 Protein	0.6842 ns	0.0731 ns	0.1003 ns	x	x	x	x	x
E	CV- ATP5A	0.0887 ns	0.3752 ns	0.2122 ns	x	x	x	x	x
	CIII- UQCRC2	0.0051 **	0.4232 ns	0.0333 *	**	ns	ns	ns	ns
	CIV- MTCO1	0.0009 ***	0.5227 ns	0.5080 ns	ns	ns	ns	*	*
	CII-SDHB	0.1553 ns	0.3967 ns	0.5272 ns	x	x	x	x	x
	CI- NDUFB8	0.5153 ns	0.5942 ns	0.6341 ns	x	x	x	x	x
F	*Pgargc1A*	<0.0001 ****	0.0001 ***	0.0003 ***	*	****	ns	ns	****
	Acaca	0.4454 ns	0.7594 ns	0.0273 *	ns	ns	ns	ns	ns
	Mlycd	0.7006 ns	0.0952 ns	0.0012 **	ns	ns	**	ns	*
	Cs	0.0004 ***	0.1864 ns	0.0011 **	ns	**	ns	ns	****
	Lipe	0.0955 ns	0.7623 ns	0.0165 *	ns	ns	ns	ns	*
	Cidea	<0.0001 ****	0.1151 ns	<0.0001 ****	ns	****	ns	***	****
G	iBAT	0.1182 ns	0.0089 **	0.8367 ns	ns	ns	ns	*	ns
	iWAT	0.0591 ns	0.0102 *	0.0090 **	ns	ns	**	*	*
	gWAT	0.1282 ns	0.7922 ns	0.3803 ns	x	x	x	x	x
Figure 14									
A	*Dio2*	0.3127 ns	0.0832 ns	0.0015 **	*	ns	ns	ns	ns
	Ucp1	0.1494 ns	0.0336 *	0.0736 ns	ns	ns	ns	ns	ns
	Cidea	0.8605	0.7035	0.0061	ns	ns	ns	ns	ns

		ns	ns	**					
	Ppargc1A	0.8091 ns	0.5341 ns	0.0265 *	ns	ns	ns	ns	ns
	Mlycd	0.8373 ns	0.0287 *	0.0018 **	ns	ns	ns	ns	ns
B	*Pnpla2*	0.6769 ns	0.2420 ns	0.0174 *	ns	ns	ns	ns	ns
	Lipe	0.3986 ns	0.1592 ns	0.0699 ns	x	x	x	x	x
	Lpl	0.2731 ns	0.8523 ns	0.2182 ns	x	x	x	x	x
	Adrb3	0.9700 ns	0.5117 ns	0.2312 ns	x	x	x	x	x
Figure 15									
A	*Dio1*	0.3408 ns	0.2589 ns	<0.0001 ****	ns	ns	ns	ns	**
	Thrsp	0.6183 ns	0.0144 *	<0.0001 ****	*	ns	***	ns	**
	Pklr	0.0022 **	0.0114 *	0.1318 ns	ns	**	ns	ns	*
	Pck1	0.0657 ns	0.3701 ns	0.0906 ns	x	x	x	x	x
	Ldha	0.0578 ns	0.0035 **	0.1191 ns	ns	**	*	ns	ns
	Me1	0.3515 ns	0.3224 ns	0.0003 ***	**	ns	ns	ns	ns
	Acaca	0.5260 ns	0.2782 ns	0.0151 *	ns	ns	ns	ns	ns
B	Glycogen	0.3301 ns	0.8107 ns	0.0882 ns	x	x	x	x	x
Figure 16									
A	Heart Weight	0.1338 ns	0.2241 ns	0.5283 ns	x	x	x	x	x
C	Heart Rate Light	0.6444 ns	0.6065 ns	0.5549 ns	x	x	x	x	x
	Heart Rate Dark	0.7493 ns	0.8970 ns	0.6104 ns	x	x	x	x	x
Figure 18									
A	max. Heart Rate	0.4187 ns	0.3815 ns	0.0934 ns	x	x	x	x	x
B	PSNS	0.7500 ns	0.9116 ns	0.8597 ns	x	x	x	x	x
	SNS	0.8630 ns	0.5841 ns	0.2785 ns	x	x	x	x	x
C	intrinsic Heart Rate	0.9125 ns	0.7059 ns	0.7270 ns	x	x	x	x	x
Figure 19									
A	*Hcn2*	0.3559 ns	0.2543 ns	0.1073 ns	x	x	x	x	x
	Hcn4	0.8650 ns	0.7624 ns	0.2545 ns	x	x	x	x	x
	Kcna1	0.6849 ns	0.8974 ns	0.6080 ns	x	x	x	x	x

	Serca2	0.6890 ns	0.4832 ns	0.8090 ns	x	x	x	x	x
	Pln	0.6276 ns	0.8066 ns	0.8990 ns	x	x	x	x	x
	α/β-Mhc ratio	0.1814 ns	0.1581 ns	0.1447 ns	x	x	x	x	x
	Bnf	0.3518 ns	0.1818 ns	0.3524 ns	x	x	x	x	x
B	Systolic	0.0253 *	0.6498 ns	0.3564 ns	ns	ns	ns	ns	ns
	Diastolic	0.1447 ns	0.8901 ns	0.4031 ns	x	x	x	x	x
	MAP	0.0608 ns	0.8875 ns	0.8779 ns	x	x	x	x	x

*: p<0.05; **: p<0.01; ***: p<0.001; ****: p<0.0001; ns, not significant (p>0.05); WT, wildtype; x, no post-hoc test required.

Supplementary Table 2: Statistical analysis of heart rate frequency distribution of Part A – two-way ANOVA with Holm-Sidak's multiple comparisons test.

Figure 17A						
	Light phase			Dark phase		
	WT vs.			WT vs.		
Heart rate in 20 bpm intervals	*Mct8* ko	*Oatp1c1* ko	*M/O* dko	*Mct8* ko	*Oatp1c1* ko	*M/O* dko
100 - 160	ns	ns	ns	ns	ns	ns
180	ns	ns	*	ns	ns	ns
200	ns	ns	*	ns	ns	ns
220 - 280	ns	ns	ns	ns	ns	ns
300	ns	ns	ns	ns	ns	*
320	ns	ns	ns	ns	ns	ns
340	ns	ns	ns	ns	ns	ns
360	ns	ns	**	ns	ns	ns
380	ns	ns	**	ns	ns	*
400	ns	ns	*	ns	ns	**
420	ns	ns	*	ns	ns	*
440 - 800	ns	ns	ns	ns	ns	ns

*: p<0.05; **: p<0.01; ***: p<0.001; ****: p<0.0001; bpm, beats per minute; ns, not significant (p>0.05); WT, wildtype. Heart rate values with a significance of p>0.05 are not displayed individually.

6.2. Statistical Analysis of Part B

In vivo body temperature data (twenty-four-hour profile (Supplementary Table 3) and mean values for light and dark phase (Supplementary Table 4) were analyzed using two-way repeated measures ANOVA with Holm-Sidak's multiple comparisons test correcting for time, treatment (T3), and interaction. Furthermore, the heart rate frequency distribution was analyzed using two-way ANOVA with Holm-Sidak's multiple comparisons test (Supplementary Table 5).

Supplementary Table 3: Statistical analysis of the body temperature twenty-four-hour profile of Part B – two-way repeated measures ANOVA with Holm-Sidak's multiple comparisons test.

Figure 21A					
two-way repeated measures ANOVA				Holm-Sidak's post-hoc test	
	Time	T3	Interaction	Time point (30min interval)	Baseline vs. +T3
Body temperature	****	ns	****	12:00	*
				12:30	ns
				13:00	ns
				13:30	ns
				14:00	ns
				14:30	ns
				15:00	*
				15:30	*
				16:00	*
				16:30	*
				17:00	*
				17:30 – 02:30	ns
				03:00	*
				03:30	ns
				04:00	ns
				04:30	ns
				05:00	ns
				05:30	ns
				06:00	ns
				06:30	*
				07:00	**
				07:30	**
				08:00	***
				08:30	***
				09:00	**
				09:30	***
				10:00	**
				10:30	ns
				11:00	***
				11:30	***

*: $p<0.05$; **: $p<0.01$; ***: $p<0.001$; ****: $p<0.0001$; ns, not significant ($p>0.05$). Body temperature values with a significance of $p>0.05$ are not displayed individually.

Supplementary Table 4: Statistical analysis of the mean body temperature (°C) of Part B – two-way repeated measures ANOVA with Holm-Sidak's multiple comparisons test.

Figure 21B					
two-way repeated measures ANOVA				Holm-Sidak's post-hoc test	
				Baseline vs. T3	
	Time	T3	Interaction	Light phase	Dark phase
Body temperature °C	**	ns	**	***	ns

*: p<0.05; **: p<0.01; ***: p<0.001; ****: p<0.0001; ns, not significant (p>0.05).

Supplementary Table 5: Statistical analysis of heart rate frequency distribution of Part B – two-way ANOVA with Holm-Sidak's multiple comparisons test.

Figure 27A		
	Baseline vs. +T3	
Heart rate in 20bpm intervals	Light phase	Dark phase
100 - 800	ns	ns

Bpm, beats per minute; ns, not significant (p>0.05). Heart rate values with a significance of p>0.05 are not displayed individually.

6.3. Statistical Analysis of Part C

In vivo food intake data (Supplementary Table 6) were analyzed using two-way repeated measures ANOVA with Bonferroni post-hoc test correcting for interaction, time, treatment (TA3), and subjects matching.

Supplementary Table 6: Statistical analysis of the cumulative food intake of Part C – two-way repeated measures ANOVA with Holm-Sidak's multiple comparisons test.

Figure 30E						
two-way repeated measures ANOVA					Bonferroni post-hoc test	
	Interaction	Time	Treatment	Subjects (matching)	Days	-TA3 vs +TA3
Food intake	****	****	**	****	1	ns
					2	ns
					3	ns
					4	ns
					5	ns
					6	ns
					7	*
					8	*
					9	**
					10	**
					11	***
					12	****
					13	****
					14	****

*: $p<0.05$; **: $p<0.01$; ***: $p<0.001$; ****: $p<0.0001$; ns, not significant ($p>0.05$).

6.4. List of Tables

6.5. List of Figures

6.6. Non-standard abbreviations

°C	degree Celsius
AHDS	Allan-Herndon-Dudley Syndrome
AMPK	adenosine monophosphate-activated protein kinase
ANOVA	analysis of variance
ANS	autonomic nervous system
ARs	adrenergic receptors
ATP	adenosine triphosphate
AU	arbitrary units
AUC	area under the curve
BAT	brown adipose tissue
BBB	blood brain barrier
BCSFB	blood cerebrospinal fluid barrier
bpm	beats per minute
brite adipocytes	brown in white adipocytes
BSA	bovine serum albumin
Ca^{2+}	calcium
cAMP	cyclic adenosine monophosphate
cDNA	complementary deoxyribonucleic acid
CIII-UQCRC2	complex III ubiquinol cytochrome c reductase core protein 2
CIV-MTCO1	omplex IV Cytochrome C Oxidase core subunit 1
CNS	central nervous system
cnts	counts
Ct	treshold cycle
DIO 1-3	iodothyronine deiodinase type 1-3
ELISA	enzyme linked immunosorbent assay
gWAT	gonadal white adipose tissue
HCN channel	hyperpolarization activated cyclic nucleotide gated channel
HPT axis	hypothalamu-pituitary-thyroid axis
HRP	horseradish peroxidase
i.p.	intraperitoneally
iBAT	interscapular brown adipose tissue
I_f	funny current
IRD	inner ring deiodination
iWAT	inguinal white adipose tissue
kg/g/mg/µg/ng	kilogram/gram/milligram/microgram/nanogram

ko	knockout
L/mL/µL	Liter/milliliter/microliter
LAT 1/2	L type amino acid transporter 1/2
M/mM/µM/nM	Molar/millimolar/micromolar/nanomolar
M/O dko	Mct8/Oatp1c1 double knockout
MCT8	monocarboxylate transporter 8,
MFS	major facilitator superfamily
MHC	myosin heavy chain
min	minute
mmHg	millimeter of mercury
mRNA	messenger ribonucleic acid
NCX	sodium-calcium exchanger
NE	norepinephrine
NST	non-shivering thermogenesis
OATP	organic anion transporting polypeptide
OATP1C1	organic anion transporting polypeptide 1C1
OD	optical density
ORD	outer ring deiodination
OXPHOS	oxidative phosphorylation complexes
PBS	phosphate buffered saline
PCR	polymerase chain reaction
PLN	phospholamban
PSNS	parasympathetic nervous system
qPCR	quantitative real time PCR
RNA	ribonucleic acid
RT	room temperature
RYR	ryanodine receptor
SA	sinoatrial
SR	sarcoendoplasmic reticulum
S.E.M.	standard error of the mean
SERCA	sarcoendoplasmic reticulum Ca^{2+} adenosine triphosphatase
SLC	solute carrier
SNS	sympathetic nervous system
T2	diiodothyronine
T3	3,3',5-triiodothyronine
T4	3,3',5,5'-tetraiodothyronine
TA3	3,3',5-triiodothyroacetic acid, Triac

TA4	3,3',5,5'-tetraiodothyroacetic acid, Tetrac
TBS	tris buffered saline
TBS-T	tris buffered saline with Tween20
TE	tris ethylenediaminetetraacetic acid
THs	thyroid hormones
THTs	thyroid hormone transporters
TLSs	translational starting sites
TMB	tetramethylbenzidine
TR	thyroid hormone receptors
TRH	thyrotropin-releasing hormone
TSH	thyroid-stimulating hormone
tT3	total T3
tT4	total T4
UCP1	uncoupling protein 1
WAT	white adipose tissue
WT	wildtype
xCT	cystine/glutamate transporter

7. Danksagung

Ich möchte mich bei all den Menschen bedanken, die mich während meiner Promotion unterstützt haben, und ohne die diese Dissertation nicht entstanden wäre.

An erster Stelle möchte ich meinem Doktorvater Prof. Jens Mittag dafür danken, dass er mir dieses Projekt anvertraut hat und mir die Möglichkeit gab, an einem so interessanten und anspruchsvollen Thema zu arbeiten. Danke für Deine Unterstützung, Motivation, offene Tür sowie unzählige wissenschaftliche Diskussionen – aber auch für äußerst unterhaltsame Mittagspausen und Erziehungstipps. Außerdem vielen Dank für Deine außergewöhnlich schnellen Korrekturen und für eine unvergessliche Zeit.

Weiterhin danke ich den Mitgliedern des Prüfungsausschusses für Ihre Zeit und dafür, dass Sie sich bereit erklärt haben, mich zu prüfen.

Mein Dank gilt auch der Deutschen Forschungsgemeinschaft, die mein Projekt im Rahmen des SPP1629 Thyroid Trans Act finanziert hat; der Deutschen Gesellschaft für Endokrinologie für den Bruno Allolio-Preis und zahlreiche Reisestipendien; der Young Active Research in Endocrinology und der Europäischen Gesellschaft für Endokrinologie für weitere Reisestipendien.

Außerdem möchte ich mich bei den Verantwortlichen des GRK1957 – Adipocyte Brain Crosstalk an der Universität zu Lübeck bedanken, dass Sie mich als assoziiertes Mitglied aufgenommen und mir so die Teilnahme an vielfältigen Workshops, Seminaren, „Summer Schools“ und Konferenzen ermöglicht haben. Ein besonderer Dank geht an Prof. Markus Schwaninger für die Begleitung meines Projektes als Zweitbetreuer und Dr. Nina Perwitz und Chaoqun Jiang, die auf jede erdenkliche Frage eine Antwort gefunden haben.

Danke an Prof. Heike Heuer und ihre gesamte Arbeitsgruppe – insbesondere Dr. Jiesi Chen und Markus Korkowski – für die Zeit, die ich in ihren Laboren verbringen durfte; ebenso für die *Mct8* ko, *Oatp1c1* ko und die *Mct8/Oatp1c1* dko Mäuse, die wissenschaftlichen Diskussionen und konstruktives Feedback zu meinem Paper. Mein Dank geht auch an Prof. Henrik Oster für die Benutzung des Spektralphotometers, Prof. Olaf Jöhren für die Benutzung des Stickstoff-Verdampfers und Dr. Henriette Kirchner für die Nutzung der qPCR Maschine und ihre Hilfe bei den Messungen.

Ein großes Dankeschön geht an die Gemeinsame Tierhaltung Lübeck; vor allem an Yannick, Sven und Heiko, die mich immer nach Kräften unterstützten und für einen Plausch zu haben waren.

Des Weiteren möchte ich mich bei allen ehemaligen und aktuellen Mitgliedern der Arbeitsgruppe bedanken, die mich so herzlich im Norden aufgenommen und mir immer mit Rat und Tat zur Seite gestanden haben:

Dr. Rebecca Ölkrug: danke, dass Du damals an mich gedacht hast, denn sonst hätte ich meine Promotion wohl nie geschafft! Danke für Dein offenes Ohr, die Kinderbetreuung im Labor, die Unterstützung bei Versuchen jeglicher Art und natürlich für Pat und Patterchen im Labor.

Dr. Lisbeth Harder: danke für die Ablenkung beim Yoga, beim Trampolinspringen oder in den Kaffeepausen; für Deine unermüdliche Hilfe im Labor sowie bei den Versuchen während des Mutterschutzes – und besonders dafür, dass es mit der Wohnung geklappt hat. Dr. Sogol Gachkar, meine erste Platznachbarin im UKSH und Labornachbarin im CBBM: danke für Deine immer gute Laune, die einen ansteckt, ob man will oder nicht; außerdem für Deine spontanen Einfälle und Unternehmungen, die meine Zeit in Lübeck sehr bereichert haben. Dr. Kornelia Johann: danke für die stets unterhaltsame Begleitung zu zahlreichen Konferenzen und SPP Meetings.

Dr. Sebastian Nock: danke für Deine Hilfe bei Computerproblemen und Versuchen – und für den leckeren Kuchen! Francesca Raffaelli: danke für die lebhaften Gespräche und das Perfektionieren der Mittagspausen-Organisation. Julia Resch: danke für Deine Herzlichkeit und die Einführung in Dein Western Blot Geheimnis; außerdem für Deine Hilfe im und außerhalb des Labors.

Mehdi Pedaran: danke für die netten, abwechslungsreichen Dialoge zu Labor- und Kinderthemen und Deine große Hilfsbereitschaft. Dr. Riccardo Dore und Sandro Catzeddu: danke für unterhaltsame Gespräche und den Espresso-Geruch im Büro am Nachmittag. PD Alexander Iwen: danke für überraschende Geschichten und medizinische Hilfe. Ihr habt die letzten Jahre für mich unvergesslich gemacht, dafür bin ich Euch sehr dankbar!

Vielen Dank allen ehemaligen Kolleginnen und Kollegen auf der 1. Etage des CBBM, vor allem Dr. Lisa Cherradi, Dr. Rose Kohlie, Dr. Cathleen Geißler, Dr. Christin Krause, Martina Grohs, Dr. Stephanie Fliedner, Heike Albrecht, Sylvia Grammerstorf-Roche, Dr. Jana-Thabea Kiehn, und Ludmila Skrum für die Hilfsbereitschaft und unterhaltsamen Gespräche in der Kaffeeküche. Dr. Carla Schulz: danke für Hilfe bei Fragen jeder Art und viele fröhliche Unterhaltungen!

Danke auch an Prof. Ruth Lehmann, Prof. Steven Burden and Assistenzprofessor Dr. Thomas Ryan Hurd für einen wichtigen Beitrag zu meiner wissenschaftlichen Karriere, die wissenschaftlichen Diskussionen und das Einleben in New York.

Ein ganz besonderer Dank geht an meine Freunde außerhalb des Labors, die mich immer unterstützt haben. Danke an das Office003 in Bonn – Saskia, Laia und Katarina –, für die unvergessliche Zeit, in der aus Kolleginnen echte Freunde geworden sind. Danke für die vielen Kaffeepausen, die gemeinsamen Zellkulturschichten und Western Blot Fun, aber auch für die gemeinsamen Ausflüge und, nicht zu vergessen, für Wuthering Heights. Danke an meine Kindergartenfreundin Marina für die vielen Videoanrufe und Sprachnachrichten und dafür, dass Du immer für mich da bist. Danke auch an Carmen, Christiane und Anna, denn mit Euch fing die tolle Bio-Zeit an; ich hoffe, dass wir uns bald alle wiedersehen werden. Danke an Juhee, für Videoanrufe, Motivationsschübe und Päckchen aus New York, die mir jedes Mal Heimweh bescherten.

Nicht zuletzt möchte ich den wichtigsten Menschen in meinem Leben Danke sagen, denn ohne meine tolle Patchwork-Familie wäre ich nicht da, wo ich heute bin. Danke an Wolfgang und Christa, Andreas und Anna mit Sofia und Anastasia für leckeres Essen, gemeinsame Urlaube und aufmunternde Worte. Danke an Andreas, Steffi und Simon für die großartigen Zeiten in Jülich

und Basel, das Korrekturlesen und die tollen Feste. Danke auch an meine Großeltern und meine Urgroßmutter für Eure immerwährende Unterstützung – ganz gleich, wo ich gerade bin. Danke an meinen Vater Jochen, an Jana, Alexander und Laura für den familiären Halt, wunderschöne Weihnachtsfeiern und dafür, dass es nie langweilig geworden ist. Danke an Dieter, Nora, Flo, Anne, Martin, Erik und Marc für Eure riesengroße Hilfsbereitschaft in jeder Lebenslage, für viele leckere Essen, Eure Besuche in Lübeck, Schweden oder New York, fürs Korrekturlesen, und dafür, dass ich mich immer auf Euch verlassen kann. Ein ganz großes Dankeschön geht an meine Mutter Steffi und meine Schwester Tina, die immer für mich da sind, hinter mir stehen, mich immer wieder überraschen und aufmuntern. Ganz besonders danke ich meinem Partner Boris für die Geduld und Liebe, für die Unterstützung in den vergangenen Jahren und die unzähligen Fahrten nach Lübeck. Danke, dass Du mir den Rücken freigehalten hast und immer zu mir stehst! Und natürlich Danke an Henri, meinen Sohn, für Deine bedingungslose Liebe und dafür, dass ich die Welt mit Dir neu entdecken darf. Danke für Eure grenzenlose Liebe und uneingeschränktes Vertrauen!